May / June 2024
Volume 53, Number 3

AppliedRadiology®

The Journal of Practical Medical Imaging and Management

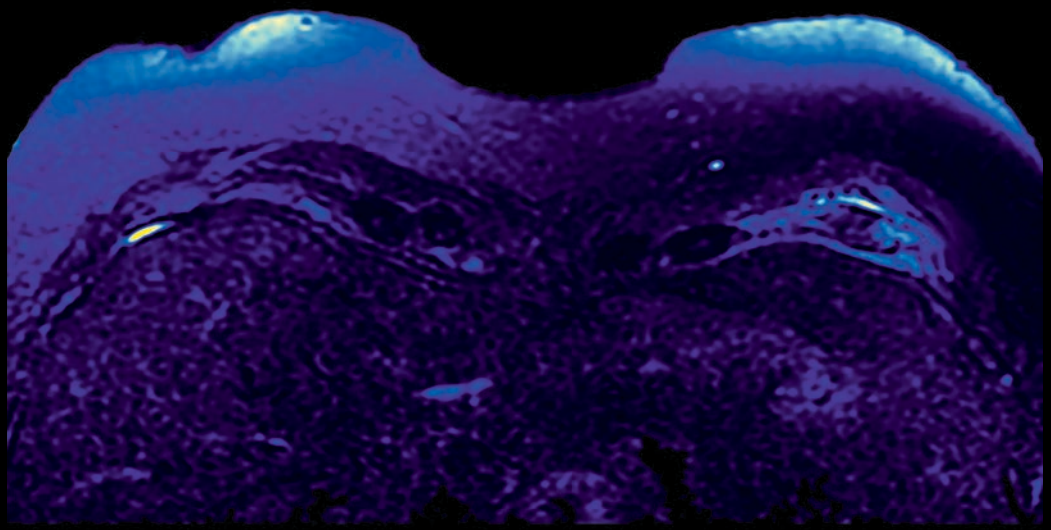

CME Making Sense of Incidental Musculoskeletal Findings on Breast MRI

CT in Nontraumatic Intraperitoneal and Retroperitoneal Hemorrhage

Chemical Exchange Saturation Transfer for Epilepsy Imaging

Reduce, Reuse, Recycle: The Three R's of Sustainability

Amyand Hernia Complicated by Acute Appendicitis

www.appliedradiology.com

Applied Radiology
May / June 2024 Volume 53, Number 3

CT Suite | MR Suite | Injectors and Digital Solutions

SmartInject
SOLUTIONS FROM BRACCO

Point-of-care imaging solutions that help promote patient safety and streamline workflow

NEXO®
Contrast management system

Advance patient care with smart injectors and digital solutions from Bracco.

Learn more at **SmartInject.com**

Bracco Diagnostics Inc.
259 Prospect Plains Road, Building H
Monroe Township, NJ 08831 USA

Phone: 609-514-2200
Toll Free: 1-877-272-2269 (U.S. only)
Fax: 609-514-2446

BRACCO
LIFE FROM INSIDE

Committed to Science,
Committed **to You.**™

AppliedRadiology®

The Journal of Practical Medical Imaging and Management

Anderson Publishing, Ltd
180 Glenside Avenue,
Scotch Plains, NJ 07076
Tel: 908-301-1995
Fax: 908-301-1997
info@appliedradiology.com

Editorial Advisory Board

Applied Radiology®

The Journal of Practical Medical Imaging and Management

May / June 2024
Vol 53 No 3

ONLINE PEDIATRIC CASE SUPPLEMENT AT APPLIEDRADIOLOGY.COM

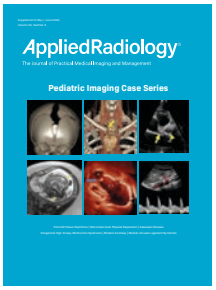

Applied Radiology (ISSN 0160-9963, USPS 943180) is published in print 6 times a year, January, March, May, July, September, and November, by Anderson Publishing Ltd at 180 Glenside Ave., Scotch Plains NJ 07076. Periodicals postage paid at Scotch Plains, NJ and additional mailing offices. Free subscriptions for US-based qualified radiology professionals. Subscriptions for the US and its territories and possessions: $115 per year, $225 for two years. Foreign and Canadian subscriptions $215 for one year payable in US funds, international money orders, or by credit card only. Postmaster: Please send address changes to Applied Radiology, PO Box 317, Lincolnshire, IL 60069-0317 (847-564-5942) or email AppliedRadiology@0meda.com.

Ch- Ch- Changes

Erin Simon Schwartz, MD

Dr Schwartz is the Editor-in-Chief of *Applied Radiology*. She is the chief of the Division of Neuroradiology and holds the Robert A. Zimmerman Chair in Pediatric Neuroradiology in the Department of Radiology at The Children's Hospital of Philadelphia. She is also professor of radiology, Perelman School of Medicine, University of Pennsylvania. Dr Schwartz can be reached at erin@appliedradiology.com.

Missing you already, JJ!

This issue marks the end of an era for *Applied Radiology*. After over 13 years with Anderson Publishing and serving as our Executive Editor since 2014, Joseph Jalkiewicz will be focusing on other adventures. JJ, as he is known in our shorthand, has been a terrific partner to us all. He has been the grease that helps keep the wheels turning, keeping track of our review articles and columns, and cracking the whip with authors when needed. Like my editorials that — without fail — come in precariously close to our publication deadline. His eye for detail and love of all things AMA Manual of Style have given our journal a consistent format and readability.

Larry Tanenbaum, our Associate Editor for AI, "always appreciated working with Joe and the unique tone he brought to my pieces." And the incomparable Wet Reader himself, Doug Phillips, said, "I have beforehand refused any editorial input on my ramblings. His were (largely) appreciated."

On a personal note, Joe has made me a better writer and editor. And his sense of humor made every interaction a pleasure. For those, and for his friendship, I am truly grateful.

Thank you, JJ. We will miss you and wish you all the best in your next chapter.

Additions

I am pleased to announce more imaging experts joining our Editorial Advisory Board:

- Avishkar (Avi) Sharma, MD, CIIP, joins our Artificial Intelligence section. Dr Sharma is a body radiologist and imaging informatics leader at Jefferson Einstein Hospitals in Philadelphia, Pennsylvania.

- Jessica K. Stewart, MD, joins the Interventional Radiology section. Dr Stewart is an interventional radiologist, director of interventional radiology global health initiatives, and an assistant professor of radiology at the University of California, Los Angeles, David Geffen School of Medicine, Los Angeles, California.

Making Sense of Incidental Musculoskeletal Findings on Breast MRI

Description

Incidental musculoskeletal findings are fairly common when reading breast MRI, as the ribs and sternum are included in the field of view. It is important that radiologists be familiar with the appearance of benign and malignant chest wall lesions on breast MRI in order to appropriately direct diagnosis and treatment, as well as to avoid unnecessary workup of benign lesions.

This activity is designed to educate radiologists about the wide range of both benign and malignant lesions which can be detected incidentally on breast MRI by reviewing the imaging findings and other pertinent demographic considerations regarding these lesions.

Learning Objectives

Upon completing this activity, the reader should be able to:

- Describe a range of both benign and malignant musculoskeletal imaging findings by their imaging features on breast MRI.
- Identify which imaging features and risk factors which would raise concern for malignant degeneration of certain musculoskeletal lesions.
- Discuss differing mineralization patterns of primary chest wall tumors.

Target Audience

- Radiologists
- Related Imaging Professionals

Authors

Paul Wojack, MD; Suzanne McElligott, MD; Pamela Walsh, MD; Nina Vincoff, MD; Ekta Gupta, MD

Affiliations: Department of Radiology, Northwell Health, and Zucker School of Medicine at Hofstra/Northwell, Hempstead, New York. Disclosures: Dr. Vincoff is also a member of the Editorial Advisory Board of *Applied Radiology*.

Commercial Support

None

Accreditation/ Designation Statement

This activity has been planned and implemented in accordance with the accreditation requirements and policies of the Accreditation Council for Continuing Medical Education (ACCME) through the joint providership of IAME and Anderson Publishing.

IAME is accredited by the ACCME to provide continuing medical education for physicians. IAME designates this enduring material for a maximum of 1 AMA PRA Category 1 Credits™. Physicians should claim only the credit commensurate with the extent of their participation in the activity.

Instructions

This activity is designed to be completed within the designated time period. To successfully earn credit, participants must complete the activity during the valid credit period. To receive CME credit, you must:

1. Review this article in its entirety.
2. Visit *appliedradiology.org/SAM2*.
3. Log into your account or create an account (new users).
4. Complete the post-test and review the discussion and references.
5. Complete the evaluation.
6. Print your certificate.

Estimated time for completion: 1 hour

Date of release and review: May 1, 2024

Expiration date: April 30, 2025

Disclosures

Planner: Erin Simon Schwartz, MD, discloses no relevant financial relationships with any ineligible companies.

Authors: Paul Wojack, MD, discloses no relevant financial relationships with ineligible companies. Suzanne McElligott, MD, discloses no relevant financial relationships with ineligible companies. Pamela Walsh, MD, discloses no relevant financial relationships with ineligible companies. Nina Vincoff, MD, discloses no relevant financial relationships with ineligible companies. Ekta Gupta, MD, discloses no relevant financial relationships with ineligible companies.

IAME has assessed conflict of interest with its faculty, authors, editors, and any individuals who were in a position to control the content of this CME activity. Any identified relevant conflicts of interest have been mitigated. IAME's planners, content reviewers, and editorial staff disclose no relationships with ineligible entities.

Making Sense of Incidental Musculoskeletal Findings on Breast MRI

Paul Wojack, MD; Suzanne McElligott, MD; Pamela Walsh, MD; Nina Vincoff, MD; Ekta Gupta, MD

Owing to its high sensitivity for cancer detection and superior soft-tissue resolution, MRI is often used for breast cancer staging and high-risk screening. Because it utilizes a dedicated coil with a large field of view, the modality often reveals incidental findings in extramammary structures of the chest wall and upper abdomen, particularly the musculature, ribs, and sternum.

To help radiologists gain confidence in interpretation and avoid unnecessary workups, we review the appearance of several of the most common musculoskeletal lesions demonstrated by breast MRI.

Figure 1. T1 fat-saturated, postcontrast axial MR image demonstrating T1 hypointense, nonenhancing mass in the sternum (circle). Additionally, this lesion was hypointense on all other sequences, consistent with a bone island.

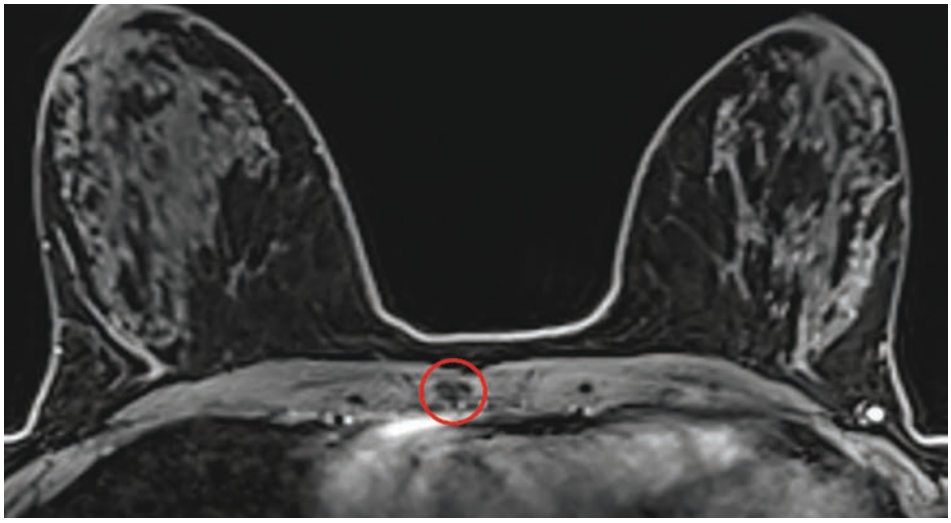

Frequency and Location of Incidental Findings

There is little question that breast MRI frequently makes incidental findings in the course of an examination performed for breast cancer screening or staging. In one study, extramammary findings were detected in up to 34% of patients.[1] While the liver and lungs are the most common sites for these entities, the chest musculature, ribs, and sternum are also common locations. Accounting for 7-10% of extramammary findings,[2,3,4] these incidental lesions may include osseous hemangiomas (also described as venous malformations), which comprise 17% of clinically insignificant abnormalities, and osseous metastases, which comprise 39% of clinically significant findings.[1]

Most lesions are determined to be benign, however up to 14% require additional workup.[1] Among patients with metastatic breast cancer, for example, about 60% will have osseous metastases.[5] Benign and malignant lesions, moreover, frequently share overlapping imaging features, making diagnosis challenging in many cases. Following is a discussion of the appearances of such entities that are likely to be encountered on breast MRI.

Benign Osseous Lesions

Bone Islands

Extremely common benign lesions, bone islands consist of masses of compacted cortical bone often seen in the sternum or ribs. Clinically asymptomatic, they do not enhance with contrast. While most occur sporadically, they can be associated with

Affiliations: Department of Radiology, Northwell Health, and Zucker School of Medicine at Hofstra/Northwell, Hempstead, New York. Disclosures: Dr. Vincoff is a member of the Editorial Advisory Board of *Applied Radiology*.
Keywords: extramammary breast MRI findings, benign and malignant osseous and soft tissue chest wall tumors, rib and sternal fractures, normal chest wall variants

Figure 2. (A) Axial T1 and (B) T2 fat-saturated MR images demonstrating a T1 isointense and T2 hyperintense mass in the sternum (circles). This mass demonstrated signal dropout on T1 fat-suppressed images and had mild enhancement (not shown). Findings are consistent with an osseous hemangioma.

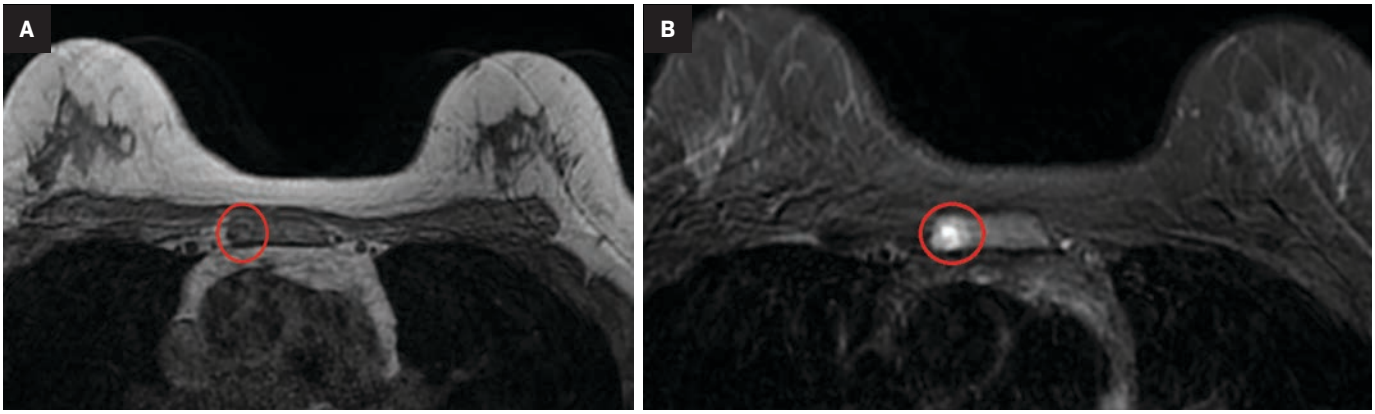

Figure 3. (A) Axial T2 fat-suppressed MR image showing a mass projecting anteriorly from the left third rib (red arrow). Note the T2 hyperintense cartilaginous cap of the lesion (white arrow). (B) Chest CT demonstrates corticomedullary continuity with the adjacent rib. Findings are consistent with an osteochondroma.

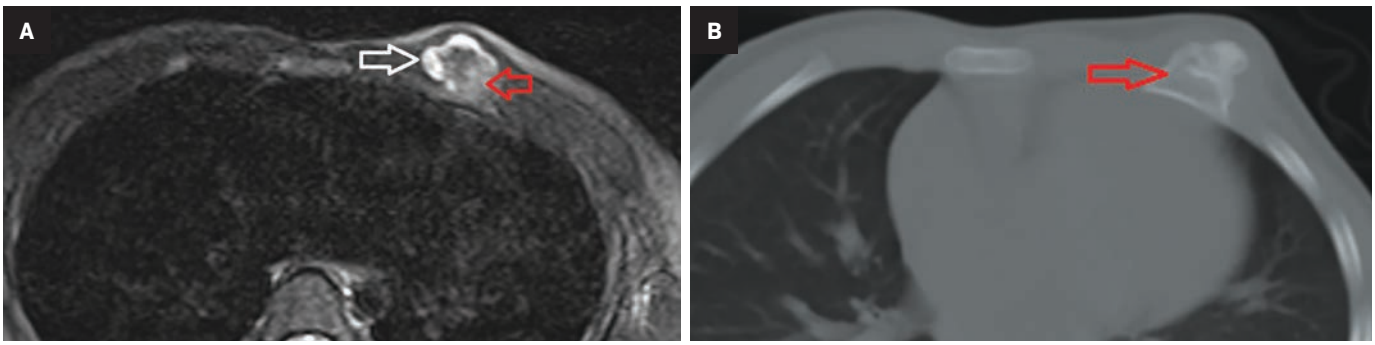

syndromes such as osteopoikilosis and Gardner syndrome (osteopoikilosis plus colonic polyps). Appearing highly sclerotic with a mean attenuation of 885 HU or greater on CT, they are deeply hypointense on all sequences on breast MRI (Figure 1).[6,7]

Hemangiomas

Osseous hemangiomas are often seen within the sternum (Figure 2). Histologically, they are composed of vascular elements with associated fat, although other components such as smooth muscle, fibrous tissue, or bone may also be seen.[8,9] Most occur sporadically, but they can be associated with a wide variety of syndromes, in which case they more often affect the extremities.[9] They are T2 hyperintense with intermediate to high T1 signal (depending on the amount of fat within the lesion) and will typically enhance. Hemangiomas may be associated with radiating trabecular thickening around the lesion; however, this finding is better appreciated with CT or radiography. Unlike osseous hemangiomas elsewhere in the body, vertebral hemangiomas have characteristic vertically oriented trabeculations, which develop as a response to the axial loading forces.[9]

Osteochondromas

As a type of exostosis, osteochondromas consist of an osseous protrusion from a bone with an associated cartilage cap. They commonly occur in the long bones and sometimes within the ribs (Figure 3).[10] Solitary osteochondromas have a low (< 1%) chance of malignant degeneration to chondrosarcoma, although the risk is greater when they are associated with syndromes such as multiple hereditary exostoses (~5%).[11] On MRI, the osseous portion of the lesion demonstrates corticomedullary contiguity with adjacent bone. The cartilage cap has low-to-intermediate T1 and high T2 signal. A cartilage cap thickness >1.5 cm is suspicious for malignant degeneration.[11] Osteochondromas may present either asymptomatically or as palpable or painful masses if they impinge on adjacent neurovascular structures or muscles.

Fibrous Dysplasia

Fibrous dysplasia develops when immature bone and fibrous stroma replace normal cancellous bone as a result of abnormal differentiation of osteoblasts.[12] The condition commonly involves the ribs, skull, mandible, and long bones.[13] It can affect patients of all ages but is most common in children and young adults. Occurring sporadically, most cases are monostotic (involving

Figure 4. (A) Axial T2 fat-suppressed MR image showing a T2 hyperintense expansile lesion in the right fourth rib (arrow). This lesion had intermediate T1 signal and enhanced with contrast (not shown). (B) Subsequent axial CT image with contrast demonstrates ground-glass matrix within the lesion (arrow). No aggressive features were seen. Findings are compatible with fibrous dysplasia.

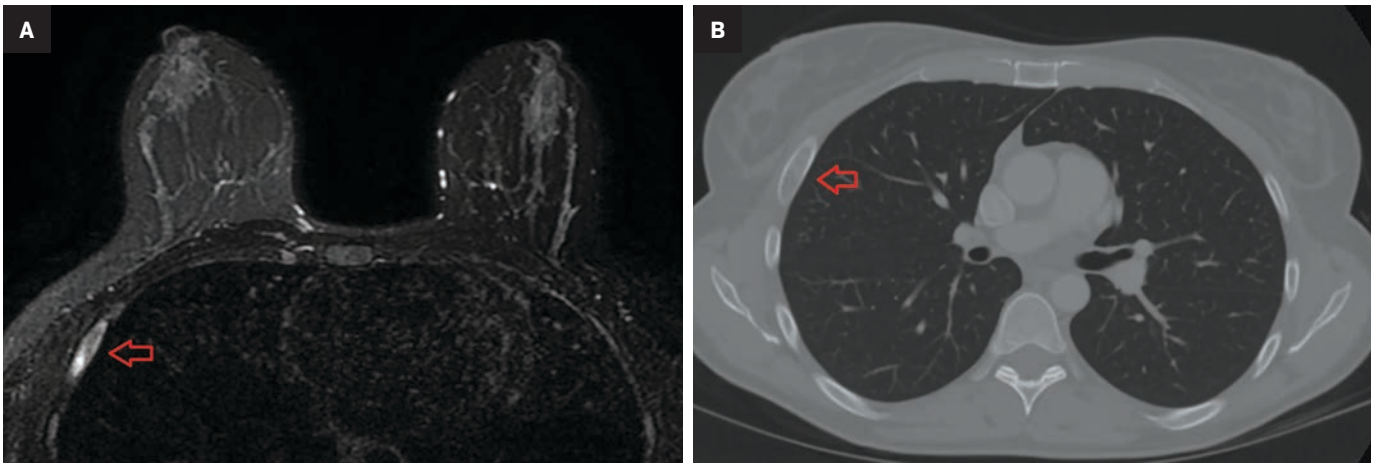

Figure 5. (A) Axial T1 and (B) T1 fat-suppressed postcontrast MR images of the right breast. There is a nonenhancing, T1 hyperintense mass in the lateral chest wall musculature that has signal loss on fat-suppressed sequence consistent with an intramuscular lipoma (circles).

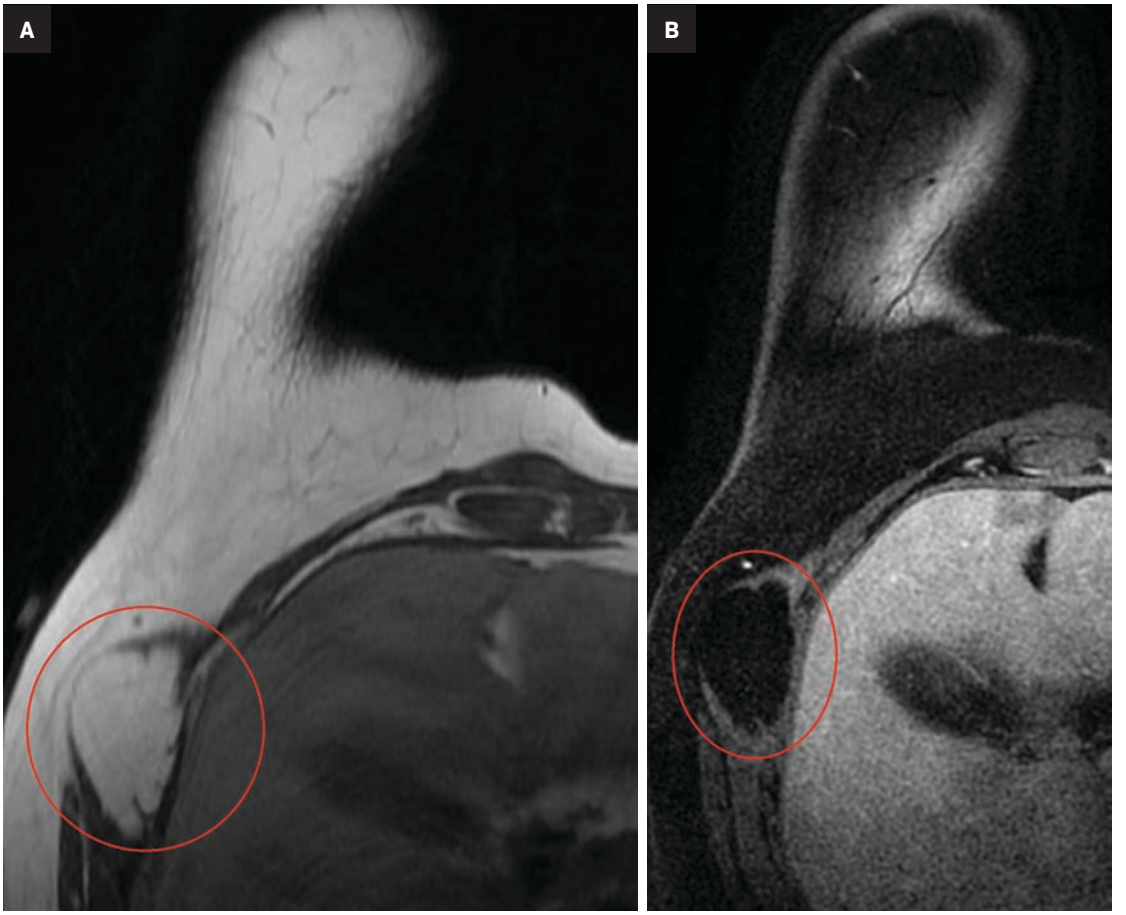

only one bone),[12] while about 20% are polyostotic (involving multiple bones) and may be associated with syndromes such as McCune-Albright and Mazabraud. Common MRI features consist of an expansile mass with low-to-intermediate T1 signal, variable T2 signal, and variable enhancement. If fibrous dysplasia is suspected, CT evaluation can help to demonstrate its typical "ground glass" matrix (Figure 4); diagnosis can often be made with imaging alone if this characteristic finding is present. Pathologic fractures are a potential complication. Malignant degeneration to osteosarcoma, fibrosarcoma, and malignant fibrous

Figure 6. (A) Axial STIR and (B) T2 fat-suppressed MR images demonstrating peripheral nerve sheath tumors in two separate patients. (A) A T2 hyperintense intercostal mass (circle) pathologically proven to represent an intercostal schwannoma. (B) Two T2 hyperintense, cutaneous masses in the lateral right breast and chest wall (arrows), consistent with neurofibromas in this patient with known type 1 neurofibromatosis. These masses demonstrated homogeneous enhancement in both patients (not shown), typical of peripheral nerve sheath tumors.

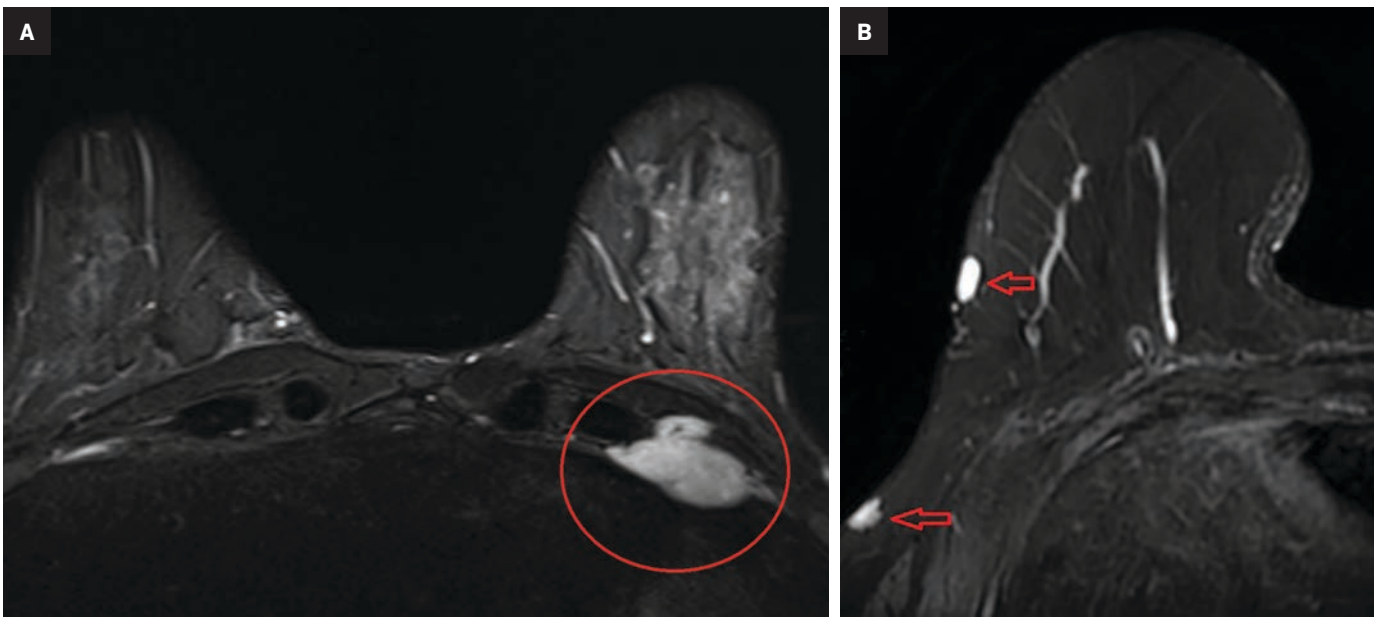

Figure 7. Axial T1 fat-suppressed precontrast MR image demonstrating a structure anterior to the medial aspect of the right pectoralis major musculature (arrow). This structure is isointense to skeletal muscle on all sequences and is compatible with a sternalis muscle.

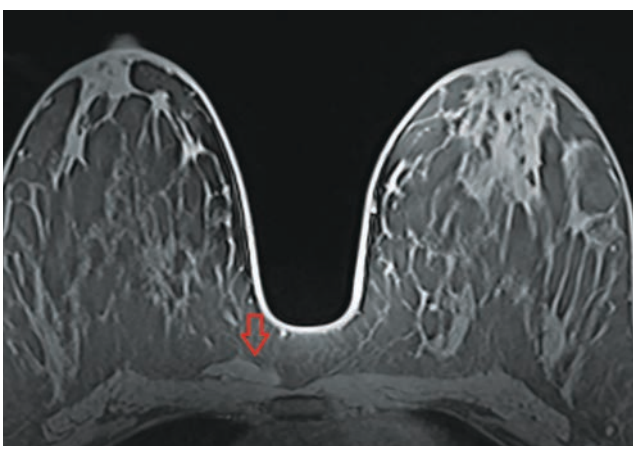

Figure 8. Axial T2 fat-suppressed MR image at the level of the sternoclavicular joints. There is a T2 hyperintense, well-circumscribed lesion adjacent to the left sternoclavicular joint (red arrow). This lesion was T1 hypointense and did not enhance, consistent with a cyst. Mild periarticular spurring is also seen at the left sternoclavicular joint (white arrow). Findings are consistent with osteoarthritis with subchondral cystic change.

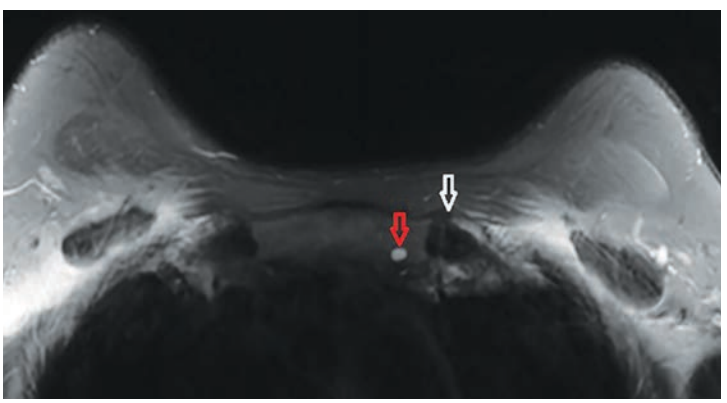

histiocytoma can also occur, albeit rarely (< 1% of cases).[12]

Benign Soft-tissue Masses

Lipoma

Composed of adipose tissue (Figure 5), these masses commonly present in the trunk and proximal extremities of middle-aged patients.[14] They appear as a circumscribed mass with signal characteristics of fat: high T1 and T2 signal with signal dropout on fat-suppressed sequences. Enhancement should be minimal or absent, although a few thin internal septa are normal. Any thick septations, nodularity, or prominent areas of enhancement should prompt further evaluation for a potential liposarcoma. When describing lipomas, their location is important to note, as superficial lipomas are easier to remove surgically than their intra- and intermuscular counterparts.

Nerve Sheath Tumors

Schwannomas and neurofibromas are common nerve sheath tumors that occur in the chest wall, typically in young and middle-aged adults.[15] They arise from the intercostal nerves or posteriorly from the spinal nerve roots. On MRI, they are isointense to slightly hyperintense

Figure 9. (A) Axial T2 fat-suppressed MR image showing a T2 hyperintense area in the sternum (circle). (B) Sagittal T1 postcontrast shows that this area represents a portion of the nonossified fibrocartilaginous disk of the normal manubriosternal joint.

relative to skeletal muscle on T1, hyperintense on T2, and enhance homogeneously with contrast.[16] Intercostal schwannomas are interposed between the ribs, reflecting the course of the intercostal nerves (Figure 6). Given their slow growth, there may be mild scalloping or remodeling of the adjacent bones.

Neurofibromas develop in younger patients, usually in their 20s and 30s, and are typically associated with type 1 neurofibromatosis.[15] They typically present as T2 hyperintense cutaneous masses (Figure 6). Some neurofibromas have a characteristic target-like appearance on T2 images; the periphery of the mass is brighter owing to the higher content of stromal material in the periphery relative to the cellular core.[17] This zonal distribution also results in more avid central enhancement of neurofibromas.

Other benign nerve sheath tumors such as ganglioneuromas and paragangliomas occur in the paraspinal regions and are less likely to be seen on breast MRI.

Sternalis Muscle

The sternalis muscle is an accessory muscle that runs vertically along the lateral margin of the sternum. Breast imagers are familiar with this anatomic variant, as it is seen on mammography and breast MRI. It typically originates from the upper sternum but demonstrates many potential insertions: the pectoral fascia, lower ribs, costal cartilages, rectus abdominis muscle sheath, and the aponeurosis of the abdominal external oblique muscle.[18,19] Mammographically, the muscle can present as an asymmetry in the posterior inner breast on the craniocaudal view. On MRI, it presents as a vertically oriented muscle just superficial to the medial aspect of the pectoralis major muscle, adjacent to the lateral margins of the sternum. It is isointense to the adjacent skeletal muscle on all sequences (Figure 7).

Sternal Arthridities

Multiple joints involving the sternum include the manubriosternal joint, the sternoclavicular joints, and multiple sternocostal joints. Like others, these joints are susceptible to various arthridities. The most common is osteoarthritis, which is characterized by joint space narrowing, periarticular osteophyte formation, and subchondral cystic changes. Subchondral cystic changes appear as T2 hyperintense cystic spaces within the bone and adjacent to the joint spaces (Figure 8).

Inflammatory arthridities can also be encountered. Rheumatoid arthritis may demonstrate periarticular erosions and joint-space narrowing, with fusion across the manubriosternal joint.[20] Psoriatic arthritis also presents with erosions but in a setting of superimposed osseous productive changes.[21] Although rare, crystalline arthropathies such as gout and calcium pyrophosphate dehydrate deposition disease (CPPD) can also affect the joints of the sternum.

A few other conditions classically involve the sternum. For example, SAPHO syndrome (synovitis, acne, psoriasis, hyperostosis, and osteitis) presents as sternocostoclavicular hyperostosis and osteitis on chest wall imaging.[22]

Monoarthritis of the manubriosternal joint, characterized by erosive changes about the joint, may also occur; this condition is often idiopathic but can occur in the setting of trauma or palmoplantar pustulosis.[23]

Tiezte syndrome is characterized by painful costochondritis of the costal cartilage.[23] It commonly occurs in young women. On imaging, the affected cartilage will appear enlarged with increased T2 signal in surrounding tissues and bone resulting from edema.

Additionally, the fibrocartilaginous disk of the manubriosternal joint demonstrates wide variability in resorption rate and degree as well as ossification over time. Therefore,

Figure 10. (A) Axial T2 fat-suppressed MR image demonstrates an acute left anterior rib fracture; the angulated, disrupted appearance of the rib cortex (arrow), along with a history of recent chest wall trauma, helped to confirm the diagnosis of acute fracture. Mild T2-hyperintense edema is seen surrounding the fracture site. (B) T1 postcontrast subtracted MR image through the sternum in a different patient with breast cancer demonstrating a mildly expansile, heterogeneously enhancing sternal lesion concerning for metastatic disease (circle). The patient also had suspected metastatic lesions involving several ribs. (C) Subsequent Tc-99m HDP SPECT CT, which confirmed metastatic disease in the sternum. Although there was suspicion for a pathologic sternal fracture, this diagnosis could not be made definitively on MRI.

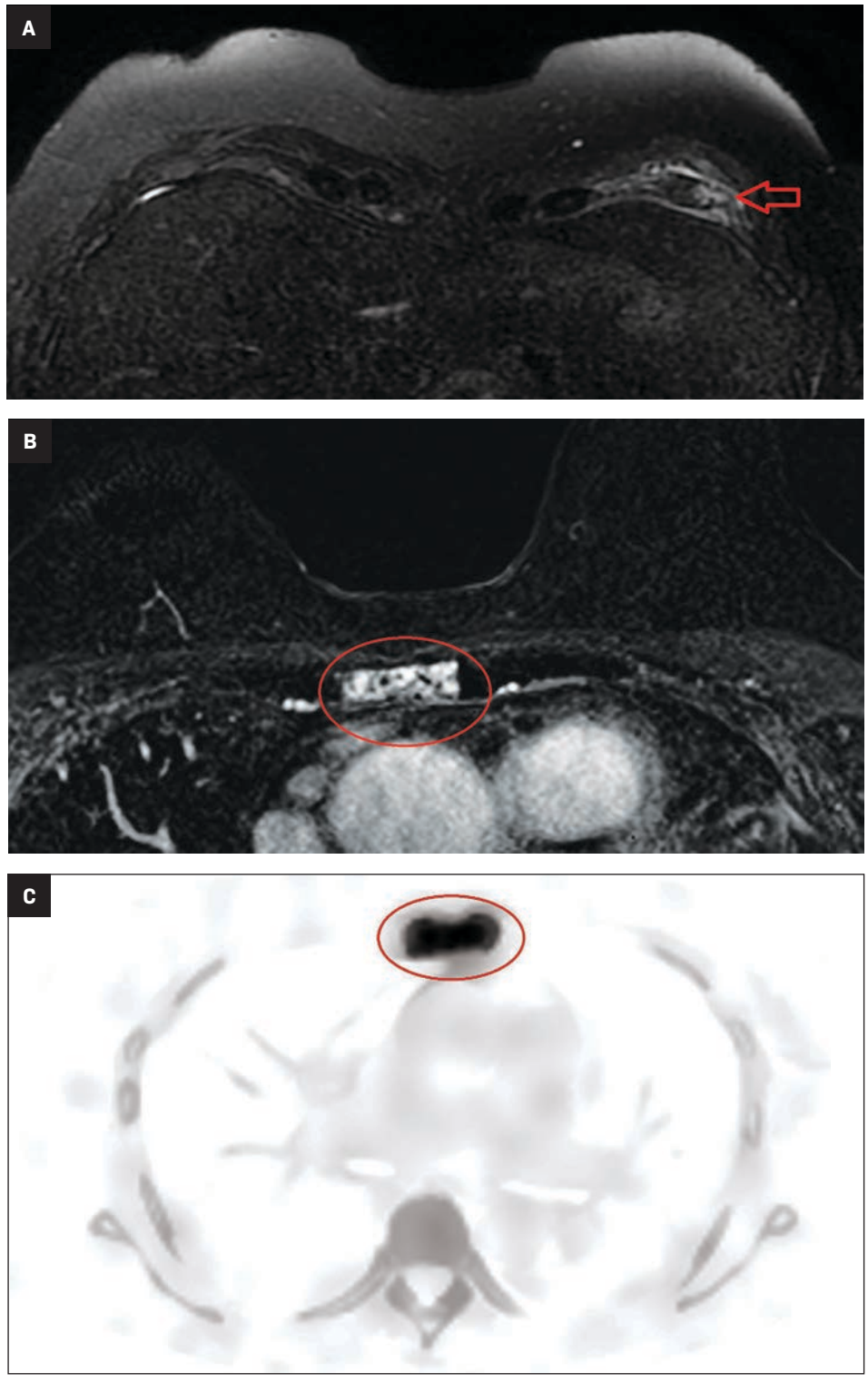

Figure 11. (A) T1 postcontrast subtracted image of the right breast in a patient with multiple myeloma showing an expansile, avidly enhancing, right anterior rib mass. Note the similar imaging features on MRI between multiple myeloma and other osseous metastases depicted in Figure 10. (B) Axial CT scan through the lesion shows the degree of associated osseous destruction (arrow).

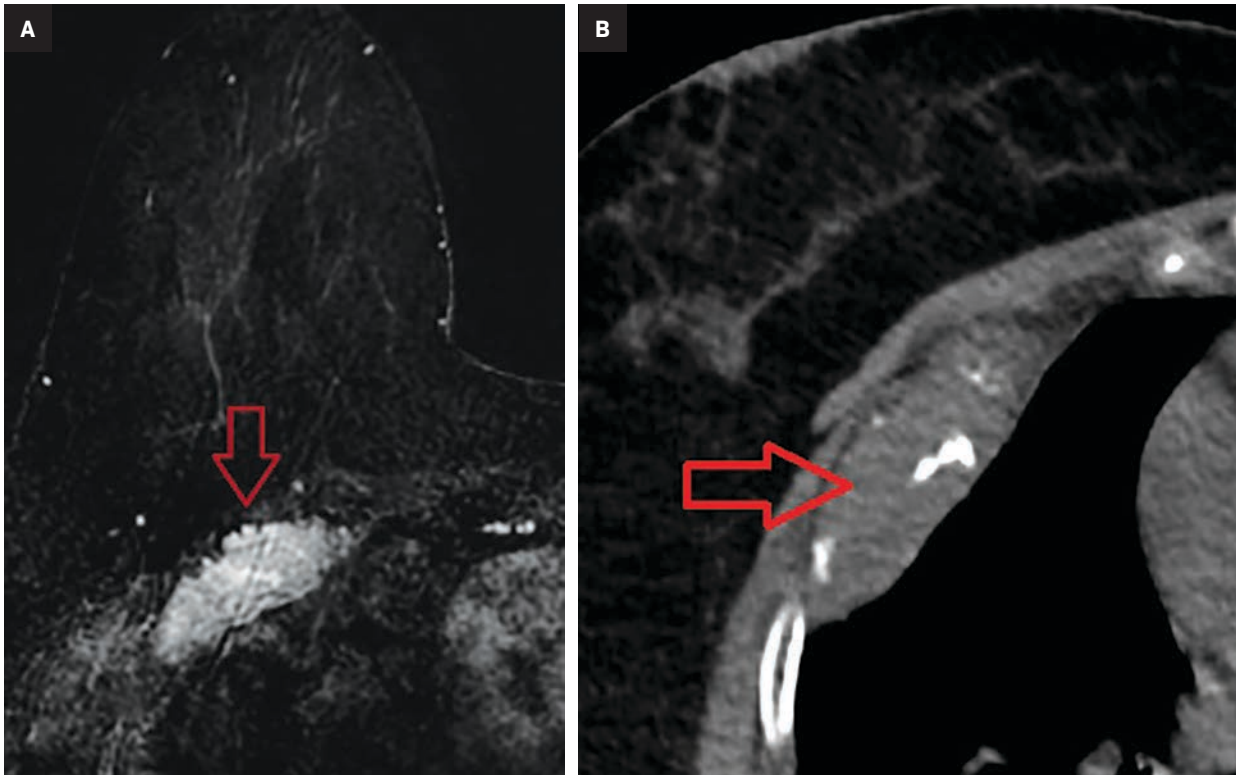

it is possible for a prominent disk to mimic a lesion to radiologists unfamiliar with its variations in appearance. Residual disks that have not ossified appear T2 hyperintense due to their cartilage content (Figure 9).

Rib and Sternal Fractures

Rib fractures are common in patients with chest wall trauma, occurring in about 10% of cases.[24] While chest CT has traditionally been the gold standard for assessing rib fractures, recent research has shown that MRI may be more sensitive for detecting acute fractures.[24] Additionally, elderly female patients and those who have received chest wall radiation are at increased risk of osteoporosis and rib fractures.[5,25,26] Although rib and sternal fractures are more likely to be detected on breast MRI given their locations, evaluating the localizer images is important, as they may show vertebral pathology, including fractures.[27]

Acute Traumatic Injuries

An acute fracture should demonstrate either a clear line extending through the cortex of the bone or the presence of cortical buckling (Figure 10). There is often a history of chest wall trauma. During the acute phase (up to four weeks), there is T2 hyperintense edema and enhancement in and around the fracture site resulting from posttraumatic inflammatory changes. Often, multiple adjacent ribs are fractured in a linear pattern. Over time, as the fracture enters the subacute phase of healing, edema and contrast enhancement decrease as surrounding bony callous forms. Once the bone is fully healed, enhancement and edema resolve and the osseous callus coalesces, typically resulting in a chronic fracture deformity.

Additionally, MRI may detect costal cartilage fractures not visible on CT or radiography. These occur at either the sternochondral or costochondral junction and most often affect the first and second ribs.[28] A T2 bright, linear fluid cleft extending through the costal cartilage with surrounding edema will be visible on MRI.

Pathologic Fractures

In contrast to their benign counterparts, pathologic fractures occur in the setting of malignancy such as metastatic disease (Figure 10) or multiple myeloma (Figure 11). The imaging features of both types of fractures can overlap; these include T2 hyperintense edema in and around the affected bone. Although diagnosing a pathologic fracture can be challenging with MRI alone, the presence of an expansile bone lesion or soft-tissue component may suggest a pathologic fracture. Discrete fracture lines may not be seen; bone lesions may slowly grow and erode through cortical bone, making it difficult to assess for an associated fracture.[29] Unless displacement is

Figure 12. (A) Large chondrosarcoma on a T1 fat-suppressed postcontrast image (star). Mineralization within the tumor is not readily apparent on MRI, but (B) axial noncontrast CT demonstrates the "ring and arc" pattern typical of chondroid lesions (red arrow). Expansion and extensive periosteal reaction of a left lateral rib denote the suspected origin site (white arrow). (C) A T1 fat-suppressed MR image demonstrates a large, irregular mass arising from a left-side rib with low-signal mineralization. (D) Axial CT shows extensive internal mineralization as areas of high density. Osteosarcoma was confirmed histologically.

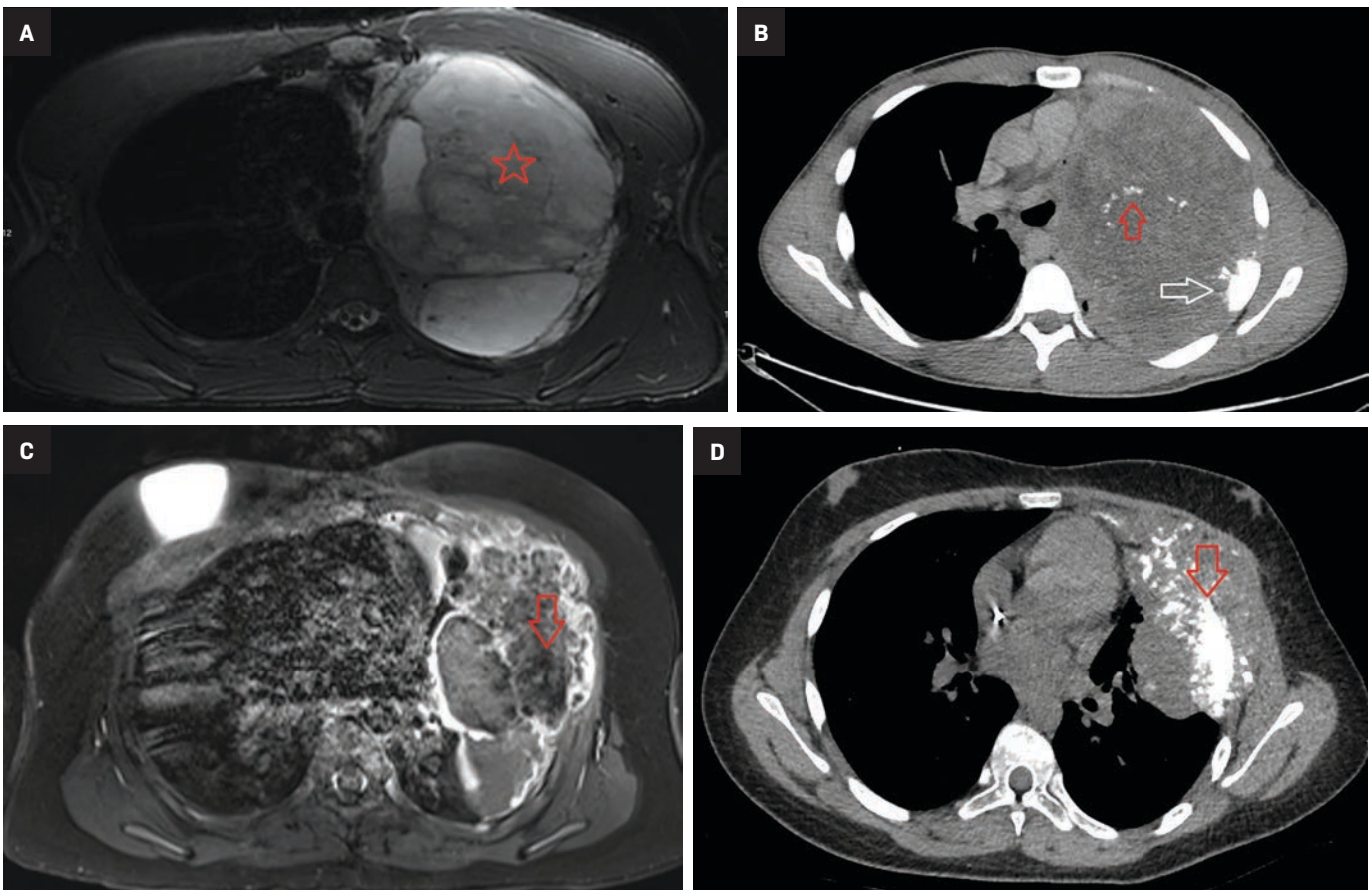

clearly visible, diagnosing a pathologic fracture on MRI may be difficult; CT may be helpful in equivocal cases. In contrast to the expected linear pattern of acute rib fractures, pathological fractures will generally follow a random distribution.

Chest Wall Malignancy

Metastatic Disease

The skeletal system is the most common site of distant breast cancer metastases (occurring in approximately 60% of patients with metastatic disease).[5] Other tumors that commonly spread to the bones include non-small cell lung cancer, hepatocellular carcinoma, renal cell carcinoma, thyroid cancer, and prostate cancer.[30] Discovery of osseous metastases on MRI immediately upstages a patient and usually alters the goal of therapy from cure to long-term remission. However, curative treatment may still be pursued if only a few metastases (oligometastases) are present.[31]

On MRI, metastatic lesions are typically T1 hypointense, owing to the replacement of normal fatty marrow by tumor cells, with associated T2 hyperintense marrow edema and avid contrast enhancement. While early osseous metastases are typically confined to bone, over time they may grow and invade through the cortex into adjacent soft tissues, increasing the risk for pathologic fracture. Metastases may become sclerotic following treatment, subjectively signifying interval healing. These changes, which are more apparent on CT, may be difficult to appreciate on MRI alone.

Multiple Myeloma

Multiple myeloma is the second-most common malignancy involving the skeleton (after metastatic disease) and is also the second-most common hematological malignancy (after non-Hodgkin lymphoma),[32] typically occurring in patients older than 50. Imaging features overlap with metastatic disease: T1 hypointense masses with intermediate or high T2 signal with avid enhancement (Figure 10). Computed tomography and radiography will demonstrate the classic "punched-out" appearance of numerous lytic lesions throughout the bones.

Multiple myeloma may also present extraskeletally as an extramedullary plasmacytoma. This lesion appears as a homogeneously enhancing mass, with variable and nonspecific T1 and T2 signal characteristics. The presence of myeloma elsewhere in the body may suggest a diagnosis of extramedullary plasmacytoma. The skin, muscles, and pleura are the most common sites of involvement.[33]

Primary Malignant Chest Wall Tumors

Multiple types of primary bone and soft-tissue tumors can occur in the chest wall, many of which share imaging features. However, some imaging features can suggest a diagnosis based on their location and appearance, with tissue sampling generally required for definitive diagnosis. Chondrosarcoma, osteosarcoma, and the Ewing sarcoma family of tumors often arise from the ribs and sternum. Soft-tissue tumors of the chest wall include angiosarcoma, liposarcoma, rhabdomyosarcoma, and lymphoma.

Malignant Tumors Arising from Ribs and Sternum

Chondrosarcoma (Figure 12) is the most common primary chest wall tumor in adults. It typically arises from the costal cartilage or the costochondral junction but may also result from malignant degeneration of an osteochondroma or enchondroma, especially in patients who have received chest wall radiation.[34] On MRI chondrosarcoma has low or intermediate T1 signal, high T2 signal, and avid enhancement. Areas of low T1 and T2 signal correspond with mineralization in the tumor, which on CT or radiographs corresponds to the typical "ring and arc" appearence of these tumors.

Osteosarcoma (Figure 12) is the most common primary bone tumor in adults. It commonly involves the long bones, but involvement of the ribs and sternum is also possible.[35] It typically arises within the marrow space of the bones, but certain subtypes can arise from the cortex (parosteal and periosteal subtypes) and soft tissues (extraskeletal osteosarcoma). While most osteosarcomas arise de novo, secondary subtypes can result from malignant degeneration of lesions such as fibrous dysplasia or Paget's disease, or radiation exposure.[35] MRI features include intermediate T1 signal, moderate-to-high T2 signal, heterogeneous enhancement, and areas of hemorrhage in the tumor. Typically, there is a high degree of mineralization within the tumor which will be T1 and T2 hypointense and be better visualized by CT or radiography.

The Ewing sarcoma family of tumors usually occurs in children and young adults and often presents as a painful, palpable, rapidly growing mass. In the chest, the ribs and scapulae are commonly involved sites.[36] On MRI, Ewing sarcoma typically has intermediate T1 signal, low or intermediate T2 signal, heterogeneous enhancement, and no internal mineralization. Rarely, the Ewing sarcoma family of tumors can arise directly from the soft tissues.[36]

Malignant Tumors Arising from Soft Tissues

The differential diagnosis of primary soft-tissue chest wall tumors is broad, with overlapping imaging features among many. A few do have a characteristic appearance on MRI. Liposarcomas are fat-containing masses with areas of enhancement or soft-tissue nodularity. Angiosarcomas demonstrate T1 intermediate signal, T2 hyperintensity, diffuse enhancement, and skin involvement.[37] Secondary angiosarcomas commonly occur following breast conservation surgery. The most common risk factors for these are prior radiation therapy and chronic lymphedema.[37] They may occur inside the breast or elsewhere in the chest wall. Angiosarcomas can be associated with a wide array of genetic syndromes, including type-1 neurofibromatosis, Maffucci syndrome, *BRCA 1* and *BRCA* 2, and others.

Lymphoma of the chest wall demonstrates greater signal homogeneity and enhancement compared to other chest wall tumors.[38] Rhabdomyosarcomas occur primarily in children, rarely in young adults. They demonstrate nonspecific imaging features and are not commonly seen on breast MRI.

Conclusion

Incidental musculoskeletal findings are common on breast MRI; it is important for radiologists to be able to identify these lesions, suggest a differential diagnosis, and guide management. While benign lesions often present with classic imaging features, many malignant lesions involving the chest share overlapping imaging features and may require correlation with CT or radiography to assess mineralization, as well as biopsy for definitive diagnosis. Recognizing these extramammary musculoskeletal findings is important, especially in patients with breast cancer, as they can impact staging, treatment, and therapeutic goals.

By reviewing the demographics and imaging features of benign and malignant chest wall lesions, radiologists can produce more specific reports, accelerate treatment planning, and help alleviate patient uncertainty and anxiety.

For further reading, we recommend the Society of Skeletal Radiology's white paper, *Guidelines for the Diagnostic Management of Incidental Solitary Bone Lesions on CT and MRI in Adults: Bone Reporting and Data System (Bone-RADS).* This document offers a step-by-step flowchart based on their signal characteristics and other features.[39]

References

1) Iodice D, Di Donato O, Liccardo I, et al. Prevalence of extramammary findings on breast MRI: a large retrospective single-centre study. *Radiol Med*. 2013;118(7):1109-1118. doi:10.1007/s11547-013-0937-8

2) Moschetta M, Telegrafo M, Rella L, Stabile Ianora AA, Angelelli G. Let's go out of the breast: prevalence of extra-mammary findings and their characterization on breast MRI. *Eur J Radiol*. 2014;83(6):930-934. doi:10.1016/j.ejrad.2014.02.022

3) Rinaldi P, Costantini M, Belli P, et al. Extra-mammary findings in breast MRI. *Eur Radiol*. 2011;21(11):2268-2276. doi:10.1007/s00330-011-2183-6

4) Padia SA, Freyvogel M, Dietz J, Valente S, O'Rourke C, Grobmyer SR. False-positive extra-mammary findings in breast MRI: Another cause for concern. *Breast J*. 2016;22(1):90-95. doi:10.1111/tbj.12524

5) Gao Y, Ibidapo O, Toth HK, Moy L. Delineating extramammary findings at breast MR imaging. *Radiographics*. 2017;37(1):10-31. doi:10.1148/rg.2017160051

6) Ulano A, Bredella MA, Burke P, et al. Distinguishing untreated osteoblastic metastases from enostoses using CT attenuation measurements. *AJR Am J Roentgenol*. 2016;207(2):362-368. doi:10.2214/AJR.15.15559

7) Bedard T, Mohammed M, Serinelli S, Damron TA. Atypical enostoses-Series of ten cases and literature review. *Medicina (Kaunas)*. 2020;56(10):534. Published 2020 Oct 13. doi:10.3390/medicina56100534

8) Nielsen G, Baumhoer D, Bredella M, Sumathi V. *WHO classification of tumours: Soft tissue and bone tumours*. 5th ed, vol. 3. Lyon, France. International Agency for Research on Cancer; 2020.

9) Murphey MD, Fairbairn KJ, Parman LM, Baxter KG, Parsa MB, Smith WS. From the archives of the AFIP. Musculoskeletal angiomatous lesions: radiologic-pathologic correlation. *Radiographics*. 1995;15(4):893-917. doi:10.1148/radiographics.15.4.7569134

10) Kadu VV, Saindane KA, Goghate N, Goghate N. Osteochondroma of the rib: a rare radiological appearance. *J Orthop Case Rep*. 2015;5(1):62-64. doi:10.13107/jocr.2250-0685.258

11) Murphey MD, Choi JJ, Kransdorf MJ, Flemming DJ, Gannon FH. Imaging of osteochondroma: variants and complications with radiologic-pathologic correlation. *Radiographics*. 2000;20(5):1407-1434. doi:10.1148/radiographics.20.5.g00se171407

12) Fitzpatrick KA, Taljanovic MS, Speer DP, et al. Imaging findings of fibrous dysplasia with histopathologic and intraoperative correlation. *AJR Am J Roentgenol*. 2004;182(6):1389-1398. doi:10.2214/ajr.182.6.1821389

13) Traibi A, El Oueriachi F, El Hammoumi M, Al Bouzidi A, Kabiri el H. Monostotic fibrous dysplasia of the ribs. *Interact Cardiovasc Thorac Surg*. 2012;14(1):41-43. doi:10.1093/icvts/ivr048

14) Gaskin CM, Helms CA. Lipomas, lipoma variants, and well-differentiated liposarcomas (atypical lipomas): results of MRI evaluations of 126 consecutive fatty masses. *AJR Am J Roentgenol*. 2004;182(3):733-739. doi:10.2214/ajr.182.3.1820733

15) Tateishi U, Gladish GW, Kusumoto M, et al. Chest wall tumors: radiologic findings and pathologic correlation: Part 1. Benign tumors. *Radiographics*. 2003;23(6):1477-1490. doi:10.1148/rg.236015526

16) Suh JS, Abenoza P, Galloway HR, Everson LI, Griffiths HJ. Peripheral (extracranial) nerve tumors: correlation of MR imaging and histologic findings. *Radiology*. 1992;183(2):341-346. doi:10.1148/radiology.183.2.1561333

17) Burk DL Jr, Brunberg JA, Kanal E, Latchaw RE, Wolf GL. Spinal and paraspinal neurofibromatosis: surface coil MR imaging at 1.5 T1. *Radiology*. 1987;162(3):797-801. doi:10.1148/radiology.162.3.3101136

18) Raikos A, Paraskevas GK, Tzika M, et al. Sternalis muscle: an underestimated anterior chest wall anatomical variant. *J Cardiothorac Surg*. 2011;6:73. doi:10.1186/1749-8090-6-73

19) Georgiev GP, Jelev L, Ovtscharoff VA. On the clinical significance of the sternalis muscle. *Folia Med (Plovdiv)*. 2009;51(3):53-56.

20) Sebes JI, Salazar JE. The manubriosternal joint in rheumatoid disease. *AJR Am J Roentgenol*. 1983;140(1):117-121. doi:10.2214/ajr.140.1.117

21) Becker NJ, de Smet AA, Cathcart-Rake W, Stechschulte DJ. Psoriatic arthritis affecting the manubriosternal joint. *Arthritis Rheum*. 1986;29(8):1029-1031. doi:10.1002/art.1780290814

22) Sugimoto H, Tamura K, Fujii T. The SAPHO syndrome: defining the radiologic spectrum of diseases comprising the syndrome. *Eur Radiol*. 1998;8(5):800-806. doi:10.1007/s003300050475

23) Ehara S. Manubriosternal joint: imaging features of normal anatomy and arthritis. *Jpn J Radiol*. 2010;28(5):329-334. doi:10.1007/s11604-010-0438-9

24) Zhang T, Wu J, Chen YC, Wu X, Lu L, Mao C. Magnetic resonance imaging has better accuracy in detecting new-onset rib fractures as compared to computed tomography. *Med Sci Monit*. 2021;27:e928463. Published 2021 Jan 11. doi:10.12659/MSM.928463

25) Prins JTH, Van Lieshout EMM, Reijnders MRL, Verhofstad MHJ, Wijffels MME. Rib fractures after blunt thoracic trauma in patients with normal versus diminished bone mineral density: a retrospective cohort study. *Osteoporos Int*. 2020;31(2):225-231. doi:10.1007/s00198-019-05219-9

26) Way AR, Wasserman PL, Mailhot R, Letter H. Radiation-Induced Rib Fractures on Magnetic Resonance Imaging Following Proton Therapy for Breast Cancer With Pencil Beam Scanning. *Cureus*. 2020;12(10):e11120. doi:10.7759/cureus.11120

27) Bazzocchi A, Spinnato P, Garzillo G, et al. Detection of incidental vertebral fractures in breast imaging: the potential role of MR localisers. *Eur Radiol*. 2012;22(12):2617-2623. doi:10.1007/s00330-012-2521-3

28) Subhas N, Kline MJ, Moskal MJ, White LM, Recht MP. MRI evaluation of costal cartilage injuries. *AJR Am J Roentgenol*. 2008;191(1):129-132. doi:10.2214/AJR.07.3396

29) Marshall RA, Mandell JC, Weaver MJ, Ferrone M, Sodickson A, Khurana B. Imaging features and management of stress, atypical, and pathologic fractures. *Radiographics*. 2018;38(7):2173-2192. doi:10.1148/rg.2018180073

30) Shupp AB, Kolb AD, Mukhopadhyay D, Bussard KM. Cancer metastases to bone: Concepts, mechanisms, and interactions with bone osteoblasts. *Cancers (Basel)*. 2018;10(6):182. Published 2018 Jun 4. doi:10.3390/cancers10060182

31) Terao M, Niikura N. Diagnosis of oligometastasis. *Transl Cancer Res*. 2020;9(8):5032-5037. doi:10.21037/tcr.2020.01.04

32) Ormond Filho AG, Carneiro BC, Pastore D, et al. Whole-body imaging of multiple myeloma: Diagnostic criteria. *Radiographics*. 2019;39(4):1077-1097. doi:10.1148/rg.2019180096

33) Bladé J, Beksac M, Caers J, et al. Extramedullary disease in multiple myeloma: a systematic literature review. *Blood Cancer J*. 2022;12(3):45. doi:10.1038/s41408-022-00643-3

34) Singh A, Chandrashekhara SH, Triveni GS, Kumar P. Imaging in sternal tumours: A pictorial review. *Pol J Radiol*. 2017;82:448-456. doi:10.12659/PJR.901226

35) Murphey MD, Robbin MR, McRae GA, Flemming DJ, Temple HT, Kransdorf MJ. The many faces of osteosarcoma. *Radiographics*. 1997;17(5):1205-1231. doi:10.1148/radiographics.17.5.9308111

36) Murphey MD, Senchak LT, Mambalam PK, Logie CI, Klassen-Fischer MK, Kransdorf MJ. From the radiologic pathology archives: Ewing sarcoma family of tumors: radiologic-pathologic correlation. *Radiographics*. 2013;33(3):803-831. doi:10.1148/rg.333135005

37) Gaballah AH, Jensen CT, Palmquist S, et al. Angiosarcoma: clinical and imaging features from head to toe. *Br J Radiol*. 2017;90(1075):20170039. doi:10.1259/bjr.20170039

38) Witte B, Hürtgen M. Lymphomas presenting as chest wall tumors. *Thorac Surg Sci*. 2006;3:Doc01.

39) Chang CY, Garner HW, Ahlawat S, et al. Society of Skeletal Radiology- white paper. Guidelines for the diagnostic management of incidental solitary bone lesions on CT and MRI in adults: Bone reporting and data system (Bone-RADS). *Skeletal Radiol*. 2022;51(9):1743-1764. doi:10.1007/s00256-022-04022-8

Chemical Exchange Saturation Transfer for Epilepsy Imaging

Joshua D. Brown, MD, PhD; Hahnsung Kim, PhD; Philip Zhe Sun, PhD; Ranliang Hu, MD

Multimodal imaging plays an important role in epilepsy evaluation to localize the source of seizures and is crucial for successful surgical intervention in drug-resistant cases. Up to one-third of epilepsy patients have nonlesional brain MRIs. Glutamate levels in the brain are known to be increased in epileptogenic foci. Magnetic resonance spectroscopy (MRS) has been used to detect brain glutamate levels, but chemical exchange saturation transfer (CEST) imaging has demonstrated higher sensitivity and spatial resolution.

Recent data suggest that glutamate CEST is promising to identify the epileptogenic zone(s) in drug-resistant epilepsy patients without identifiable lesions on more conventional imaging and thus improve their prognosis. This article serves as an introduction to CEST for radiologists in the context of epilepsy imaging applications and their accompanying challenges.

Epilepsy Facts

Epilepsy is a central nervous system disorder characterized by disruptive electrical neuronal activity that results in recurrent seizures. It is a devastating disease that affects more than 46 million people worldwide.[1] Uncontrolled seizures may prevent activities such as driving and employment, leading to stigmatization, social isolation, and psychological harm.[2] Epilepsy is associated with 11 times the odds of premature mortality compared to the general population.[3] The condition also inflicts a burden on society, costing an estimated $10-12 billion in medical expenditures and indirect costs annually in the United States.[4,5] The primary treatment for epilepsy is antiepileptogenic medication. However, approximately one-third of patients are drug-resistant and may benefit from surgical intervention,[6-8] including ablation and minimally invasive surgery.[9,10] Localization-related epilepsy (LRE) is the most common type, accounting for 80% of drug-resistant patients.[9] Localizing the epileptogenic source increases the chance of successful postsurgical outcomes by up to three times.[11,12]

Current Epilepsy Imaging

High-resolution images of brain structure and pathology can be obtained by MRI using tissue properties of T1 and T2 relaxation. Current diagnostic techniques have found 65% of LRE cases to be temporal lobe epilepsy (TLE),[13,14] resulting in favorable surgical outcomes, with 70-80% of patients seizure-free post-treatment.[15-19] Conventional MRI has found that two-thirds of TLE patients demonstrate mesial temporal sclerosis (MTS), including the hippocampus, amygdala, and parahippocampal gyrus.[15] However, subtle or early-stage epileptogenic lesions may not alter brain physiology and morphology enough to exhibit detection by conventional MRI. In addition, one-third of drug-refractory TLE patients have no detectable lesions on conventional MRI,[6,12-15,19,20] and are up to three times more likely to have worse surgical outcomes than patients with lesional MRIs.[11,21] Despite this, histopathology is abnormal in approximately 87% of nonlesional MRI epilepsy patients, suggesting current imaging technology is unable to detect the existing pathology.[22]

Positron emission tomography (PET) with fluorodeoxyglucose (FDG) measures glucose metabolism, which is tightly connected with neuronal activity. The most common PET tracer in epilepsy localization for clinical practice, FDG is transported into the blood cells and phosphorylated by hexokinase to form FDG-6-phosphate. This step essentially traps it in the cell, and the positron radiation produced is subsequently measured.

Affiliations: Department of Radiology and Imaging Sciences, Emory University, Atlanta, Georgia (Drs Brown, Zhe Sun, Hu); Emory National Primate Research Center, Atlanta, Georgia (Drs Kim, Zhe Sun).
Disclosures: This project was supported by the RSNA Research & Education Foundation through grant number RR2234. The authors are solely responsible for the content, which does not necessarily represent the official views of the RSNA R&E Foundation. The authors report no conflicts of interest.
Keywords: Epilepsy, Chemical Exchange Saturation Transfer, MRI, Nonlesional, Glutamate

Figure 1. Overview of CEST. (A) A small concentration of solute exists within the tissue. (B) The solute of choice is selectively saturated with a radiofrequency pulse that reduces the signal of the solute (white H). (C) The saturated solute hydrogen (white H) is then exchanged with an unsaturated hydrogen from water (yellow H), reducing the overall signal of water. (D) The process is repeated until a measurable water signal reduction is reached, indirectly detecting the solute concentration.[9]

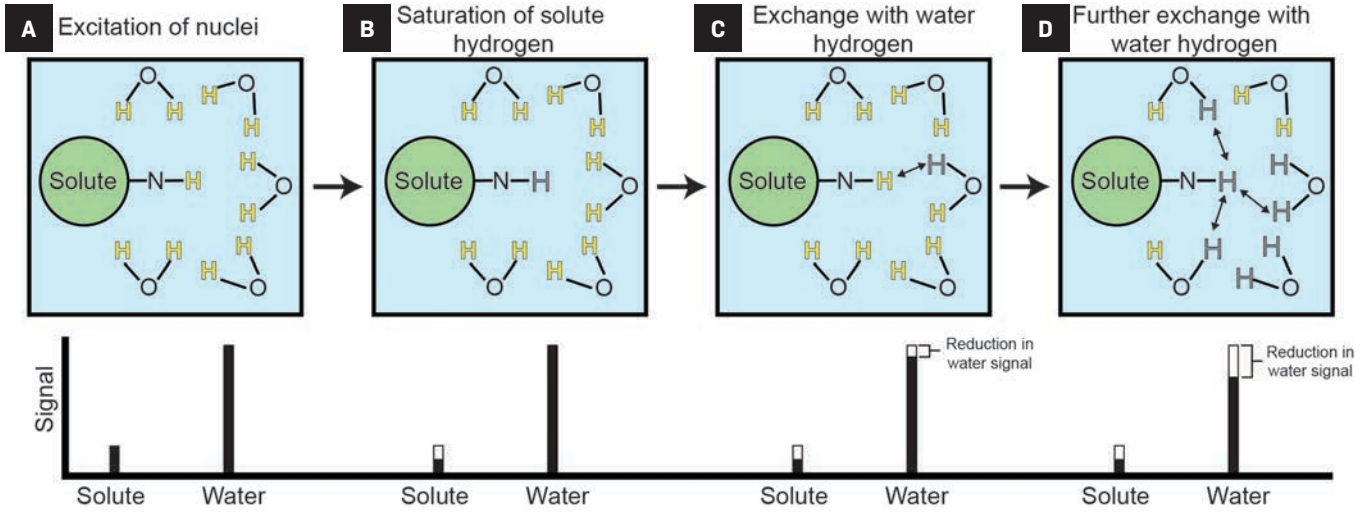

Interictal FDG-PET imaging reveals decreased uptake, reflecting hypometabolism, at epileptogenic foci; resection of these correlates with positive surgical outcomes.[23-25]

In pediatric patients, PET has been found to be more effective than conventional MRI in detecting subtle lesions; a recent study found that lesions were missed by MRI in up to 66% of patients but detected by PET in 77% of patients.[26] FDG-PET imaging is usually combined with another modality, such as computed tomography (PET/CT). However, combining with MRI (PET/MR) results in equivalent sensitivity to PET/CT while providing the advantages of lower radiation exposure and lower dose to the brain and eyes owing to the acquisition of images in a single session.[27] Overall, hybrid PET/MR imaging, compared to MRI alone, increases sensitivity and epileptogenic abnormality identification, resulting in improved seizure-free outcomes.[28,29]

Nevertheless, there are several limitations to PET utilization, including availability, radiation exposure, high cost, relatively long scan times, and preprocedural requirements such as fasting, tight blood glucose control, and avoidance of caffeine, alcohol, or drugs that may affect cerebral glucose metabolism.[30] Studies are optimally performed during the interictal period, requiring the patient to be seizure free for at least 24 hours.[31] PET's ability to precisely define the surgical margin is also limited, as areas of hypometabolism may extend beyond the anatomical epileptogenic zone.[32] Overall, standard multimodal imaging has been unable to identify a clear cause of seizures for one-third of epilepsy patients, half of whom are drug resistant.[33] Owing to water's abundance in the body, MRI relies heavily on the molecule's protons, which produce contrasts based on relaxation rates of different gross tissue structures.

There is great interest in expanding the use of novel molecules; however, direct detection using a multinuclear imaging system is technically challenging and expensive.[34] Magnetic resonance spectroscopy (MRS) is a technique that allows probing of the metabolic environment. Nevertheless, the current clinically available MRS sequences are limited by long acquisition times, low sensitivity, poor spectral and spatial resolution, and volume voxel overlapping with non-targeted tissue.[35]

Chemical Exchange Saturation Transfer Imaging

Chemical exchange saturation transfer (CEST) is an advanced MR imaging technique that addresses many limitations of current techniques. CEST takes advantage of proton exchange between solutes and water, providing an amplification strategy to detect metabolites and proteins with labile groups by using a frequency-selective radiofrequency saturation pulse (Figure 1). Saturation is a magnetic resonance state in which the selected tissue or, in this case, solute produces zero net magnetization or signal.

During radiofrequency saturation, low-concentration solutes with exchangeable protons can be selectively saturated. Owing to proton exchange, this saturation is continuously transferred to the much more abundant water molecules, leading to a proportional signal reduction for water.[34,36] The difference in the water signal obtained with and without saturation essentially allows indirect detection of low-concentration solutes.

Glutamate is a key excitatory transmitter in the brain; however, an imbalance can result in seizure activity.[39] Dysfunctional glutamate

Figure 2. Axial sections from four patients with drug-resistant temporal lobe epilepsy (TLE) showing the increased GluCEST signal in the nonlesional epileptogenic hippocampus. (A, B) Right TLE; (C, D) Left TLE. Images courtesy of Davis et al. Reprinted with permission of AAAS.[56]

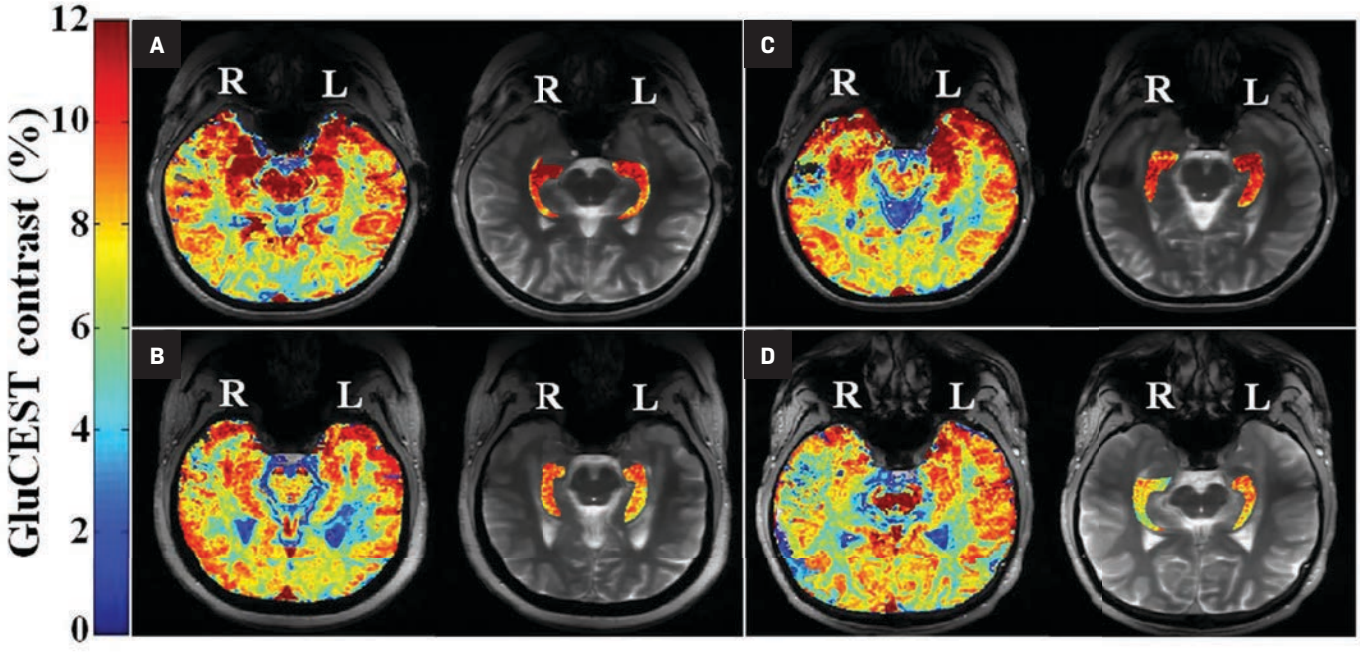

cycling by glutamine synthetase in astrocytes slows glutamate clearance and subsequently elevated levels of glutamate in the epileptogenic hippocampus.[40-43] Studies in animals and humans demonstrate glutamate's potential to serve as a marker for localizing epileptogenic foci. Microdialysis studies in human subjects have shown increased glutamate concentrations at the epileptogenic focus ictally, interictally, and postmortem.[41,42,44-47]

Increased glutamate concentration has also correlated with decreased hippocampal volume on MRI.[47] Using MRS, Pfund et al found the combined glutamate and glutamine signal to be increased in the epileptogenic hippocampus of patients with morphologically nonlesional epilepsy.[48] Decreased levels in sclerotic hippocampi were also noted; however, their observation could have been limited by the hippocampal volume loss and relatively large voxel size.[48]

This result has led to the investigation of glutamate as a metabolic agent for noninvasive imaging to correlate and potentially map epileptogenic networks using CEST (GluCEST).

GluCEST has been found to have higher spatial resolution and twice the sensitivity for glutamate compared with traditional MRS methods.[38]

GluCEST has already been demonstrated in healthy subjects and Alzheimer disease mouse models.[49-52] Davis et al have utilized GluCEST for epileptogenic source lateralization in four nonlesional, drug-resistant, epilepsy patients and 11 healthy controls.[53] Using a two-dimensional single-slice GluCEST sequence on a 7 Tesla (T) MRI, the epileptogenic hippocampus was lateralized in all of the epilepsy patients, including two right-sided and two left-sided temporal epilepsy patients (Figure 2).[53-55] GluCEST findings matched EEG and subsequent histopathology results.[53] In addition, no significant difference in hippocampal volume was found between the epileptogenic and the contralateral sides.

Subsequently, Hadar et al applied GluCEST to three-dimensional imaging and found similar results with increased GluCEST signal in the epileptogenic hippocampus,[55] and Lucas et al found a GluCEST correlation with lesional and nonlesional hippocampi.[54]

CEST has also been used to distinguish the physical signs of tuberous sclerosis complex (TSC), a disease that affects more than 1 million people and is caused by mutations in the *TSC1* or *TSC2* genes.[56,57] Neurological manifestations of TSC include seizures, intellectual disability, and behavioral problems.[56,57] Hamartomas in the brain or tubers, major hallmarks of TSC, have been shown to correlate with seizure burden.[58] Wen et al were able to utilize CEST imaging to differentiate tubers from normal brain tissue, with a probable major metabolic contributor being glutamate levels.[59] In addition, CEST showed the potential to reveal tubers undetected by conventional T2 sequences.[59]

Challenges and Future Directions

Chemical exchange saturation transfer imaging provides a more sensitive and robust method to detect and measure biological metabolites. However, specific resonance of the biological metabolites can

overlap and the CEST signal of two biological metabolites may contribute to each other. This includes a small contribution of the neurotransmitter gamma-aminobutyric acid and creatinine to GluCEST and glucose, contributing to glycogen detection.[38,60] Users must be precise and mindful when selecting the proper offset. Also, there could be concomitant changes not only in glutamate concentration but also mild pH change.[61]

Third, CEST signal magnitude and spectral separation are enhanced at higher magnetic field strengths, requiring many of these studies to be performed on 7T scanners.[53-55,60] The need for high field strengths has thus far limited the broader research and clinical implementation of CEST MRI; more research is needed to assess the potential of CEST to be utilized at lower and more widely available magnetic field strengths. Standardization and quantification across scanners also must be improved to allow reliable CEST imaging interpretation.[62] Methods to address this issue are currently being explored.[63,64]

Conclusion

There are multiple diagnostic imaging approaches to epilepsy imaging, but there is still a subpopulation of treatment-refractory epilepsy patients whose lesions cannot be detected with conventional imaging. CEST provides direct interrogation of the metabolic composition of biological tissue and has been demonstrated to reveal epileptogenic foci not detectable with conventional MRI, including those in temporal lobe epilepsy and TSC patients. Additional work is needed to translate this capability to more widely available 3T MRI scanners and to standardize CEST acquisition and postprocessing.

Lastly, increased awareness of the CEST technique and its potential clinical use in epilepsy imaging is important as the field increasingly incorporates metabolic and precision imaging into clinical practice.

References

1) Collaborators GE. Global, regional, and national burden of epilepsy, 1990-2016: a systematic analysis for the Global Burden of Disease Study 2016. *Lancet Neurol.* 2019;18(4):357-375.

2) Baker GA, Jacoby A, Buck D, Stalgis C, Monnet D. Quality of life of people with epilepsy: a European study. *Epilepsia.* 1997;38(3):353-362.

3) Fazel S, Wolf A, Langstrom N, Newton CR, Lichtenstein P. Premature mortality in epilepsy and the role of psychiatric comorbidity: a total population study. *Lancet.* 2013;382(9905):1646-1654.

4) Yoon D, Frick KD, Carr DA, Austin JK. Economic impact of epilepsy in the United States. *Epilepsia.* 2009;50(10):2186-2191.

5) Begley CE, Famulari M, Annegers JF, et al. The cost of epilepsy in the United States: an estimate from population-based clinical and survey data. *Epilepsia.* 2000;41(3):342-351.

6) Kwan P, Brodie MJ. Early identification of refractory epilepsy. *N Engl J Med.* 2000;342(5):314-319.

7) Sultana B, Panzini MA, Veilleux Carpentier A, et al. Incidence and Prevalence of Drug-Resistant Epilepsy: A Systematic Review and Meta-analysis. *Neurology.* 2021;96(17):805-817.

8) Vakharia VN, Duncan JS, Witt JA, Elger CE, Staba R, Engel J, Jr. Getting the best outcomes from epilepsy surgery. *Ann Neurol.* 2018;83(4):676-690.

9) Gross RE, Stern MA, Willie JT, et al. Stereotactic laser amygdalohippocampotomy for mesial temporal lobe epilepsy. *Ann Neurol.* 2018;83(3):575-587.

10) Morrell MJ, Group RNSSiES. Responsive cortical stimulation for the treatment of medically intractable partial epilepsy. *Neurology.* 2011;77(13):1295-1304.

11) Tellez-Zenteno JF, Hernandez Ronquillo L, Moien-Afshari F, Wiebe S. Surgical outcomes in lesional and non-lesional epilepsy: a systematic review and meta-analysis. *Epilepsy Res.* 2010;89(2-3):310-318.

12) Siegel AM, Jobst BC, Thadani VM, et al. Medically intractable, localization-related epilepsy with normal MRI: presurgical evaluation and surgical outcome in 43 patients. *Epilepsia.* 2001;42(7):883-888.

13) Callaghan BC, Anand K, Hesdorffer D, Hauser WA, French JA. Likelihood of seizure remission in an adult population with refractory epilepsy. *Ann Neurol.* 2007;62(4):382-389.

14) Wiebe S, Camfield P, Jette N, Burneo JG. Epidemiology of epilepsy: prevalence, impact, comorbidity and disparities. *Can J Neurol Sci.* 2009;36 Suppl 2:S7-16.

15) Jette N, Wiebe S. Update on the surgical treatment of epilepsy. *Curr Opin Neurol.* 2013;26(2):201-207.

16) Spencer SS, Berg AT, Vickrey BG, et al. Predicting long-term seizure outcome after resective epilepsy surgery: the multicenter study. *Neurology.* 2005;65(6):912-918.

17) Wiebe S. Epilepsy. Outcome patterns in epilepsy surgery--the long-term view. *Nat Rev Neurol.* 2012;8(3):123-124.

18) Mohammed HS, Kaufman CB, Limbrick DD, et al. Impact of epilepsy surgery on seizure control and quality of life: a 26-year follow-up study. *Epilepsia.* 2012;53(4):712-720.

19) de Tisi J, Bell GS, Peacock JL, et al. The long-term outcome of adult epilepsy surgery, patterns of seizure remission, and relapse: a cohort study. *Lancet.* 2011;378(9800):1388-1395.

20) French JA. Refractory epilepsy: clinical overview. *Epilepsia.* 2007;48 Suppl 1:3-7.

21) Carne RP, O'Brien TJ, Kilpatrick CJ, et al. MRI-negative PET-positive temporal lobe epilepsy: a distinct surgically remediable syndrome. *Brain.* 2004;127(Pt 10):2276-2285.

22) Cohen-Gadol AA, Wilhelmi BG, Collignon F, et al. Long-term outcome of epilepsy surgery among 399 patients with nonlesional seizure foci including mesial temporal lobe sclerosis. *J Neurosurg.* 2006;104(4):513-524.

23) Ergun EL, Saygi S, Yalnizoglu D, Oguz KK, Erbas B. SPECT-PET in Epilepsy and Clinical Approach in Evaluation. *Semin Nucl Med.* 2016;46(4):294-307.

24) Elkins KC, Moncayo VM, Kim H, Olson LD. Utility of gray-matter segmentation of ictal-Interictal perfusion SPECT and interictal (18)F-FDG-PET in medically refractory epilepsy. *Epilepsy Res.* 2017;130:93-100.

25) Theodore WH, Sato S, Kufta CV, Gaillard WD, Kelley K. FDG-positron emission tomography and invasive EEG: seizure focus detection and surgical outcome. *Epilepsia.* 1997;38(1):81-86.

26) Kim YH, Kang HC, Kim DS, et al. Neuroimaging in identifying focal cortical dysplasia and prognostic factors in pediatric and adolescent epilepsy surgery. *Epilepsia.* 2011;52(4):722-727.

27) Oldan JD, Shin HW, Khandani AH, Zamora C, Benefield T, Jewells V. Subsequent experience in hybrid PET-MRI for evaluation of refractory focal onset epilepsy. *Seizure.* 2018;61:128-134.

28) Salamon N, Kung J, Shaw SJ, et al. FDG-PET/MRI coregistration improves detection of cortical dysplasia in patients with epilepsy. *Neurology.* 2008;71(20):1594-1601.

29) Lin Y, Fang YD, Wu G, et al. Quantitative positron emission tomography-guided magnetic resonance imaging postprocessing in magnetic resonance imaging-negative epilepsies. *Epilepsia.* 2018;59(8):1583-1594.

30) Juhasz C, John F. Utility of MRI, PET, and ictal SPECT in presurgical evaluation of non-lesional pediatric epilepsy. *Seizure.* 2020;77:15-28.

31) Kuruva M, Moncayo VM, Peterson RB. PET and SPECT Imaging of Epilepsy: Technical Considerations, Pathologies, and Pitfalls. *Semin Ultrasound CT MR.* 2020;41(6):551-561.

32) Sarikaya I. PET studies in epilepsy. *Am J Nucl Med Mol Imaging.* 2015;5(5):416-430.

33) Nguyen DK, Mbacfou MT, Nguyen DB, Lassonde M. Prevalence of nonlesional focal epilepsy in an adult epilepsy clinic. *Can J Neurol Sci.* 2013;40(2):198-202.

34) Wu B, Warnock G, Zaiss M, et al. An overview of CEST MRI for non-MR physicists. *EJNMMI Phys.* 2016;3(1):19.

35) Simister RJ, Woermann FG, McLean MA, Bartlett PA, Barker GJ, Duncan JS. A short-echo-time proton magnetic resonance spectroscopic imaging study of temporal lobe epilepsy. *Epilepsia.* 2002;43(9):1021-1031.

36) Kogan F, Hariharan H, Reddy R. Chemical Exchange Saturation Transfer (CEST) Imaging: Description of Technique and Potential Clinical Applications. *Curr Radiol Rep.* 2013;1(2):102-114.

37) Ward KM, Aletras AH, Balaban RS. A new class of contrast agents for MRI based on proton chemical exchange dependent saturation transfer (CEST). *J Magn Reson.* 2000;143(1):79-87.

38) Cai K, Haris M, Singh A, et al. Magnetic resonance imaging of glutamate. *Nat Med.* 2012;18(2):302-306.

39) Eid T, Tu N, Lee TS, Lai JC. Regulation of astrocyte glutamine synthetase in epilepsy. *Neurochem Int.* 2013;63(7):670-681.

40) Eid T, Thomas MJ, Spencer DD, et al. Loss of glutamine synthetase in the human epileptogenic hippocampus: possible mechanism for raised extracellular glutamate in mesial temporal lobe epilepsy. *Lancet.* 2004;363(9402):28-37.

41) Eid T, Lee TS, Wang Y, et al. Gene expression of glutamate metabolizing enzymes in the hippocampal formation in human temporal lobe epilepsy. *Epilepsia.* 2013;54(2):228-238.

42) Petroff OA, Errante LD, Rothman DL, Kim JH, Spencer DD. Glutamate-glutamine cycling in the epileptic human hippocampus. *Epilepsia.* 2002;43(7):703-710.

43) Eid T, Hammer J, Runden-Pran E, et al. Increased expression of phosphate-activated glutaminase in hippocampal neurons in human mesial temporal lobe epilepsy. *Acta Neuropathol.* 2007;113(2):137-152.

44) Wilson CL, Maidment NT, Shomer MH, et al. Comparison of seizure related amino acid release in human epileptic hippocampus versus a chronic, kainate rat model of hippocampal epilepsy. *Epilepsy Res.* 1996;26(1):245-254.

45) Millan MH, Chapman AG, Meldrum BS. Extracellular amino acid levels in hippocampus during pilocarpine-induced seizures. *Epilepsy Res.* 1993;14(2):139-148.

46) Cavus I, Kasoff WS, Cassaday MP, et al. Extracellular metabolites in the cortex and hippocampus of epileptic patients. *Ann Neurol.* 2005;57(2):226-235.

47) Cavus I, Pan JW, Hetherington HP, et al. Decreased hippocampal volume on MRI is associated with increased extracellular glutamate in epilepsy patients. *Epilepsia.* 2008;49(8):1358-1366.

48) Pfund Z, Chugani DC, Juhasz C, et al. Evidence for coupling between glucose metabolism and glutamate cycling using FDG PET and 1H magnetic resonance spectroscopy in patients with epilepsy. *J Cereb Blood Flow Metab.* 2000;20(5):871-878.

49) Kogan F, Singh A, Debrosse C, et al. Imaging of glutamate in the spinal cord using GluCEST. *Neuroimage.* 2013;77:262-267.

50) Cai K, Singh A, Roalf DR, et al. Mapping glutamate in subcortical brain structures using high-resolution GluCEST MRI. *NMR Biomed.* 2013;26(10):1278-1284.

51) Haris M, Nath K, Cai K, et al. Imaging of glutamate neurotransmitter alterations in Alzheimer's disease. *NMR Biomed.* 2013;26(4):386-391.

52) Crescenzi R, DeBrosse C, Nanga RP, et al. In vivo measurement of glutamate loss is associated with synapse loss in a mouse model of tauopathy. *Neuroimage.* 2014;101:185-192.

53) Davis KA, Nanga RP, Das S, et al. Glutamate imaging (GluCEST) lateralizes epileptic foci in nonlesional temporal lobe epilepsy. *Sci Transl Med.* 2015;7(309):309ra161.

54) Lucas A, Nanga RPR, Hadar P, et al. Mapping hippocampal glutamate in mesial temporal lobe epilepsy with glutamate weighted CEST (GluCEST) imaging. *Hum Brain Mapp.* 2022.

55) Hadar PN, Kini LG, Nanga RPR, et al. Volumetric glutamate imaging (GluCEST) using 7T MRI can lateralize nonlesional temporal lobe epilepsy: A preliminary study. *Brain Behav.* 2021;11(8):e02134.

56) Marcotte L, Crino PB. The neurobiology of the tuberous sclerosis complex. *Neuromolecular Med.* 2006;8(4):531-546.

57) Crino PB, Nathanson KL, Henske EP. The tuberous sclerosis complex. *N Engl J Med.* 2006;355(13):1345-1356.

58) Holmes GL, Stafstrom CE, Tuberous Sclerosis Study G. Tuberous sclerosis complex and epilepsy: recent developments and future challenges. *Epilepsia.* 2007;48(4):617-630.

59) Wen Q, Wang K, Hsu YC, et al. Chemical exchange saturation transfer imaging for epilepsy secondary to tuberous sclerosis complex at 3 T: Optimization and analysis. *NMR Biomed.* 2021;34(9):e4563.

60) van Zijl PC, Jones CK, Ren J, Malloy CR, Sherry AD. MRI detection of glycogen in vivo by using chemical exchange saturation transfer imaging (glycoCEST). *Proc Natl Acad Sci U S A.* 2007;104(11):4359-4364.

61) Lu D, Ji Y, Sundaram P, et al. Alkaline brain pH shift in rodent lithium-pilocarpine model of epilepsy with chronic seizures. *Brain Research.* 2021;1758:147345.

62) Sun PZ. Numerical simulation-based assessment of pH-sensitive chemical exchange saturation transfer MRI quantification accuracy across field strengths. *NMR Biomed.* 2023:e5000.

63) Kim J, Wu Y, Guo Y, Zheng H, Sun PZ. A review of optimization and quantification techniques for chemical exchange saturation transfer MRI toward sensitive in vivo imaging. *Contrast Media Mol Imaging.* 2015;10(3):163-178.

64) Zhou J, Zaiss M, Knutsson L, et al. Review and consensus recommendations on clinical APT-weighted imaging approaches at 3T: Application to brain tumors. *Magn Reson Med.* 2022;88(2):546-574.

Computed Tomography: An Optimal Modality for the Detection of Nontraumatic Intraperitoneal and Retroperitoneal Hemorrhage

Robin Okpara, BS; Kaustubh G. Shiralkar, MD; Eduardo J. Matta, MD; Steven S. Chua, MD, PhD

Acute nontraumatic abdominopelvic hemorrhage is a medical emergency that requires prompt diagnosis; imaging is often crucial to localize the source and extent of bleeding. Ultrasound may be useful as an initial screening tool but is not sensitive enough to detect subtle injuries or small bleeds.[1] Computed tomography (CT) is most commonly used and typically the best option in emergency settings, owing to its reliability, speed, and typical proximity to the emergency department.[2] Indeed, the modality has been shown to be superior to other imaging modalities in detecting intra-abdominal bleeding, particularly when the bleeding rate is low.[1]

Signs of acute hemorrhage on CT scans include the triangle sign of mesenteric bleeding, sentinel clot, mesenteric/hyperdense fluid, and active arterial extravasation. These findings may allow radiologists to localize the source and site of intraperitoneal hemorrhage, which can aid management.[1,2] This review article focuses on common sources of nontraumatic hemoperitoneum while highlighting salient CT findings.

Figure 1. Coronal CT reformation showing expansile and necrotic right renal cell carcinoma (##) with perinephric (**) and intralesional hematoma, as well as expansile tumor thrombus extending from the right renal vein (RRV) into the IVC (white arrows).

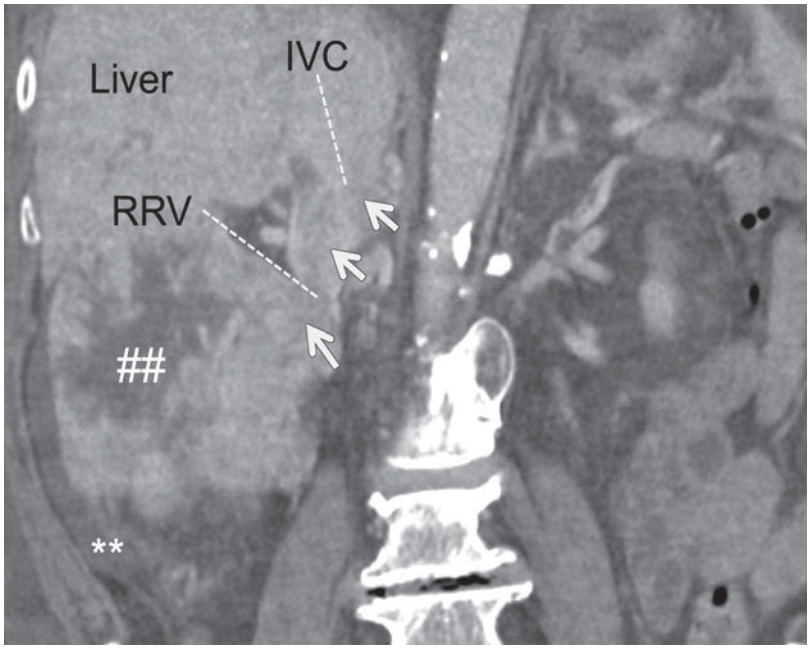

Appearance of Hemorrhage

The CT appearance of hemorrhage depends on the location, age, and extent of the bleeding. On unenhanced images, bleeding attenuates at 35-45 Hounsfield units (HU) in the hyperacute stage due to high protein concentration.[3] In the next few hours, the attenuation will increase to over 60 HU as hemoglobin concentration increases in the

Affiliations: Texas Tech University Health Sciences School of Medicine, Lubbock, Texas (Ms Okpara); Department of Diagnostic and Interventional Imaging, McGovern Medical School at UTHealth, Houston, Texas (Drs Shiralkar, Matta, Chua).
Disclosures: None.
Prior publication/presentation: Portions of this article were presented as an exhibit at RSNA 2020, Chicago, Illinois: Chua SS, Chaudhary L, Shiralkar KG, Ocazionez D, Matta E. Don't bleed to know the bleeds: Systematic cased-based approach for correct localization of bleeds/hemorrhages.
Keywords: Hemorrhage, computer tomography, nontraumatic hemoperitoneum, rupture, coagulopathy.

Figure 2. (A) Left-sided coronal CT reformation showing interpolar renal angiomyolipoma. (white arrow) with foci of macroscopic fat and extensive perinephric hemorrhage (***). (B) Catheter angiogram indicates pseudoaneurysms (white arrows), which were subsequently embolized (C). Typically, AMLs undergo prophylactic embolization if > 4 cm and if pseudoaneurysms are > 0.5 cm.

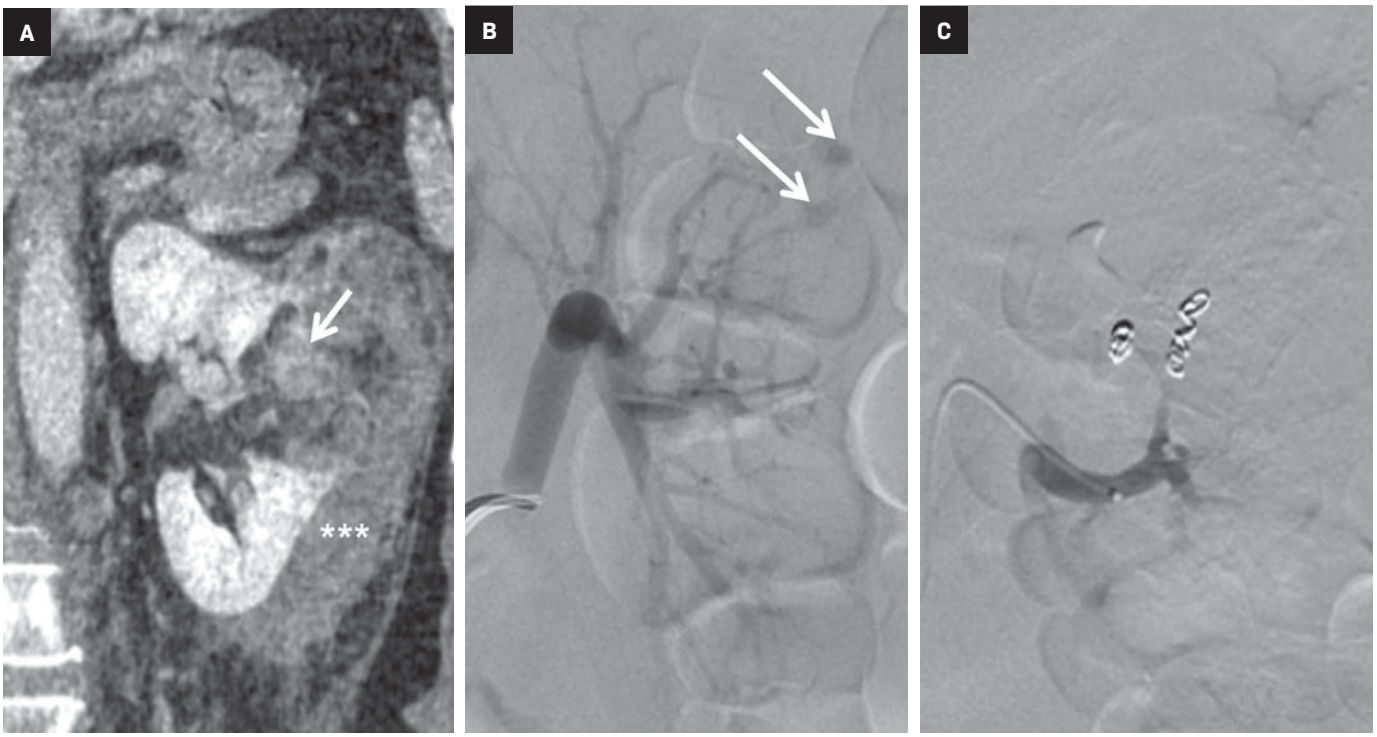

acute stage. This will subsequently decrease over time. Typically, blood will tend to clot near the bleeding site (the "sentinel clot sign") further pinpointing the hemorrhage location.[2] Over time, the clot will shrink with progressive lysis of hemoglobin and liquefaction. On contrast-enhanced CT, a site of active bleeding may demonstrate higher attenuation ranging from 85 to 300 HU.[2] Such high attenuation suggests contrast extravasation and may indicate the need for emergency embolization or surgery.

Tumor-related Causes of Hemorrhage

Absent a history of anticoagulant use or trauma, spontaneous hemoperitoneum is rare. In these cases, excluding rupture by neoplasm or vasculopathy is essential.[4] While uncommon, a primary or metastatic tumor can rupture and bleed into the peritoneal or retroperitoneal cavity with devastating effects.

Figure 3. Axial contrast-enhanced CT through the upper abdomen in a patient with metastatic angiosarcoma with hemoperitoneum (**) from rupture of the hepatic and splenic lesions (##). The splenic angiosarcoma contains abnormally dilated, serpentine, and leaky vessels (white arrow).

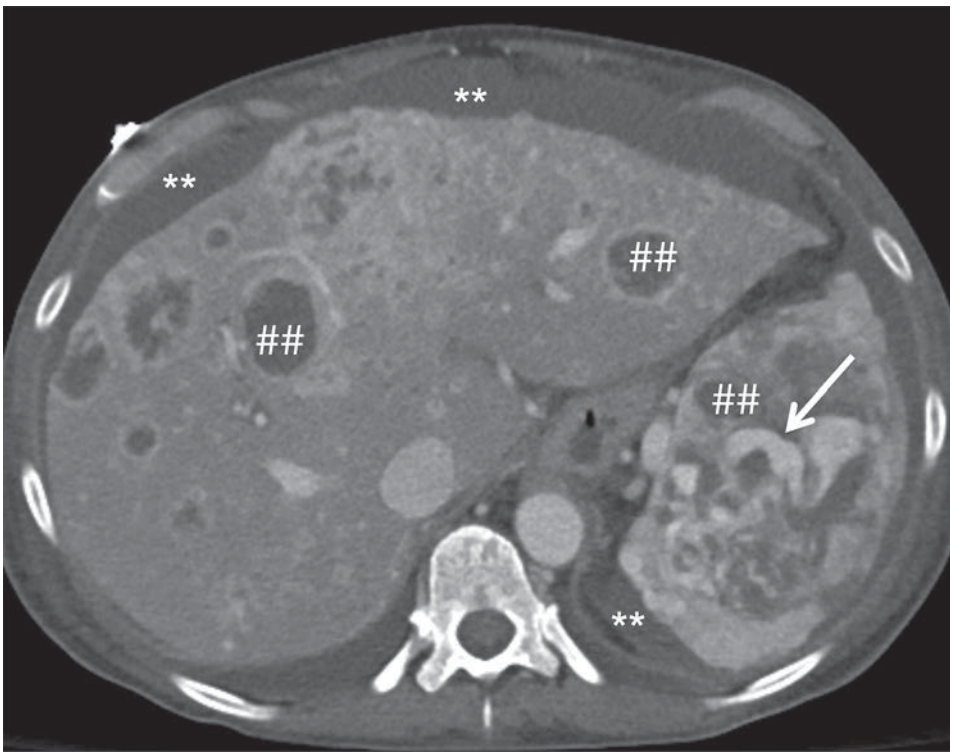

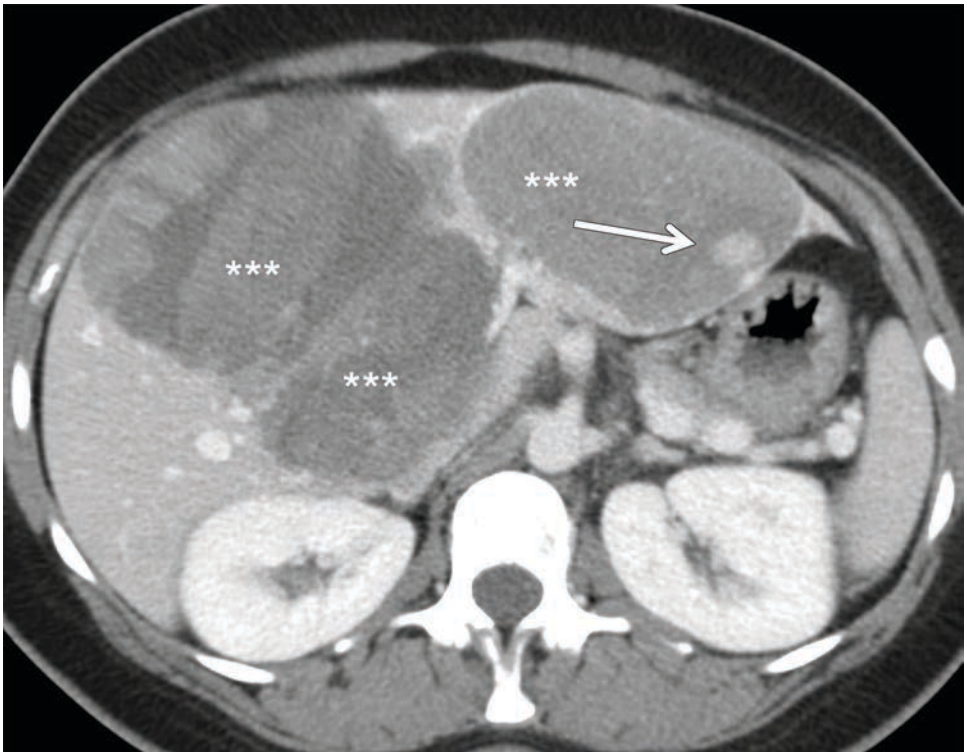

Figure 4. Axial contrast-enhanced CT through the abdomen in a patient with three large hepatocellular adenomas with internal hemorrhage (***) and one with a focus of active bleeding (white arrow).

Figure 5. (A) Axial contrast-enhanced CT through the upper abdomen in a patient with two right hepatic-lobe, arterially enhancing, hepatocellular carcinomas (white arrows) with washout in the (B) portal venous phase (white arrows), tumoral bleeding, and perihepatic hematoma (A, B,***)

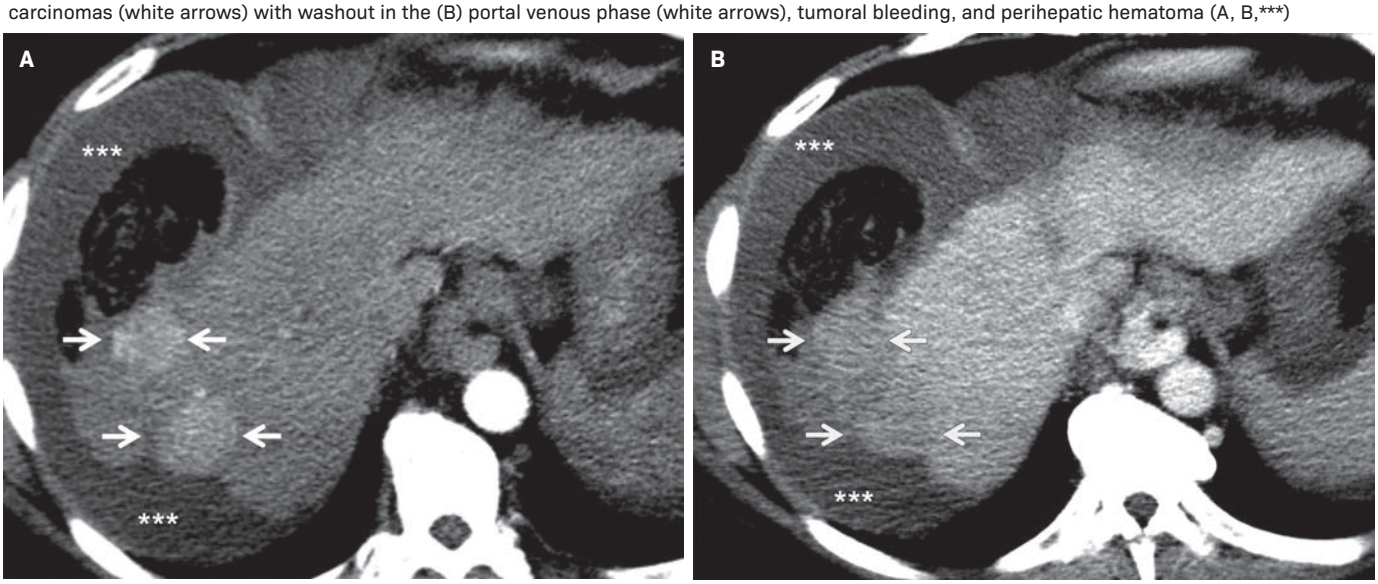

Renal Cell Carcinoma

Accounting for 3% of overall adult malignancies and 90% of neoplasms derived from the kidneys, renal cell carcinoma (RCC) is the most common renal cancer in adults.[5,6] Spontaneous hemorrhaging of these tumors more commonly accompanies the clear cell and collecting duct subtypes and typically presents with hematuria, pain, and a palpable abdominal mass.[7] On contrast-enhanced CT images, RCC is suggested by a solid, enhancing, and often necrotic mass (Figure 1).[3] Spontaneous rupture of RCC is rare; however, the condition is life-threatening and prompt imaging and intervention may be necessary.[8]

Angiomyolipoma

Angiomyolipoma (AML) is the most common benign renal neoplasm. It consists of fat, smooth muscle, and abnormally thick-walled vessels.[9] This entity commonly affects women, usually between the ages of 40 and 70 years,[9] and can present with a wide range of signs and symptoms,

Figure 6. (A-C) A patient with a positive ß-HCG without an intrauterine gestational sac in the endometrium was found on ultrasound and CT to have a left adnexal lesion with tubal ring configuration with peripheral vascularity (#) with accompanying hemorrhage (**), indicative of a ruptured ectopic pregnancy. U = Uterus.

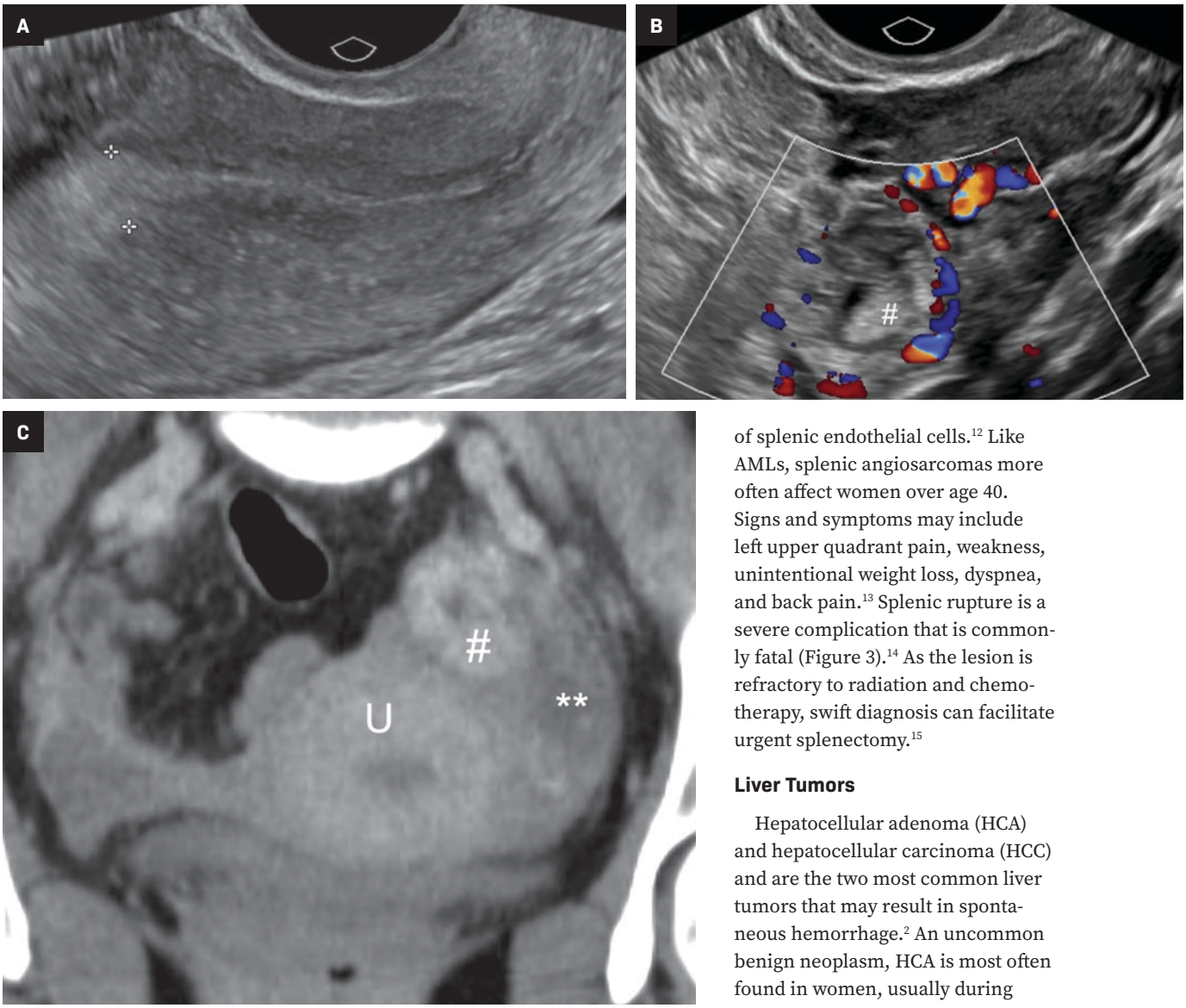

including hematuria, flank mass, hypertension, urinary tract infection, and renal failure in severe cases.[10,11] While the tumor is benign, there is a risk of rupture (Figure 2). This is especially true for tumors larger than 4 cm and for those with pseudoaneurysms greater than 0.5 cm, which frequently call for embolization.[10] A lipid-rich AML will often demonstrate internal enhancement on contrast-enhanced CT with low-attenuation areas of macroscopic fat density.[3] Surveillance may be indicated in certain situations, as the risk of rupture increases with tumor size.[10] There are no established guidelines for AML surveillance; however, the International Tuberous Sclerosis Complex Consensus Conference recommends that abdominal MRI or CT should be performed every 1-3 years to assess AML progression over the life of the patient.[10]

Splenic Angiosarcoma

A rare and aggressive type of hypervascular cancer, splenic angiosarcoma is typically composed of splenic endothelial cells.[12] Like AMLs, splenic angiosarcomas more often affect women over age 40. Signs and symptoms may include left upper quadrant pain, weakness, unintentional weight loss, dyspnea, and back pain.[13] Splenic rupture is a severe complication that is commonly fatal (Figure 3).[14] As the lesion is refractory to radiation and chemotherapy, swift diagnosis can facilitate urgent splenectomy.[15]

Liver Tumors

Hepatocellular adenoma (HCA) and hepatocellular carcinoma (HCC) and are the two most common liver tumors that may result in spontaneous hemorrhage.[2] An uncommon benign neoplasm, HCA is most often found in women, usually during their reproductive years. It may be associated with hyperestrogenic states associated with obesity and the use of estrogen-based oral contraceptives.[16] Accurately diagnosing an HCA as soon as possible is vital,[16] as hemorrhage—often associated with large HCAs (> 5 cm)—can cause right upper quadrant pain and hemodynamic instability (Figure 4),[17] as well as spread into the liver or intraperitoneal cavity, requiring tumor resection.[2] In many cases, rupture can lead to hemorrhagic shock, which requires emergent treatment.

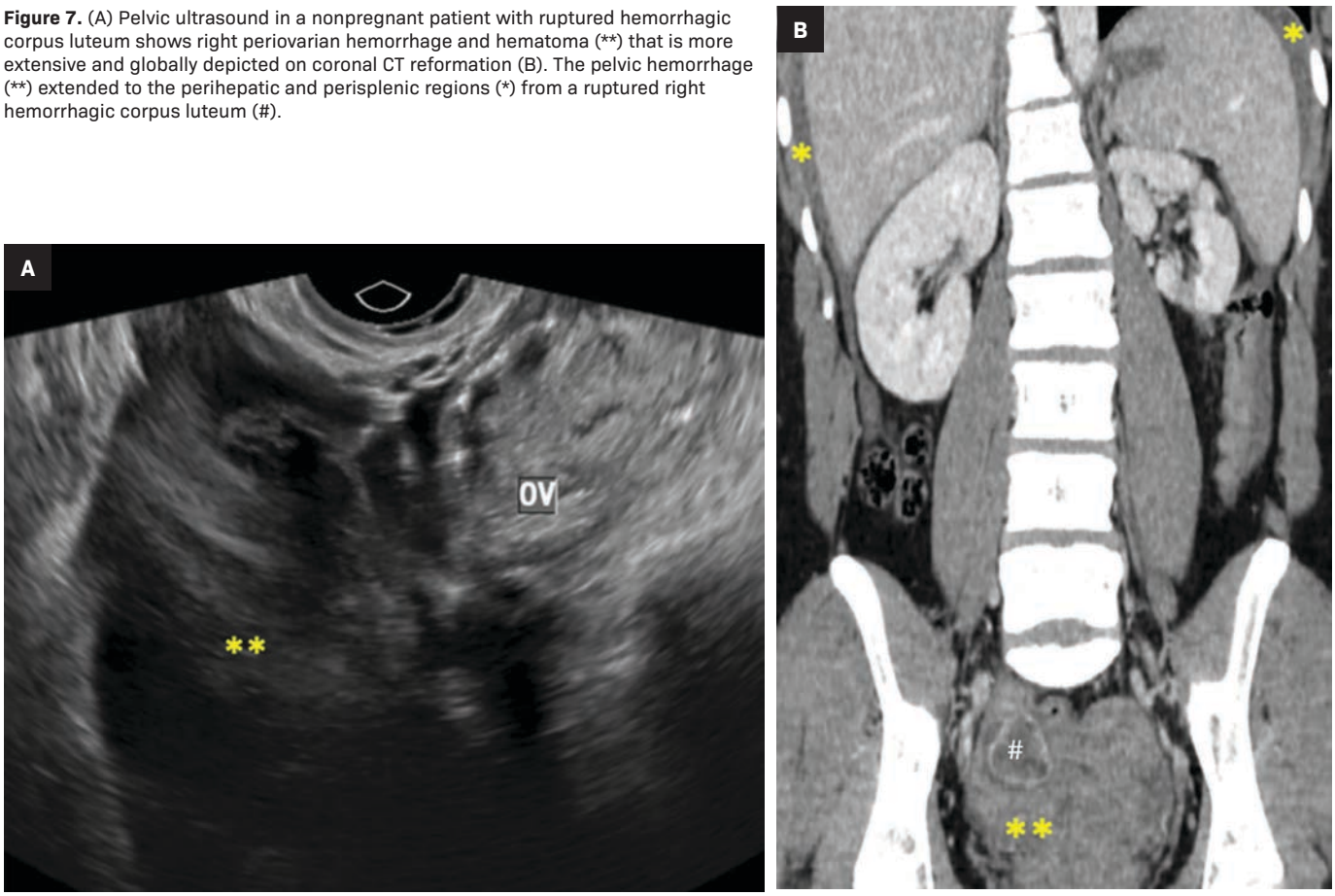

Figure 7. (A) Pelvic ultrasound in a nonpregnant patient with ruptured hemorrhagic corpus luteum shows right periovarian hemorrhage and hematoma (**) that is more extensive and globally depicted on coronal CT reformation (B). The pelvic hemorrhage (**) extended to the perihepatic and perisplenic regions (*) from a ruptured right hemorrhagic corpus luteum (#).

Further highlighting the importance of prompt identification of these tumors, some subtypes can undergo malignant transformation into HCC.[18]

Hepatocellular carcinoma is the second-most common cause of cancer-related mortality in the world.[18] This cancer is typically found in patients with cirrhosis and chronic hepatic inflammation, usually as a consequence of hepatitis B or hepatitis C.[2,18] Rupture with hemorrhage into the peritoneal or subscapular space is a complication of HCC, occurring in 3-15% of cases (Figure 5).[18] Larger and/or peripherally located tumors are at a higher risk of rupture; CT or contrast-enhanced MRI using a liver-mass protocol are the best modalities for diagnosis.[19] Images of HCC rupture typically demonstrate discontinuity of the liver capsule, subcapsular/peritoneal hematoma, and active contrast extravasation.[19]

Gynecologic and Obstetric Causes

Ectopic Pregnancy Rupture

The most common causes of gynecological nontraumatic hemoperitoneum are ectopic pregnancy and hemorrhagic cyst ruptures.[3]

Ectopic pregnancy ruptures can be life threatening; thus, they should be considered for every person of childbearing capability who presents with abdominal pain or vaginal bleeding (Figure 6). Affecting about 1-3% of all pregnancies, ectopic pregnancy most often occurs in the ampulla of the fallopian tube.[20] The diagnostic workup typically begins with serum β-HCG measurement and pelvic sonography. Patients with a β-HCG level over 2000 mIU/mL and an empty uterine cavity are at increased risk of ectopic pregnancy.[2] On imaging, an adnexal mass with hemorrhage is concerning for the condition;[3] if confirmed, these patients may require emergent surgery.

Ovarian Cyst Rupture

Ovarian cyst (typically a corpus luteal or follicular cyst) rupture is common in premenopausal people. Clinical findings are nonspecific but may include pelvic pain. The patient may not be pregnant, in which case the β-HCG levels are normal.[3] However, it should be noted that a positive β-HCG does not exclude cyst rupture which, though rarely life threatening, should be promptly diagnosed and treated. In addition, while rarely causing severe hemorrhage (Figure 7), a ruptured cyst can mimic conditions such as appendicitis that require emergent surgery.[2] Imaging will demonstrate a thick-walled cystic structure in the adnexa with internal echoes and

Figure 8. Axial CT images from a patient with HELLP syndrome. Ascites and hyperdense amorphous material external to the liver in the portal hepatic region appear (arrow) to be associated with segment IVb of the liver. There is no significant change in attenuation or appearance in the noncontrast (A) and arterial (B) phases, compatible with hematoma. These findings suggest likely hepatic hemorrhage prior to the exam, resulting in a perihepatic hematoma. There was also no active extravasation on the CTA. Axial CT (C) image with sagittal reformation (D) in a different patient shows linear, heterogeneous striations through the right posterior and left lobe of the liver which are worrisome for infarcts (arrows). The sagittal image captures the hepatic infarction (arrow), ascites (**), and enlarged postpartum uterus (U).

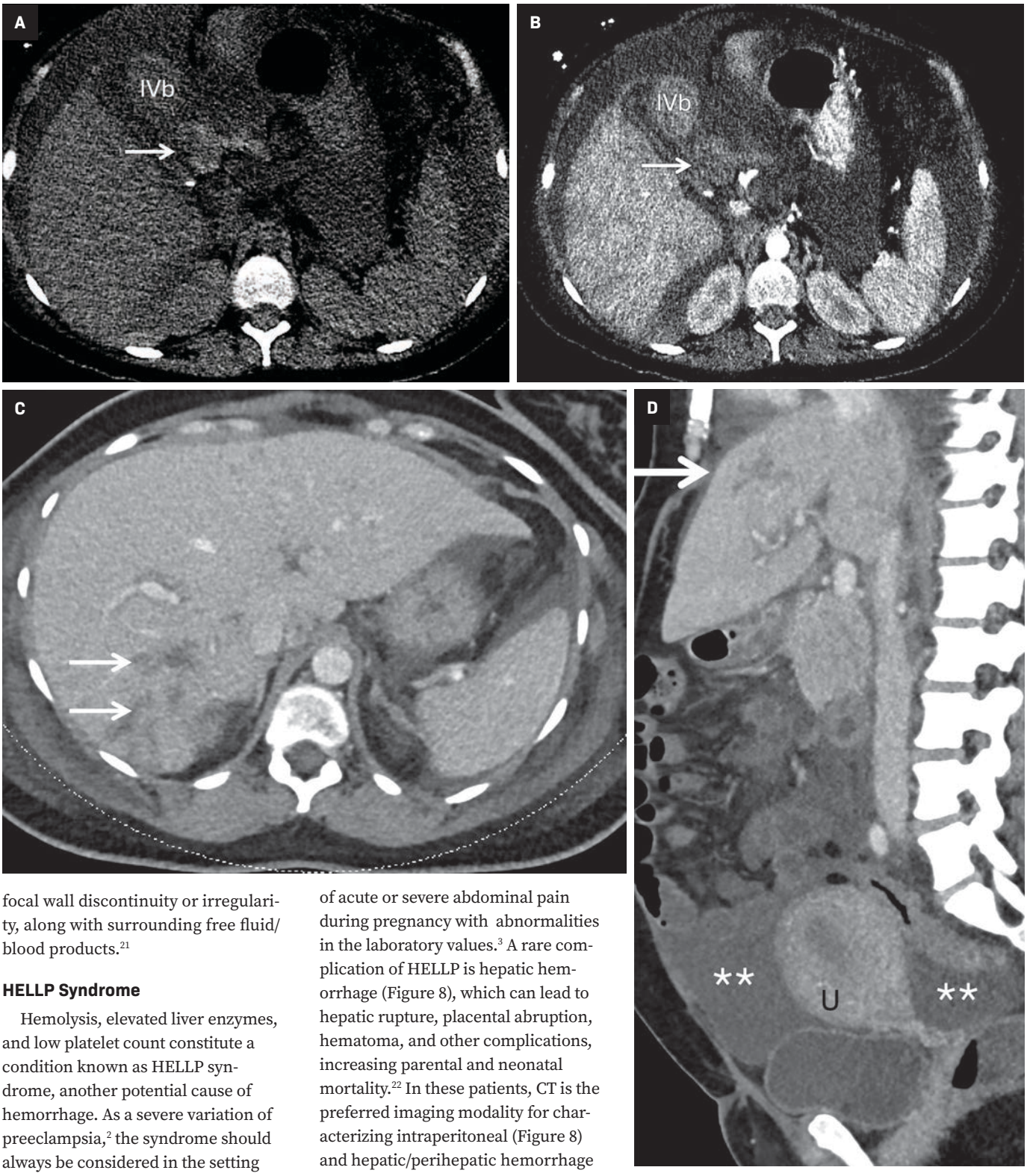

focal wall discontinuity or irregularity, along with surrounding free fluid/blood products.[21]

HELLP Syndrome

Hemolysis, elevated liver enzymes, and low platelet count constitute a condition known as HELLP syndrome, another potential cause of hemorrhage. As a severe variation of preeclampsia,[2] the syndrome should always be considered in the setting of acute or severe abdominal pain during pregnancy with abnormalities in the laboratory values.[3] A rare complication of HELLP is hepatic hemorrhage (Figure 8), which can lead to hepatic rupture, placental abruption, hematoma, and other complications, increasing parental and neonatal mortality.[22] In these patients, CT is the preferred imaging modality for characterizing intraperitoneal (Figure 8) and hepatic/perihepatic hemorrhage

and infarctions.[3,22] Hepatic infarction can appear on CT as low-attenuation, wedge-shaped areas around the liver periphery.[23] Owing to the life-threatening nature of HELLP complicated by hepatic rupture, prompt evaluation and diagnosis are imperative.

Vascular Causes of Hemorrhage

Abdominal Aortic Artery Rupture

Arterial bleeding can be caused by the rupture of an underlying vascular pathology. The most common cause of intra-abdominal vascular bleeding is a ruptured abdominal aortic aneurysm (AAA).[24] Risk factors include male gender, advanced age, a history of cigarette smoking, a family history of AAA, hypertension, and hypercholesteremia.[25] A ruptured AAA should be suspected in patients over 50 who present with severe abdominal or back pain and a pulsating abdominal mass.[26] Computed tomography will show signs of active bleeding, loss of aortic wall continuity, the high-attenuation crescent sign, and retroperitoneal hemorrhage (Figure 9).[24,27] Although many physicians prefer to proceed with immediate treatment

Figure 9. Coronal CT reformation in a coagulopathic patient with abdominal aortic aneurysm and an expanding sac (white double-headed arrow) containing intramural hematoma and subacute hemorrhage (***).

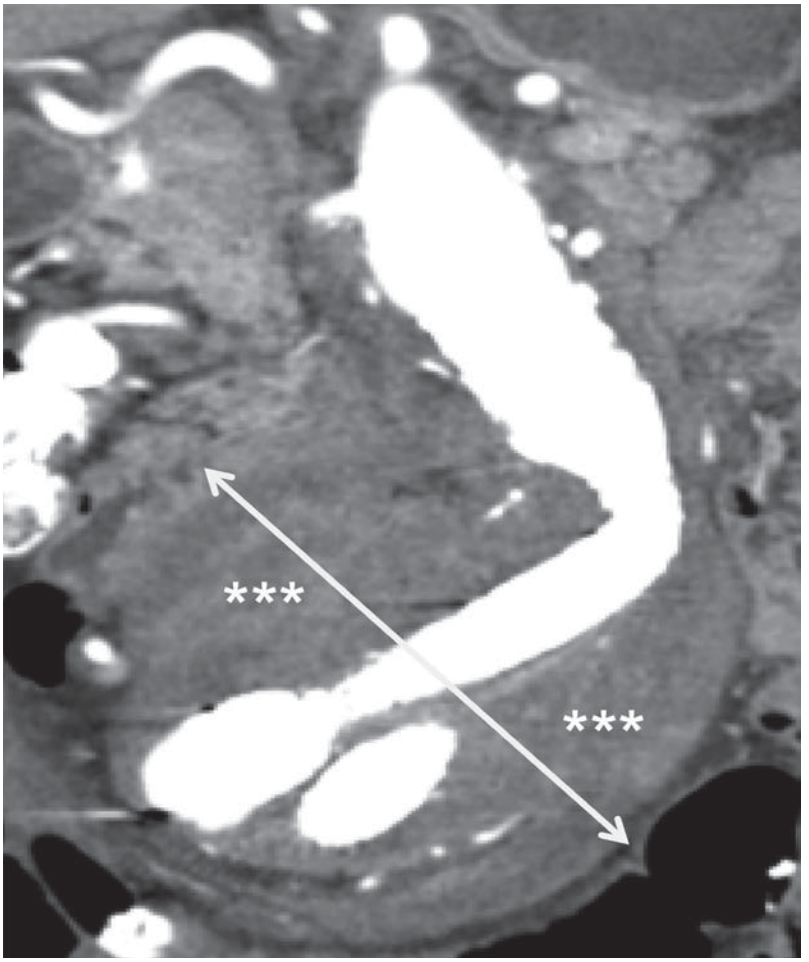

Figure 10. Oblique CT reformation (A) in a coagulopathic patient demonstrates foci of active bleeding in a left rectus sheath hematoma (white arrow). (B) Axial CT in the same patient demonstrates left psoas major hematoma (white arrow).

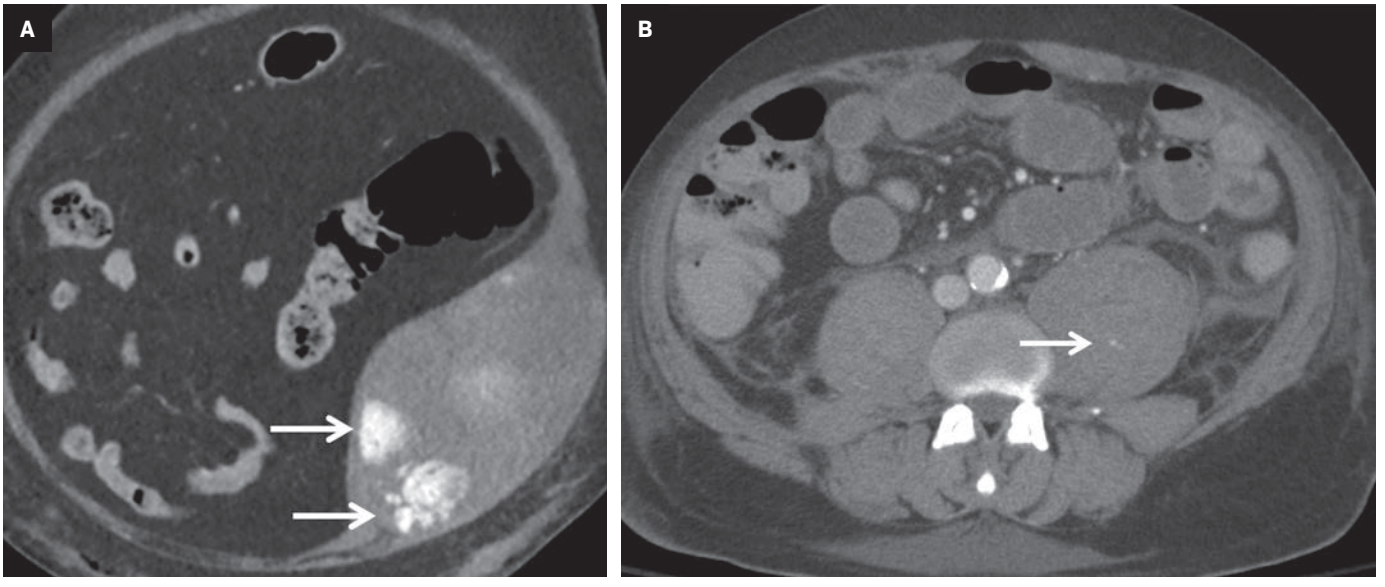

without imaging, CT angiography is the preferred imaging modality for diagnosis.[25]

Iatrogenic Causes of Hemorrhage

Anticoagulation Therapy

Hemoperitoneum following anticoagulation therapy is not uncommon.[28] Anticoagulants such as heparin and coumadin increase bleeding time, which in some cases can lead to life-threatening hemorrhage.[28] The risk of bleeding, however, is typically related to medication dosage.[2] Spontaneous hemorrhage commonly occurs in the rectus abdominis or the psoas muscles. Occasionally, anticoagulation therapy can cause spontaneous hemoperitoneum or retroperitoneal hemorrhage. Computed tomography is beneficial in coagulopathic patients with suspected intra-abdominal bleeding.[29]

Hematomas of the Abdomen and Psoas Muscle

Rectus sheath hematoma (RSH) is often a clinically misdiagnosed cause of acute abdominal pain. This is due to an accumulation of blood in the sheath of the rectus abdominis (Figure 10), typically secondary to rupture of the inferior or superior epigastric vessel, or from a direct muscle tear.[30] A common presenting feature is lower abdominal pain that never crosses the midline; the Carnett test can distinguish between tenderness occurring intra-abdominally and that occurring directly in the abdominal wall.[30,31] During a straight-leg raise, abdominal pain that remains the same or gets worse (a positive test) suggests a somatic source, while pain that improves (a negative test) suggests an intra-abdominal/visceral source. Additional signs and symptoms include nausea, vomiting, chills, fever, and abdominal guarding.[31] Because RSH is uncommon and frequently misdiagnosed, emergency physicians and radiologists should be familiar with this condition, which can mimic many other acute abdominal conditions. In these instances, failure to make a prompt and correct diagnosis could lead to a futile laparotomy.[30]

Psoas muscle hematomas occur when blood accumulates either under or within the psoas muscle (Figure 10).[32] They can present as unilateral or bilateral, the latter being most common. They affect only about 0.1-0.6% of the population, mainly elderly patients on anticoagulants or receiving dialysis.[32] The Cullen sign, which is ecchymosis in the periumbilical area, and the Grey-Turner sign, which is ecchymosis in the flanks, are common.[33] Additional abnormalities may include muscle dysfunction and nerve palsy.[34] Most psoas muscle hematomas, however, will resolve spontaneously without complication if they are not too large and/or compressing important surrounding structures.[33]

Conclusion

There are numerous sources of spontaneous, nontraumatic hemoperitoneum. Radiologist familiarity with their imaging features is crucial for accurate diagnosis and workup. While several imaging options are available, multidetector CT is generally the most efficient for diagnosis. Hemorrhage can be ascertained by the presence of a sentinel clot, active vascular blush, or hyperdense fluid near the organ of interest. Narrowing the site of hemorrhage can have important implications for treatment.

References

1) Gomez E, Horton KM, Fishman EK, Johnson PT. CT of acute abdominopelvic hemorrhage: protocols, pearls, and pitfalls. *Abdominal Radiology*. 2021;47(1):475-484. doi:10.1007/s00261-021-03336-w.

2) Lubner MG, Menias CC, Rucker CM, et al. Blood in the belly: CT findings of hemoperitoneum. *RadioGraphics*. 2007;27(1):109-125. doi:10.1148/rg.271065042.

3) Furlan A, Fakhran S, Federle MP. Spontaneous abdominal hemorrhage: Causes, CT findings, and clinical implications. *American Journal of Roentgenology*. 2009;193(4):1077-1087. doi:10.2214/ajr.08.2231.

4) Mortelé KJ, Cantisani V, Brown DL, Ros PR. Spontaneous intraperitoneal hemorrhage. *Radiologic Clinics of North America*. 2003;41(6):1183-1201. doi:10.1016/s0033-8389(03)00118-0.

5) Linehan MW, Berton Z, Bates S. Cancer of kidney and ureter. In: Devita VT Jr, Hellman S, Rosenberg SA, eds. *Principles and Practice of Oncology*, 6th ed. Philadelphia, PA: Lippincott Williams & Wilkins; 2001:1362–1396.

6) Simon JW, Marshall FF. Kidney and ureter. In: Abeloff MD, Armitage J, Niederhuber J, Kastan M, McKenna W, eds. *Clinical Oncology*, 2nd ed. New York, NY: Churchill Livingstone; 2000:1784–1799.

7) Ray RP, Mahapatra RS, Khullar S, Pal D, Kundu AK. Clinical characteristics of renal cell carcinoma: Five years review from a tertiary hospital in Eastern India. *Indian Journal of Cancer*. 2016;53(1):114. doi:10.4103/0019-509x.180851.

8) Pummer K, Lämmer J, Wandschneider G, Primus G. Renal cell carcinoma presenting as spontaneous retroperitoneal haemorrhage. *International Urology and Nephrology*. 1990;22(4):307-311. doi:10.1007/bf02549788.

9) Muttarak M, Pattamapaspong N, Lojanapiwat B, Chaiwun B. Renal angiomyolipoma with bleeding. *Biomedical Imaging and Intervention Journal*. 2007;3(4). doi:10.2349/biij.3.4.e8.

10) Hatano T, Egawa S. Renal angiomyolipoma with tuberous sclerosis complex: How it differs from sporadic angiomyolipoma in both management and care. *Asian Journal of Surgery*. 2020;43(10):967-972. doi:10.1016/j.asjsur.2019.12.008.

11) Altuwayr RM, Almutairi FS, Alkhaibari SH, et al. Spontaneous rupture of large angiomyolipoma of the kidney: a rare case. *Cureus*. November 2021. doi:10.7759/cureus.19908.

12) Kania B, Vasani S. A case report of splenic rupture secondary to underlying angiosarcoma. *Cureus*. July 2020. doi:10.7759/cureus.9439.

13) Autry JR, Weitzner S. Hemangiosarcoma of spleen with spontaneous rupture. *Cancer*. 1975;35(2):534-539. doi:10.1002/1097-0142(197502)35:2.

14) Xu B, Xie X, Zhou X, Zhai M, Yang W. Spontaneous rupture of primary splenic angiosarcoma: A case report. *Oncology Letters*. 2015;10(5):3271-3273. doi:10.3892/ol.2015.3714.

15) Hamid KS, Rodríguez J, Lairmore TC. Primary splenic angiosarcoma. *JSLS*. 2010;14(3):431-435. doi:10.4293/108680810x12924466006521.

16) Dokmak S, Aussilhou B, Rasoaherinomenjanahary F, et al. Hemorrhage of hepatocellular adenoma: a complication that can be treated by conservative management without surgery. *HPB*. 2018;20(12):1198-1205. doi:10.1016/j.hpb.2018.06.1796.

17) Papanikolaou, Giakoustidis D, Patsiaura K, et al. Management of a giant ruptured hepatocellular adenoma. Report of a case. *PubMed*. 2007. https://pubmed.ncbi.nlm.nih.gov/19582184. Accessed June 12, 2022.

18) Thomas AJ, Menias CO, Pickhardt PJ, et al. Bleeding liver masses: imaging features with pathologic correlation and impact on management. *American Journal of Roentgenology*. 2019;213(1):8-16. doi:10.2214/ajr.19.21240.

19) Sahu S, Chawla Y, Dhiman RK, et al. Rupture of hepatocellular Carcinoma: A review of literature. *Journal of Clinical and Experimental Hepatology*. 2019;9(2):245-256. doi:10.1016/j.jceh.2018.04.002.

20) Della-Giustina D, Denny MW. Ectopic pregnancy. *Emergency Medicine Clinics of North America*. 2003;21(3):565-584. doi:10.1016/s0733-8627(03)00036-1.

21) Pulappadi VP, Manchanda S, Sk P, Hari S. Identifying corpus luteum rupture as the culprit for haemoperitoneum. *British Journal of Radiology*. 2021;94(1117):20200383. doi:10.1259/bjr.20200383.

22) Nunes JO, Turner MA, Fulcher AS. Abdominal Imaging Features of HELLP Syndrome: A 10-Year Retrospective Review. *American Journal of Roentgenology*. 2005;185(5):1205-1210. doi:10.2214/ajr.04.0817.

23) Mortelé KJ, Cantisani V, Brown DL, Ros PR. Spontaneous intraperitoneal hemorrhage. *Radiologic Clinics of North America*. 2003;41(6):1183-1201. doi:10.1016/s0033-8389(03)00118-0.

24) Larrañaga N, Kozima S, Villarroel N, et al. Spontaneous abdominal hemorrhage: imaging evaluation. *Revista interamericana de radiología*. 2015. https://webcir.org/revistavirtual/articulos/2015/noviembre/argentina/rar/spontaneous.pdf. Accessed June 12, 2022.

25) Gawenda M, Brunkwall J. Ruptured abdominal aortic aneurysm: the state of play. *Dtsch Arztebl Int*. 2012;109(43):727-732. doi:10.3238/arztebl.2012.0727.

26) Wilmink A, Quick CRG. Epidemiology and potential for prevention of abdominal aortic aneurysm. *British Journal of Surgery*. 1998;85(2):155-162. doi:10.1046/j.1365-2168.1998.00714.x.

27) Siegel C, Cohan RH, Korobkin M, Alpern M, Courneya DL, Leder RA. Abdominal aortic aneurysm morphology: CT features in patients with ruptured and nonruptured aneurysms. *American Journal of Roentgenology*. 1994;163(5):1123-1129. doi:10.2214/ajr.163.5.7976888.

28) Lucey BC, Varghese JC, Anderson SW, Soto JA. Spontaneous hemoperitoneum: a bloody mess. *Emergency Radiology*. 2007;14(2):65-75. doi:10.1007/s10140-007-0594-0.

29) Nazarian LN, Lev-Toaff AS, Spettell CM, Wechsler RJ. CT assessment of abdominal hemorrhage in coagulopathic patients: impact on clinical management. *Abdominal Radiology*. 1999;24(3):246-249. doi:10.1007/s002619900489.

30) Siu WT, Tang CN, Law BKB, Chau CH, Li MKW. Spontaneous rectus sheath hematoma. *PubMed*. 2003;46(5):390. https://pubmed.ncbi.nlm.nih.gov/14577716. Accessed June 15, 2022.

31) Hatjipetrou A, Anyfantakis D, Kastanakis M. Rectus sheath hematoma: A review of the literature. *International Journal of Surgery*. 2015;13:267-271. doi:10.1016/j.ijsu.2014.12.015.

32) Abedini L, Mehrabi S, Hosseinpour R, Jahantab MB, Salehi V, Barhaghtalab MJY. Non-penetrating traumatic psoas muscle hematoma presenting with gross hematuria: a case report. *International Journal of Emergency Medicine*. 2021;14(1). doi:10.1186/s12245-021-00345-w.

33) Seo JG, Yang JC, Kim TW, Park KH. Intramuscular hematoma on the psoas muscle. *Korean Journal of Neurotrauma*. 2019;15(2):234. doi:10.13004/kjnt.2019.15.e29.

34) Zidouh S, Belkouch A, Mostafa R, Hicham B, Belyamani L. Conservative treatment of a psoas hematoma revealed by a lower limb palsy. *Pan Afr Med J*. 2017;28. doi:10.11604/pamj.2017.28.138.9930.

AppliedRadiology®

The Journal of Practical Medical Imaging and Management

UPDATE YOUR SUBSCRIPTION

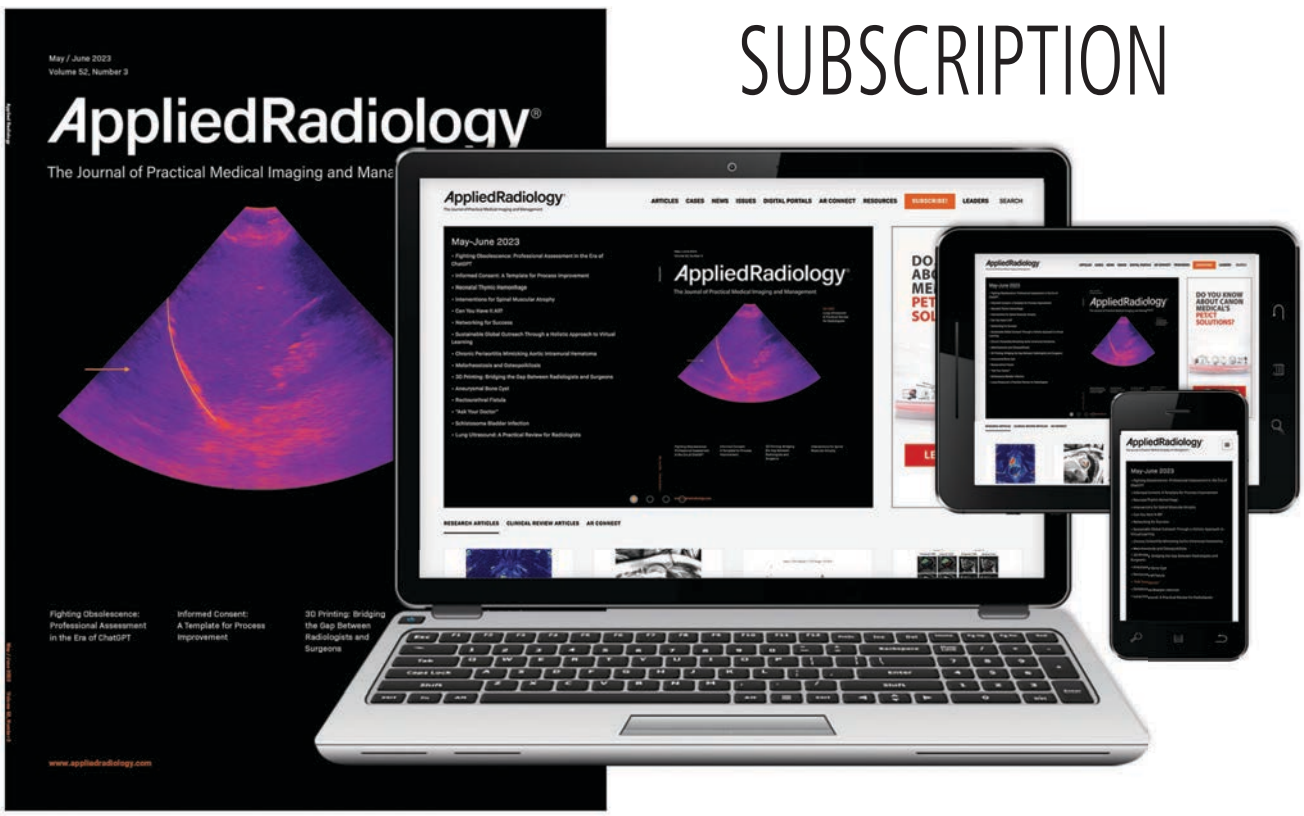

Since 1972, *Applied Radiology* has brought physician-authored clinical review articles to the radiology community.

Applied Radiology content includes clinical review articles, radiological cases, and specialty columns such as Eye on AI and the ever-popular Wet Read by C. Douglas Phillips, MD, FACR.

Now you can have it all your way (FREE) without missing a single issue.

Please take a moment to update your subscription preferences.

appliedradiology.com/#subscribe

Setting the Stage for Preventive Radiology

Leander Maerkisch; Benedikt Schneider; Christian Wiedemeyer, MD, CMO

Consider 57-year-old Elise (anonymized), who recently received a diagnosis of advanced osteoporosis after suffering an unexpected fracture, despite having undergone several other recent radiological exams for unrelated conditions.

This real patient case prompts a critical question: Could those prior scans have resulted in a much earlier diagnosis? Quite possibly. With the emergence of "opportunistic AI screening," radiologists may have a potentially powerful way to detect hidden health conditions within otherwise routine scans before they progress to more advanced stages.

Understanding Opportunistic AI Screening

At its core, opportunistic AI screening transforms standard medical imaging scans into proactive health checks. Unlike condition-specific screening exams, such as annual mammograms, this approach leverages AI to analyze more routine images for early signs of osteoporosis, cardiovascular issues, cancer, and other medical conditions.[1]

Affiliations: Mr Schneider is co-founder and chief executive officer; Mr Maerkisch is co-founder and chief product officer; and Dr Wiedemeyer is chief marketing officer of Floy, based in Munich, Germany.

The Silent Threat of Asymptomatic Conditions

In the US alone, over 50 million people are at risk for preventable conditions like osteoporotic fractures,[2] many of which are underdiagnosed.[3] This endangers individual health outcomes[4] and also significantly burdens the healthcare system with resource-intensive and expensive later-stage care.[5]

While they remain valuable tools, traditional screening programs often fail to achieve their full potential because of low participation rates.[6] For instance, only 4.5% of those eligible for lung cancer screening in the US actually avail themselves of this opportunity.[7] The economic burden of underdiagnosed conditions runs into the billions of dollars,[8] underscoring the need for more effective ways to catch them early.

Turning Routine Scans into Comprehensive Health Insights

Every year, more than 120 million CT and MRI scans offer a detailed glimpse into the human body.[9,10] Yet their diagnostic potential is often confined to the specific reason(s) for which they are requested.[1] For instance, an abdominal CT scan can not only answer the primary question facing the clinician, but it can also potentially offer quantitative assessment of bone mineral density, calcification in large arteries, body composition, and liver volume/attenuation.[1]

This wealth of unused data represents a missed opportunity for early disease detection. Opportunistic screening seeks to fill this gap by analyzing these scans for additional imaging-based biomarkers. However, expecting already overburdened radiologists to undertake these extra, time-intensive measurements is unrealistic.[11]

Providing a Scalable Solution with AI

What if AI could step in to help assess the images for potential signs of disease beyond those for which a given imaging exam is requested? Enter opportunistic AI screening.

Opportunistic screening leverages AI to analyze large volumes of scans for imaging-based biomarkers with minimal impact on radiologist workload. In the case of osteoporosis, AI can perform precise 3D segmenta-

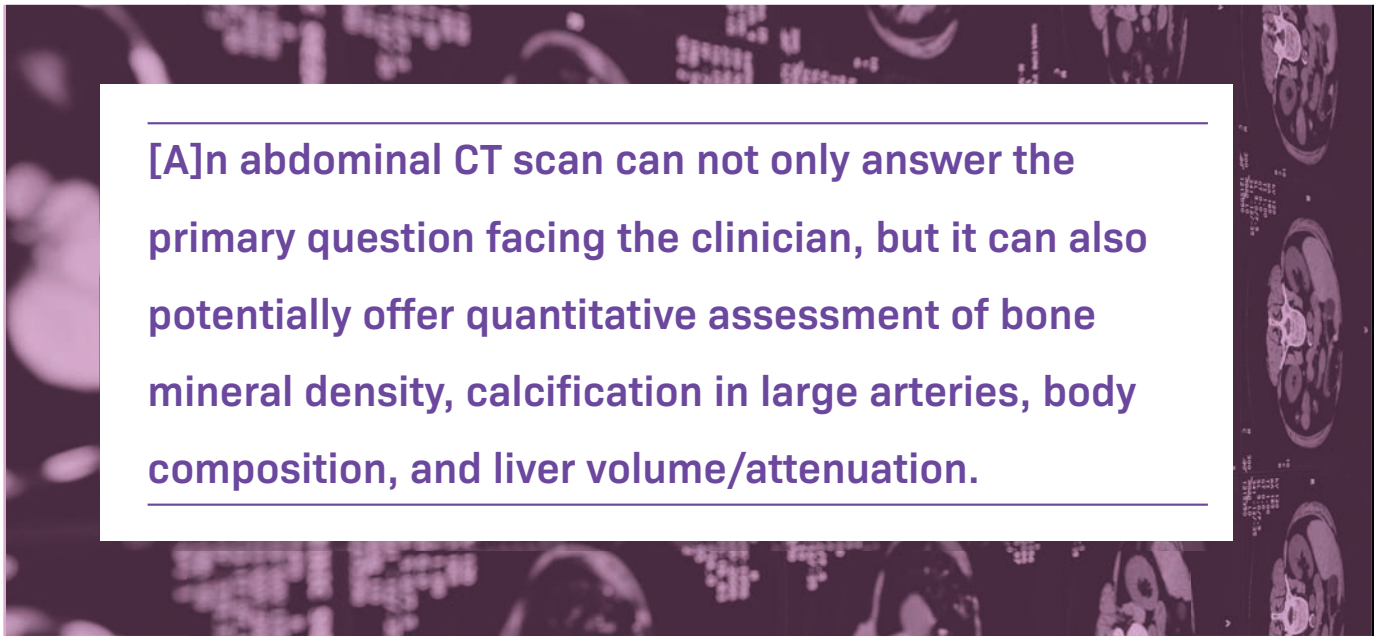

[A]n abdominal CT scan can not only answer the primary question facing the clinician, but it can also potentially offer quantitative assessment of bone mineral density, calcification in large arteries, body composition, and liver volume/attenuation.

tion of the trabecular bone structures, calculate the bone mineral density, and compare the results with reference population data to provide equivalent scoring to dual X-ray absorptiometry (DEXA) scanning.[12]

Several companies are at the forefront of this shift towards what could be considered "preventive radiology." By developing AI-based medical devices capable of detecting aneurysms in T2 MRI scans and assessing bone density in CT scans, companies like HeartLungAI (Los Angeles, California), VirtuOst (Berkeley, California), and Floy (Munich, Germany) are aiming toward transforming "routine" scans into holistic health assessments at the point of care. Such scans may thus be used as a baseline for future comparison and more nuanced risk stratification at follow-up exams.

Driving Down Costs and Unlocking New Use Cases

The advantages of opportunistic screening extend beyond improving individual care. Already showing early success in Europe, the approach also presents the US with a model to help extend healthcare access to underserved populations while also reducing the resource-intensive and costly impacts of later-stage disease treatment.[13]

Embracing the Future of Preventive Imaging

By transforming standard imaging studies into a powerful tool for comprehensive health assessment, opportunistic AI screening has the potential to deliver actionable insights earlier in the disease process without additional, costly examinations. In doing so, it can help pave the way to a future of precision medicine where treatment can be tailored to the unique needs of each patient, and cases like Elise's become a thing of the past.

References

1) Pickhardt PJ. Value-added opportunistic CT screening: state of the art. *Radiology.* 2022;303(2):241-254.

2) Wright NC, Looker AC, Saag KG, et al. The recent prevalence of osteoporosis and low bone mass in the United States based on bone mineral density at the femoral neck or lumbar spine. *J Bone Miner Res.* 2014;29(11):2520-2526.

3) Nguyen TV, Center JR, Eisman JA. Osteoporosis: underrated, underdiagnosed and undertreated. *Med J Aust.* 2004;180(S4):S18-S22.

4) Rizzo M, Cappello F, Marfil R, et al. Quality of life in osteoporotic patients. *Orthop Rev (Pavia).* 2022;14(1):38562.

5) Rashki Kemmak A, Zendehtalab HR, Miri MR, et al. Economic burden of osteoporosis in the world: a systematic review. *Med J Islam Repub Iran.* 2020;34:154.

6) Gillespie CW, Morin PE. Trends and disparities in osteoporosis screening among women in the United States, 2008-2014. *Am J Med.* 2017;130(3):306-316.

7) American Lung Association. State of lung cancer. Accessed March 15, 2024. https://www.lung.org/research/state-of-lung-cancer/key-findings.

8) Shrank WH, Rogstad TL, Parekh N. Waste in the US health care system: estimated costs and potential for savings. *JAMA.* 2019;322(15):1501-1509.

9) Shah A, Aran S. A review of magnetic resonance (MR) safety: the essentials to patient safety. *Cureus.* 2023;15:e47345.

10) Mettler FA Jr, Bhargavan M, Faulkner K, et al. Radiologic and nuclear medicine studies in the United States and worldwide: frequency, radiation dose, and comparison with other radiation sources—1950-2007. *Radiology.* 2009;253(2):520-531.

11) Chen M, Gholamrezanezhad A. Burnout in radiology. *Acad Radiol.* 2023;30(8):1031-1032.

12) Löffler MT, Sollmann N, Mei K, et al. Automatic opportunistic osteoporosis screening in routine CT: improved prediction of patients with prevalent vertebral fractures compared to DXA. *Eur Radiol.* 2021;31(9):6069-6077.

13) Pickhardt PJ, Correale L, Hassan C. AI-based opportunistic CT screening of incidental cardiovascular disease, osteoporosis, and sarcopenia: cost-effectiveness analysis. *Abdom Radiol (NY).* 2023;48(4):1181-1198.

Reduce, Reuse, Recycle: The Three R's of Sustainability

Kerri Reeves

Kerri Reeves is a freelance writer based in Ambler, PA.

Kate Hanneman, MD, MPH

While I was interested in sustainability personally, from an academic perspective, I didn't initially think this was in my lane as a radiologist.

The origins of the "Go Green" and sustainability movements to reduce man-made impacts on the environment can be traced to the 1960s and '70s, which gave birth to the first celebration of Earth Day in 1970.

However, Kate Hanneman, MD, MPH, vice chair of research and deputy lead for sustainability in the Department of Medical Imaging at the University of Toronto, Ontario, Canada, admits she didn't consider sustainability relevant to her role until rather recently.

"While I was interested in sustainability personally, from an academic perspective, I didn't initially think this was in my lane as a radiologist," says Dr Hanneman. But that changed during the pandemic, when she started reading papers about the impact of radiology on the environment. Suddenly, she says, "a light bulb went off. I realized we do have a big role to play."

She's not alone. Many medical imaging industry and clinical stakeholders are joining their peers in transportation, manufacturing, farming, and other industries in rethinking energy use and waste disposal practices to help curb greenhouse gas (GHG) production, believed to be a leading cause of climate change.

"There's been a ton of momentum and engagement in sustainability in healthcare, especially in radiology," says Reed Omary, MD, MS, noting that he has witnessed standing-room-only sessions at radiology conferences and read numerous academic publications on the topic. Dr Omary, who is on a climate-learning sabbatical, is the Carol D. & Henry P. Pendergrass Professor in the Department of Radiology and Radiological Sciences, and a professor of biomedical engineering at Vanderbilt University Medical Center & School of Medicine in Nashville, Tennessee.

"The heart of the momentum is coming from medical professionals who are projecting a new energy around sustainability … and engaging us about our own efforts," adds Amy King, sustainability lead at Bracco Diagnostics. King notes that recent federal legislation enacting grants and tax credits for sustainability action is also advancing GHG reduction efforts in healthcare.

Reduce Energy Consumption

Globally, healthcare emits the equivalent of more than 2 gigatons of carbon dioxide each year. That amounts to between 5% and 8% of total GHG emissions in developed nations and up to 1% of emissions worldwide.[1]

"Healthcare is an industry that drives one of the largest carbon footprints—more than aviation or shipping—and in hospitals, imaging accounts for a big part of this," says Olesya Struk, senior director of sustainability and access to care at Philips.

Medical imaging equipment—especially MRI and CT scanners—consumes significant amounts of energy that generates GHGs. The estimated energy expenditure for MRI for every 1,000 U.S. citizens annually is 1648 kWh; CT energy expenditure comes in at an estimated 298 kWh per 1,000 citizens.[2]

In response, vendors are taking steps to reduce the carbon footprints of their technologies. Philips, for example, has added a standby mode to all its MRI and CT scanners to reduce energy consumption when they are not in use, says Struk, adding that scan duration is also optimized for energy efficiency.

Philips' new MRI scanners also now employ efficient micro-cooling technology that requires just 7 liters of liquid helium—a fraction of the 1,500 liters of helium used by conventional magnets. This has saved more than 1.9 million liters of liquid helium since 2018, says Struk.

Bracco, meanwhile, offers consulting services to help radiology teams convert from single-dose to multi-dose contrast vials, as well as to help implement weight-based contrast dosing, says King. She adds that the company now offers a contrast agent that uses only half the dose of gadolinium previously needed to obtain diagnostic-quality images, and also encourages its customers to switch from single kits to efficiency packs of its ultrasound contrast agent.

Medical imaging departments and private practices are likewise joining the sustainability fight. Considering equipment life and rising case volumes, Dr Hanneman says, it is imperative that providers power down scanners to their lowest settings when not in use. She argues that reducing energy use and waste is one of the best steps radiology departments can take to make a significant step toward sustainability.

"Energy that is not being used to contribute to patient care, generate images, or run our workstations should be preserved," Dr Hanneman says, recommending establishment of department policies to power down machines during prolonged idle times, such as after hours. Department leaders can also inquire about their hospital's energy provider, suggests Dr Hanneman, who says that switching to renewable energy can have a big impact on emissions.

She similarly recommends using only the imaging sequences that are absolutely necessary to a procedure to reduce energy consumption.

"In general, the shorter the protocol, the less energy per patient," Dr Hanneman says. Aligning department policy with campaigns to reduce low-value imaging and following guidelines for managing incidental findings can further reduce unnecessary imaging, she says.

"The greenest radiology is avoiding the radiology that isn't needed," agrees Dr Omary.

Reduce Waste

Reducing energy use isn't the only way to go green in radiology; reducing waste is another effective strategy to improve sustainability efforts. Dr Hanneman suggests that imaging practice leaders work with their vendors to expand the lifespan of existing machines. Philips, for example, takes back whole systems and/or parts for upgrading, refurbishing, reusing, or recycling.

"Healthcare is an industry that drives one of the largest carbon footprints—more than aviation or shipping—and in hospitals, imaging accounts for a big part of this," says Struk.

Dr Omary says interest is growing in performing MRI scans either without gadolinium or with the absolute minimum dose required, particularly in pediatric cases. The environmental impact of gadolinium-based contrast agents in the water system is a growing problem.[3] Packaging of contrast in single-use vials is also a concern.

"We have structured ourselves with well-meaning intention to be disposable radiology departments," Dr Omary says, suggesting that by switching to multi-dose bottles, departments could save "an immense amount of money, plastic waste, and contrast agent waste."

Beware the "Double-edged Sword"

Software that now allows imaging and image interpretation to be performed remotely can reduce the need for travel and thereby indirectly reduce

Reed Omary, MD, MS

The greenest radiology is avoiding the radiology that isn't needed.

Amy King

The heart of the momentum is coming from medical professionals who are projecting a new energy around sustainability.

Olesya Struk

Healthcare is an industry that drives one of the largest carbon footprints. [I]maging accounts for a big part of this.

GHG emissions. Artificial intelligence (AI) is gaining attention for its potential to improve sustainability in radiology in multiple ways, including accelerating imaging and optimizing scanners to improve patient workflows, says Dr Hanneman. However, she is quick to label AI a "doubled-edged sword."

"The data and storage required for AI and the energy to train models and run interference is massive," she explains, recommending that data storage providers that prioritize renewable energy sources be used to help lower AI's impact on the environment.

Collaborate for Successful Change

Implementing the tools, technologies, and policies needed to create sustainability requires collaboration among key stakeholders. For example, department leaders can quantify energy savings and patient benefits when proposing changes to their administrators. They can also look for opportunities to collaborate with vendors while also requiring transparency about their carbon footprint and procurement principles.

"Through our collective efforts, imaging teams and industry can work together to create more of an impact on our society and less of an imprint on our environment," says King.

Like-minded radiology professionals can also form communities—like the one growing around Dr Omary's "The Green Leap blog" to make healthcare sustainable.

"Climate change will affect us all … but those who are already most vulnerable will be affected the most," explains Dr Hanneman, who says that health equity and the sustainability of our planet are "intrinsically linked."

In the US, 100 healthcare systems have joined a Department of Health and Human Services pledge to reduce carbon emissions by 50% before the end of the decade, and to achieve net zero emissions by 2050.[1] California-based Kaiser Permanente achieved carbon neutrality in 2020.[1]

"We have many opportunities to reduce waste, which is good for the planet," concludes Dr Omary. "By taking care of the planet, we take care of our patients and of our health systems."

References

1) Brown M, Schoen JH, Gross J, Omary R, Hanneman K. Climate change and radiology: Impetus for change and a toolkit for action. *Radiology.* 2023; 307(4):e230229. https://doi.org/10.1148/radiol.230229

2) Chaban Y, Vosshenrich J, McKee H, Gunasekaran S, et al. Environmental sustainability and MRI: Challenges, opportunities, and a call for action. *JMRI.* 2024; 59(4) 1149-1167. https://doi.org/10.1002/jmri.28994

3) Dekker HM, Stroomberg GJ, Van der Molen AJ, et al. Review of strategies to reduce the contamination of the water environment by gadolinium-based contrast agents. *Insights Imaging*. 2024; 15(62). https://doi.org/10.1186/s13244-024-01626-7

The 2024 Leaders on the Horizon Residents' Program

This exclusive program is designed to identify, cultivate, and highlight the future stars in medical imaging.

Residents are encouraged to submit a clinical research paper and/or a clinical review article for consideration. All papers should be focused on topics related to medical imaging and will be reviewed by a committee of key opinion leaders in radiology.

Residents authoring the top three (3) papers selected for each category will receive a scholarship.

Clinical Research Papers	
1st place	$7500
2nd place	$5000
3rd place	$3000

Clinical Review Papers	
1st place	$3000
2nd place	$2000
3rd place	$1000

Paper Submission Deadline: October 1, 2024

Visit appliedradiology.com/leaders to submit a paper topic today!

Supported through an unrestricted educational grant from Bracco Diagnostics, Inc.

BRACCO

LIFE FROM INSIDE

Amyand Hernia Complicated by Acute Appendicitis

Nicholas A. Jaeger, DO; Midhir J. Patel, MD

Case Summary

An elderly patient presented to the emergency department with acute right testicular pain and vomiting following a recent diagnosis of right inguinal hernia. In addition to the hernia, the physical exam was notable for tenderness in the right groin and scrotum.

Imaging Findings

Scrotal ultrasound (Figures 1, 2) demonstrated a blind-ending, non-compressible tubular structure in the right inguinal canal, measuring up to 9 mm in diameter, with moderate peripheral color flow.

While scanning the spermatic cord, the sonographer noticed a tubular structure within the inguinal canal and proceeded to perform the scan with compression. The reading radiologist recommended abdominopelvic CT (Figure 3), which confirmed the presence of a noncompressible, inflamed appendix within the hernia. The appendix measured up to 10 mm and the proximal portion was found to be mildly thickened with mild surrounding inflammatory fat stranding.

Affiliation: AdventHealth, Orlando, Florida..

Diagnosis

Amyand hernia with acute appendicitis.

The main differential diagnosis is a strangulated inguinal hernia, which can have a similar presentation.

Discussion

Amyand hernia is named for Claudius Amyand, the French surgeon who discovered an inflamed appendix within a right inguinal hernia sac while performing the first recorded successful appendectomy on an adolescent in 1735.[1,2]

Amyand hernia is rare, making up 0.19% to 1.7% of inguinal hernias; a 2003 study of 1,341 inguinal hernias found only 0.6% of cases contained the appendix.[2-4] Amyand hernia can occur at any age but is up to 3 times more common in children than adults.[5] Incidence of concurrent appendicitis is even more uncommon, occurring in an estimated 0.07-0.13% of inguinal hernias.[4]

Most cases are diagnosed at surgery, as imaging is not routinely performed prior to inguinal hernia repair. Incarceration of the appendix, however, is thought to be a predisposing risk factor for acute inflammatory changes that can prompt imaging.[2]

The pathophysiology of acute appendicitis in Amyand hernia is not clear. It is thought that extraluminal compression of the appendix inside the hernia, rather than intraluminal obstruction as seen in most cases of appendicitis, leads to ischemia, bacterial overgrowth, and inflammation within the appendix.[6]

Surgery is the mainstay of treatment. In most cases, the hernia is repaired concurrently with the appendectomy; however, this is at the surgeon's discretion.[2,4] If the hernia is to be repaired with a mesh, the surgeon may choose to wait until the inflammation/infection has resolved to repair the hernia.

Our patient underwent laparoscopic appendectomy and returned two months later for hernia repair with mesh placement.

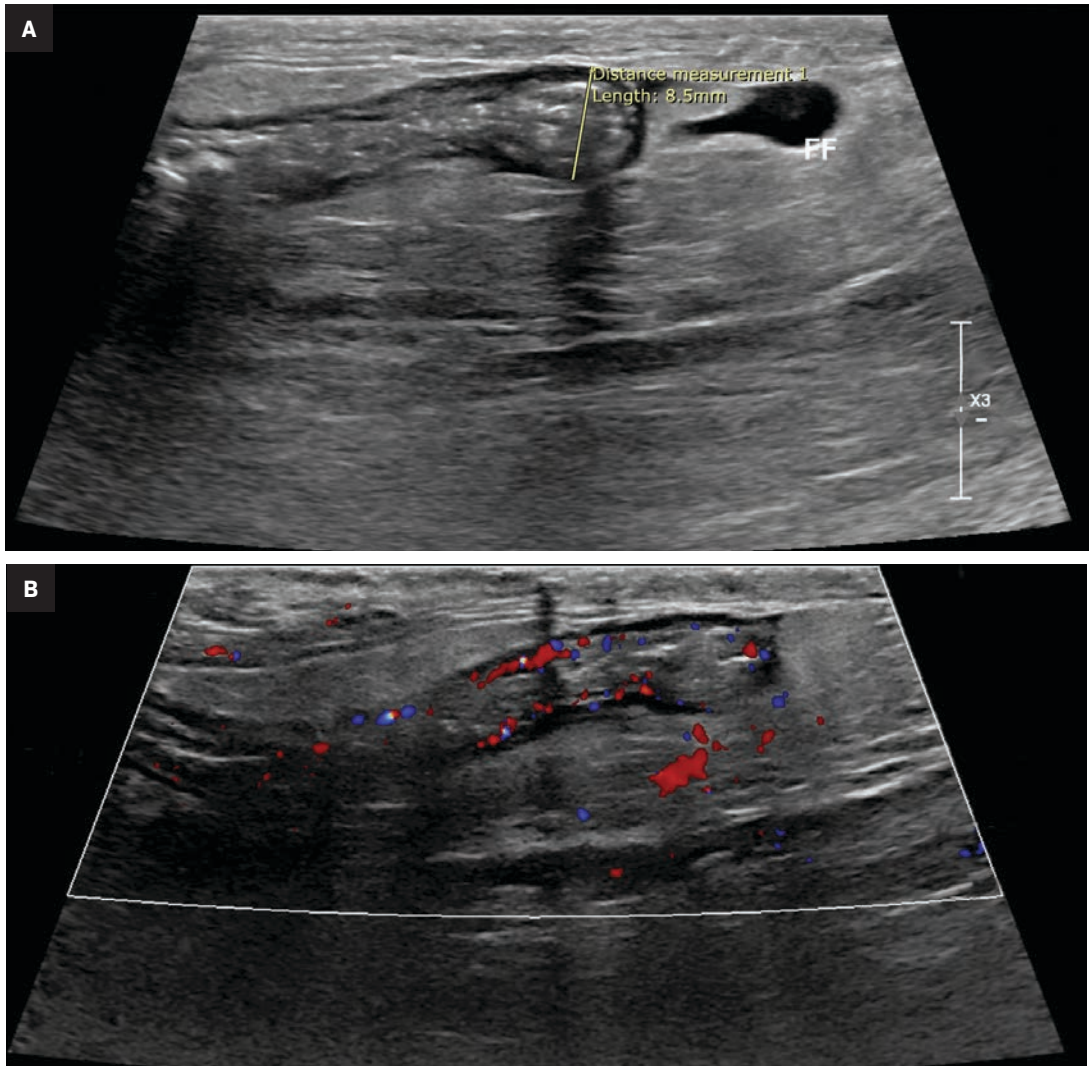

Figure 1. (A) Sagittal grayscale ultrasound of the right inguinal canal demonstrates a blind-ending tubular structure measuring approximately 9 mm consistent with a mildly dilated appendix. (B) Sagittal ultrasound with color of the right inguinal canal demonstrates a blind-ending tubular structure with increased peripheral color flow.

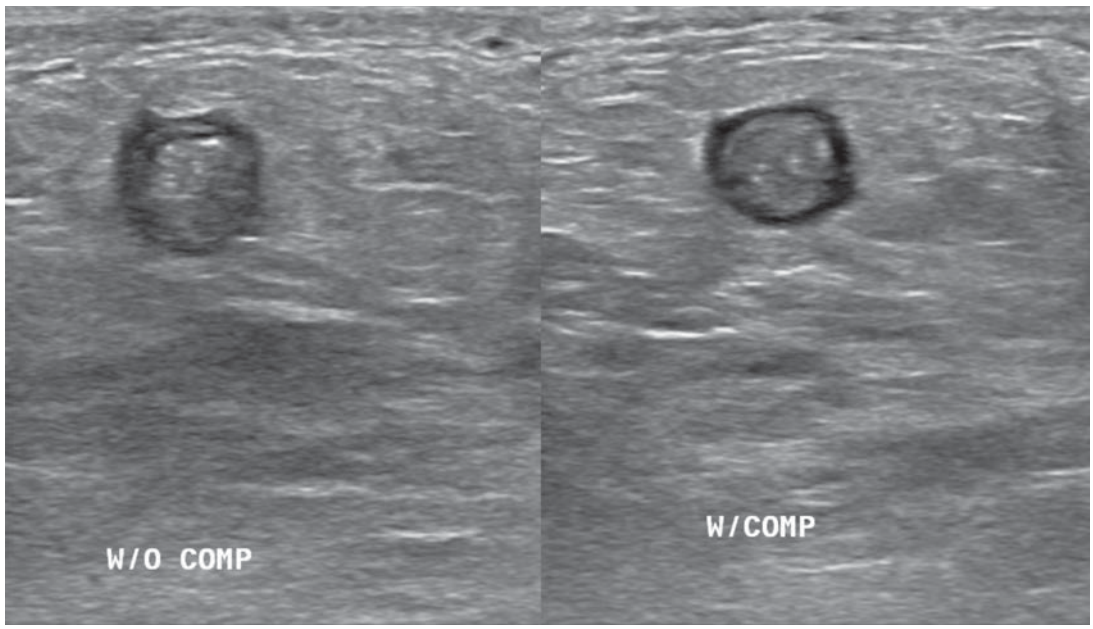

Figure 2. Transverse grayscale ultrasound of the right inguinal canal without (left) and with (right) compression, demonstrating lack of compressibility of the blind-ending tubular structure, consistent with a noncompressible appendix.

Figure 3. Contrast-enhanced coronal (A) and axial (B) CT abdomen and pelvis demonstrate the dilated base of the appendix within the proximal right inguinal canal with mild surrounding fat stranding.

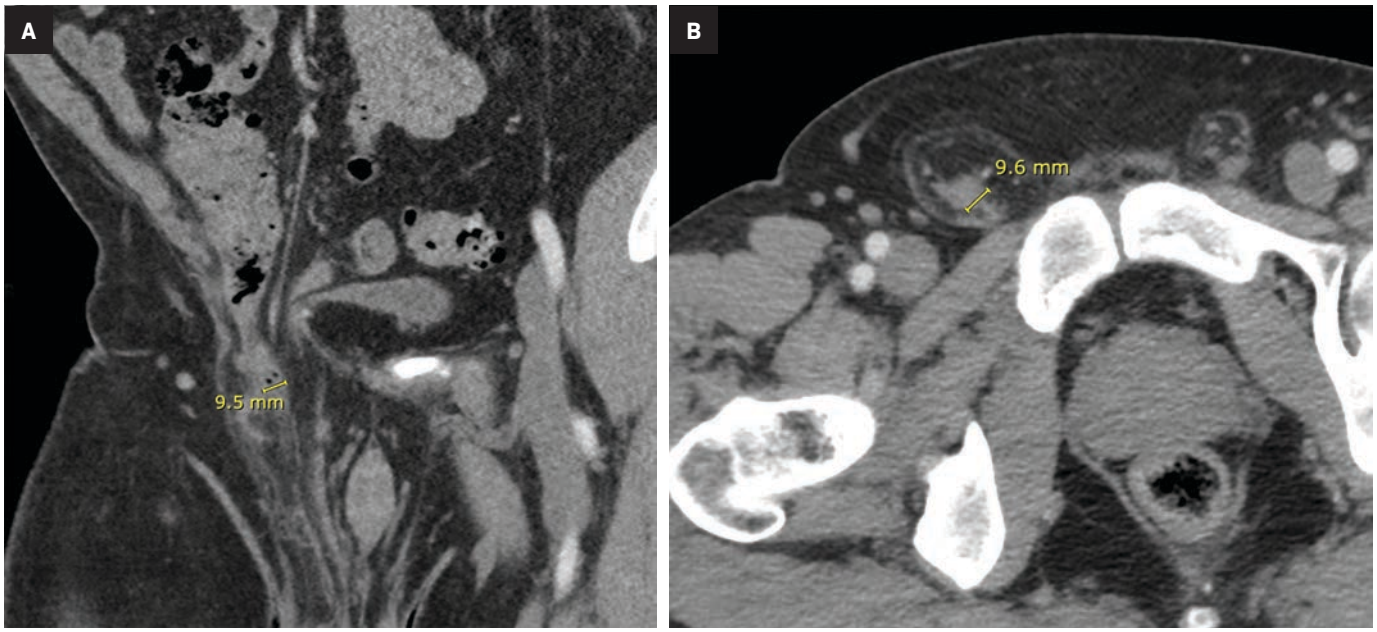

Conclusion

Because Amyand hernia itself is rare, and imaging is not necessary prior to most inguinal hernia surgeries, preoperative diagnosis of the condition is exceedingly rare. On ultrasound, a blind-ending structure within the hernia sac should raise suspicion for Amyand hernia. To assess for acute appendicitis, compression and color flow ultrasound images should be obtained; CT may be performed to confirm the findings in equivocal cases. Treatment consists of surgery.

References

1) Amyand C. Of an inguinal rupture, with a pin in the appendix caeci, incrusted with stone; and some observations on wounds in the guts. *Phil Trans R Soc Lond*. 1973;39:329.

2) Ivanschuk G, Cesmebasi A, Sorenson EP, Blaak C, Loukas M, Tubbs SR. Amyand's hernia: a review. *Med Sci Monit*. 2014;20:140-6. doi: 10.12659/MSM.889873. PMID: 24473371; PMCID: PMC3915004.

3) D'Alia C, Lo Schiavo, M G, Tonante A, et al. Amyand's hernia: case report and review of the literature. *Hernia*. 2003;7(2): 89–91. https://doi.org/10.1007/s10029-002-0098-5

4) Sharma H, Gupta A, Shekhawat NS, Memon B, Memon MA. Amyand's hernia: a report of 18 consecutive patients over a 15 year period. *Hernia*. 2007;11:31–35.

5) Baldassarre E, Centozea A, Mazzei A, et al. Amyand's hernia in premature twins. *Hernia*. 2009;13:229–230.

6) Singal R, Gupta S. Amyand's Hernia - Pathophysiology, role of investigations and treatment. *Maedica* (Bucur). 2011; 6(4):321-327. PMID: 22879848; PMCID: PMC3391951.

Groin Spindle Cell Sarcoma

Jonathan E. Henning, BS; Maryam H. Kazelka, BS; Christopher Declue, MD; Katie Bailey, MD; Nazeel Ahmad, MD

Case Summary

An elderly patient with a history of a malignant kidney tumor and aortic aneurysm presented with chronic right inguinal pain. The patient denied recent trauma, swelling, and skin changes to the right groin, and they endorsed upper respiratory symptoms and a recent "popping" sensation in the right groin after coughing. Pelvic and abdominal CT scan raised concern for acute hemorrhage in the right groin. Coil embolization was successfully performed.

One month later, CT angiography demonstrated mild interval enlargement of the right inguinal canal region hematoma, consistent with a chronic hematoma, which characteristically expands following a hemorrhagic event.[1]

In this case, however, the patient also began experiencing lower abdominal discomfort, fatigue, and tachycardia. The growing mass and onset of new symptoms, some of which are common in cancer patients,[2] prompted exploratory surgery, which demonstrated a right groin mass suspicious for malignancy. Biopsy and histopathology subsequently resulted in a diagnosis of malignant spindle cell neoplasm.

Affiliations: University of South Florida Morsani College of Medicine, Tampa, Florida (Mr Henning, Ms Kazelka, Drs Declue, Bailey, Nazeel Ahmad).

Imaging Findings

The initial abdominopelvic CT demonstrated a 10 cm x 5 cm x 6 cm heterogeneous collection with a blush (contrast pooling) appearing as an acute hemorrhage in the right inguinal canal (Figure 1). Catheter angiography prior to embolization demonstrated several irregular branches arising from the right inferior epigastric artery without contrast extravasation (Figure 2). One month postembolization, abdominopelvic CT revealed mild interval enlargement of the right inguinal canal region mass to 14.7 cm (Figure 3). Biopsy was performed (Figure 4).

Diagnosis

Malignant spindle cell sarcoma

Discussion

We present an unusual occurrence of a right groin spindle cell sarcoma disguised as a hematoma. Spindle cell sarcomas are a rare and heterogeneous type of soft-tissue sarcoma.[3] They arise from layers of connective tissue and may occur in any anatomical location, including soft tissue, bone, and viscera.[4] Given the heterogeneity of soft-tissue sarcomas, the clinical presentation is not well characterized. Owing to this obscurity, collections in the inguinal region can be mistaken for hematomas on imaging modalities such as ultrasound.[5] In these cases of uncertainty, follow up and/or contrast-enhanced imaging plays an important role in correct diagnosis.

In most settings a metastatic inguinal neoplasm is an unlikely explanation for inguinal pain or mass. More probable causes include inguinal hernia, hydrocele, abscess, and hematoma.[6] Visual and physical examination, however, can lower the probability of hernia, which presents as a bulge in the inguinal region.[6] The absence of recent trauma, swelling, and skin changes of the right groin also reduce the likelihood of hernia.[6]

An effective tool for diagnosing the cause of inguinal pain, CT can typically distinguish among abdominal wall masses, tumors, hematomas, and unsuspected hernias.[7] In this case, CT revealed a heterogeneous collection, as well as what was thought to be contrast extravasation, which may indicate active bleeding in the area.[8]

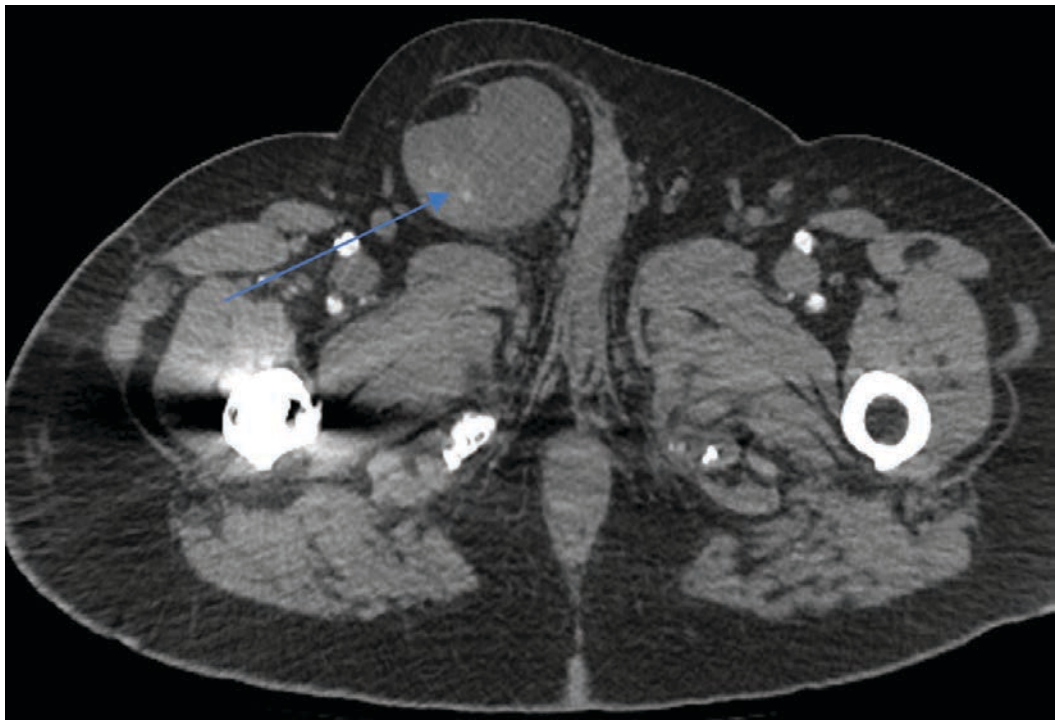

Figure 1. Axial pelvic CT scan at initial presentation demonstrates a right groin heterogeneous, rounded region of soft tissue density measuring 10cm x 5cm x 6cm with blushing. This is seen as hyperdensity at the inferior aspect of the lesion thought to depict intravenous contrast extravasation (arrow).

Figure 2. (A) Catheter angiogram displaying several irregular branches arising from the right inferior epigastric artery. Blue arrows show hyperemia within the mass without active contrast extravasation. (B) Catheter angiogram following coil embolization.

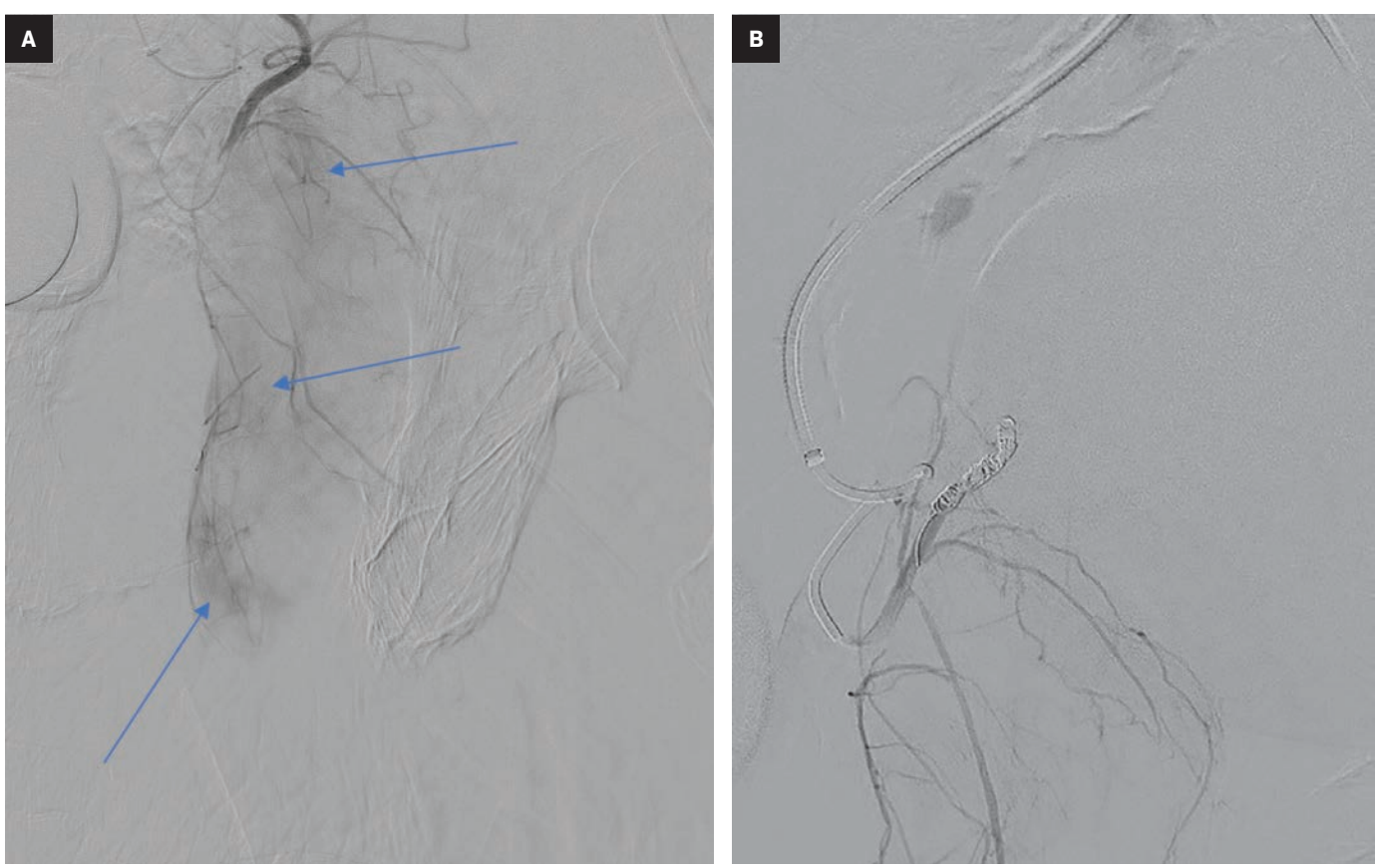

Figure 3. CT angiogram one month after initial CT demonstrates mild interval enlargement of the right groin lesion to 14.7 cm.

Figure 4. H&E stain of the spindle cell neoplasm at 30 X magnification demonstrates a multinucleated giant cell tumor along with background spindle cells. Arrows indicate the typical spindle-shaped cells.

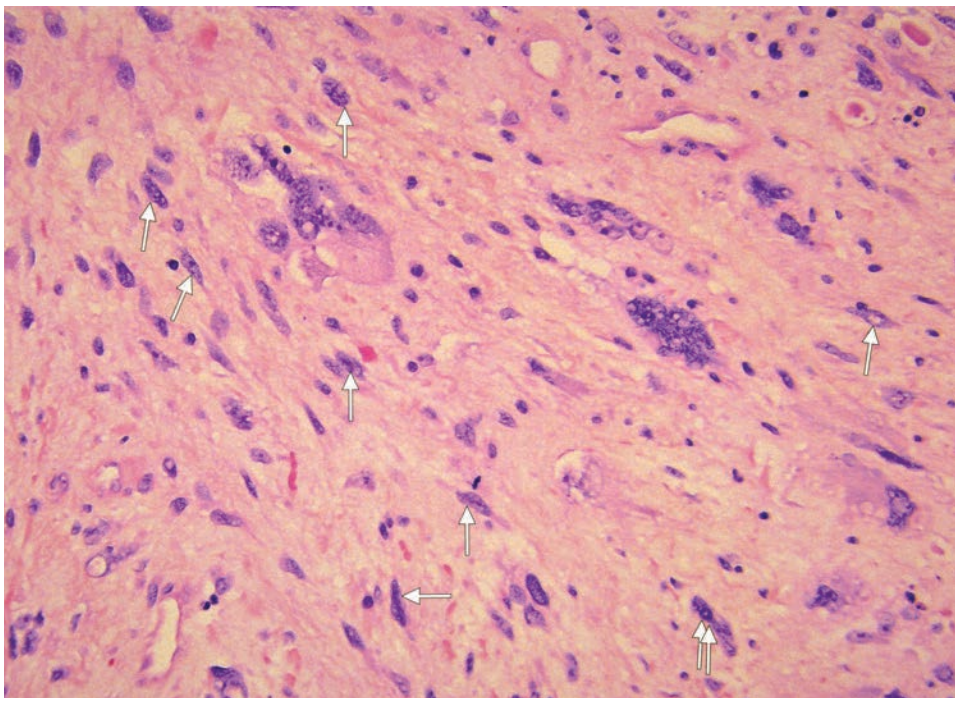

Given the concerns about bleeding, catheter angiography and coil embolization were performed. The procedure is indicated in cases of suspected active arterial hemorrhage to identify and occlude blood vessels and stop the bleeding.[9]

Conclusion

Malignant spindle cell sarcoma in the inguinal region is rare and may be missed because it can present with signs and symptoms that overlap with a groin hematoma. Imaging is essential to accurate diagnosis.

References

1) Manenti G, Cavallo AU, Marsico S, et al. Chronic expanding hematoma of the left flank mimicking a soft-tissue neoplasm. *Radiol Case Rep.* 2017;12(4):801-806. doi: 10.1016/j.radcr.2017.07.019

2) Cleeland CS. Cancer-related symptoms. *Semin Radiat Oncol.* 2000; 10(3):175-90. doi: 10.1053/srao.2000.6590

3) Panthi S, Poudel S, Khanal N, et al. Spindle cell sarcoma: a case report of diagnostic and therapeutic quandary in a low resource setting. *J Surg Case Rep*. 2022 Jan 21; 2022(1):rjab612. doi: 10.1093/jscr/rjab612. PMID: 35079340.

4) Feng L, Wang M, Yibulayin F, Zhang H, Yang YL, Ren F, Wushou A. Spindle cell sarcoma: a SEER population-based analysis. *Sci Rep*. 2018; 8(1): 5024. doi: 10.1038/s41598-018-23145-4

5) Vodanovich DA, M Choong PF. Soft-tissue sarcomas. *Indian J Orthop*. 2018; 52(1):35-44. doi: 10.4103/ortho.IJOrtho_220_17

6) Hammoud M, Gerken J. Inguinal hernia. In: StatPearls [Internet]. Treasure Island (FL): StatPearls Publishing; 2023 Available at: https://www.ncbi.nlm.nih.gov/books/NBK513332/

7) Lee GH, Cohen AJ. CT imaging of abdominal hernias. *AJR Am J Roentgenol.* 1993; 161(6):1209-13. doi: 10.2214/ajr.161.6.8249727

8) Godt J C, Eken T, Schulz A, et al. Do we really need the arterial phase on CT in pelvic trauma patients? *Emerg Radiol.* 2021;28:37–46. doi: https://doi.org/10.1007/s10140-020-01820-2

9) Lopera JE. Embolization in trauma: principles and techniques. *Semin Intervent Radiol.* 2010; 27(1):14-28. doi: 10.1055/s-0030-1247885

Leiomyosarcoma of the Inferior Vena Cava

Christopher D. Terrill, MD; Kevin Shady, MD

Case Summary

An adult with a history of metastatic prostate cancer presented for routine surveillance CT.

Imaging Findings

Contrast-enhanced CT of the chest, abdomen, and pelvis showed no evidence of metastatic bone disease or pelvic lymphadenopathy. A low-density filling defect was observed within the inferior vena cava (IVC) contrast column (Figure 1). Low-density tissue extended beyond the lumen of the IVC into the adjacent right adrenal gland, forming a 2.7 × 2.4 × 2.4 cm nodule. Initial prostate cancer staging CT seven years prior showed the tumor to be centered along the IVC with 50% being intraluminal and 50% extraluminal (Figure 1). The patient underwent adrenalectomy and resection of the involved portion of the IVC.

Retrospective evaluation of multiple studies showed growth of the intra- and extraluminal components, with greater growth extraluminally into the adrenal gland with varying degrees of intraluminal conspicuity related to contrast bolus timing. The lesion also demonstrated significant F-18 fluciclovine uptake adjacent to physiologic liver activity (Figure 2).

Affiliations: SSM Saint Louis University Hospital, St. Louis, MO (Dr Terrill), John Cochran Veterans Hospital, St. Louis, MO (Dr Shady). Disclosures: None

Diagnosis

Leiomyosarcoma of the IVC.

Differential diagnosis includes metastasis and adrenal origin neoplasms such as low-grade adrenal malignancies, including pheochromocytoma, low-grade adrenal carcinoma, and primary adrenal lymphoma.

Discussion

Venous leiomyosarcomas predominantly involve the IVC and represent fewer than 1% of malignant tumors.[1] Roughly 300 have been reported since 2006.[2] This tumor affects women more than men, with a ratio of 3:1, and occurring most frequently between the ages of 40 and 60 years.[3]

The appearance of an IVC leiomyosarcoma on imaging can be somewhat variable. Most commonly, these tumors grow extraluminally at a rate of 2:1 versus intraluminal growth.[3] They typically appear as heterogeneously enhancing masses with at least some intraluminal component causing a filling defect.

Filling defects on routine contrast-enhanced CT present a frequent dilemma for the radiologist. The most common reason for poor contrast opacification of a vein or portion of a vein is admixture of blood containing contrast with blood not yet saturated with contrast. These wispy or streaking filling defects are readily recognized by the radiologist and determined to be normal. Occasionally, these filling defects demonstrate a more distinct border, which can indicate thrombus, neoplasm, or often simply an atypical appearance of admixture.

Intravenous neoplasms are commonly associated with solid organ tumors which extend into the venous drainage of the organ. The benign primary tumor of the venous smooth muscle layer, leiomyoma, and its malignant counterpart, leiomyosarcoma, are rarer causes for venous filling defects. These tumors may develop cystic necrosis. Leiomyosarcoma uptake of F-18 fluciclovine has not previously been reported.

The level of the IVC involved is important for prognosis and treatment planning. Renal and suprarenal levels are most common (42%-50%) and have the most favorable prognosis. Intrahepatic is the rarest level of involvement (6%-20%) and has the worst prognosis. Approximately 37%-44% of leiomyosarcomas of the IVC are infrarenal. Although indolent, significant mortality is associated

Figure 1. (A) Axial contrast-enhanced CT (CECT) images through the inferior vena cava showing an irregular nodule (arrowheads) involving the right adrenal gland and IVC with intraluminal extension. (B) Initial axial CECT images of the lesion obtained seven years prior. The nodule (arrowhead) is smaller and more circumscribed.

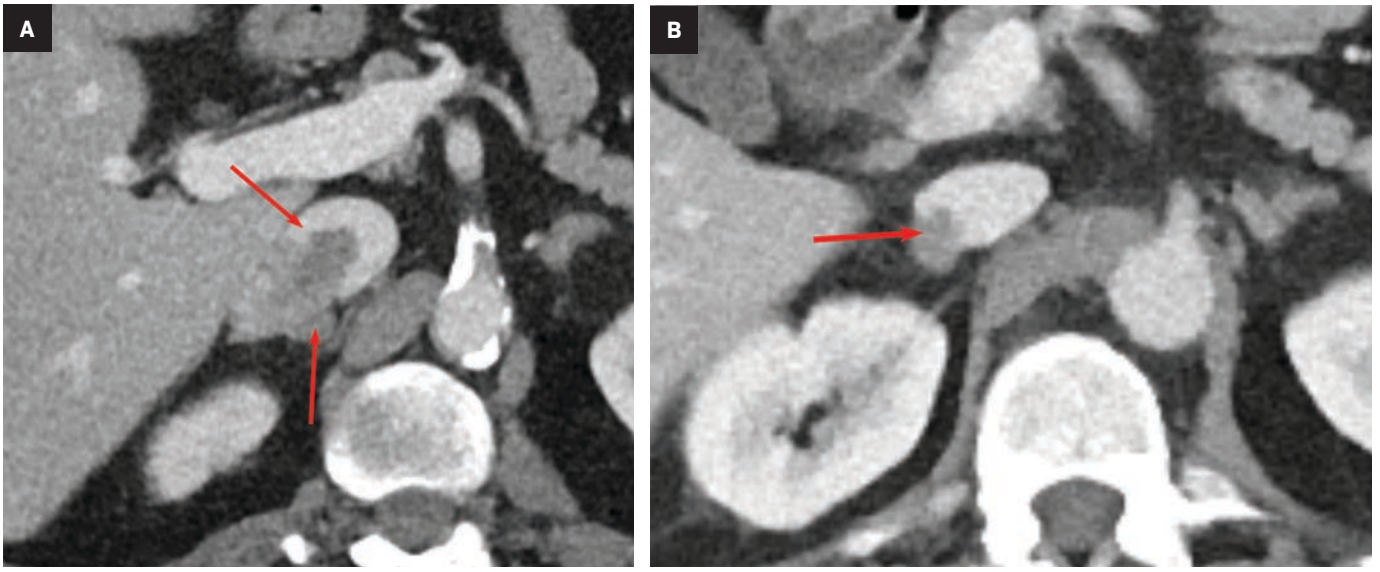

with these tumors, with an overall 10-year survival of 14% after complete resection.[4]

Conclusion

Inconsistent contrast opacification on CT makes the IVC prone to artifact from admixture. Inclusion of the IVC into the radiologist search pattern is essential for identifying true pathology, including the rare leiomyosarcoma, as well as relatively common pathologies such as bland and tumor thrombus.

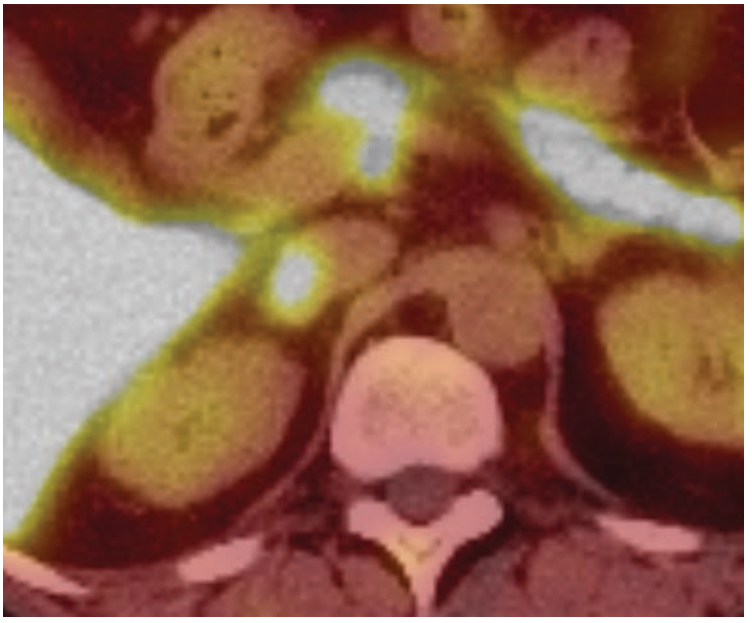

Figure 2. Axial F-18 fluciclovine PET/CT images show hypermetabolism within the nodule.

References

1) Jenkins S, Marshall GB, Gray R. Leiomyosarcoma of the inferior vena cava. *Can J Surg*. 2005; 48(3):252-253. PMID: 16013635; PMCID: PMC3211549.

2) Rare disease database: leiomyosarcoma. Nov2022. http://rarediseases.org/rare-diseases/leiomyosarcoma/2012.

3) Smillie RP, Shetty M, Boyer AC, Madrazo B, Jafri SZ. Imaging evaluation of the inferior vena cava. *Radiographics*. 2015; 35(2):578-592. doi: 10.1148/rg.352140136. PMID: 25763740.

4) Bednarova I, Frellesen C, Roman A, Vogl TJ. Case 257: leiomyosarcoma of the inferior vena cava. *Radiology*. 2018; 288(3):901-908. doi: 10.1148/radiol.2018160821. PMID: 30125223.

Cerebral Amyloid Angiopathy-related Inflammation

Krunal Moradiya, BS, BBA; Sundeep Patel, MD

Case Summary

An elderly patient presented to the emergency department with confusion, upper-extremity weakness, and slurred speech. Noncontrast head CT revealed a right temporoparietal lesion with surrounding vasogenic edema, which was confirmed by MRI. The patient was admitted and anticoagulation for their atrial fibrillation was discontinued.

The patient experienced improvement and was discharged after several days. Follow-up outpatient MRI four weeks later demonstrated persistent vasogenic edema and multiple new petechial lesions, necessitating a second hospitalization and steroid treatment.

Imaging Findings

Initial noncontrast head CT revealed a 1.5 x 2.3 cm hyperdense ovoid lesion in the right temporoparietal region surrounded by widespread, frond-like areas of hypodensity. T2 FLAIR MRI further characterized this temporoparietal lesion as a subcortical hemorrhage with out-of-proportion hyperintense vasogenic edema. T2* GRE demonstrated concentric deoxyhemoglobin around the hemorrhage (Figure 1). One month later, T2 FLAIR demonstrated persistence of prior temporoparietal hyperintensities. Susceptibility-weighted imaging revealed interval development of punctate foci of signal loss, co-localized to the hyperintensities seen on FLAIR (Figure 2).

Affiliations: Michigan State University College of Osteopathic Medicine, East Lansing, Michigan (Mr Moradiya); Henry Ford Macomb Hospital, Clinton Township, Michigan (Dr Patel).

Diagnosis

Cerebral amyloid angiopathy-related inflammation (CAARI). The differential diagnosis includes posterior reversible encephalopathy syndrome, leukoencephalopathy, brain tumor, primary angiitis of the central nervous system, acute disseminated encephalomyelitis, and neurosarcoidosis.

Discussion

CAARI is a rare variant of cerebral amyloid angiopathy (CAA). In CAA, amyloid β (Aβ) is deposited in the walls of cortical and leptomeningeal vessels, producing vasculopathy.[1] Hereditary CAA is associated with Down syndrome and mutations in genes encoding amyloid precursor and presenilin proteins, whereas sporadic CAA is age-related.[2]

Both types can present with acute, recurrent intracerebral hemorrhage (ICH), progressive dementia, and transient focal neurological episodes.[1,2] CAARI shares these manifestations, in addition to specific features like subacute encephalopathy, cognitive changes, stroke-like deficits, headaches, and seizures. The average age of patients affected by CAARI is 67, with no clear gender predominance.[2,3]

In CAARI, Aβ is believed to trigger an autoimmune response, resulting in either perivascular inflammation (inflammatory cerebral amyloid angiopathy [ICAA]) or intramural/transmural inflammation (Aβ-related angiitis [ABRA]). ICAA and ABRA are reconciled as distinct histologic forms of CAARI that have equivalent clinicoradiologic presentations. Regardless of the form, brain biopsy is needed to definitively diagnose CAARI.[2] Increasingly, MRI is preferred for noninvasive probable diagnosis of CAARI.

Although infrequent, symptomatic, large ICH is a classic imaging finding of CAA. Other characteristic MRI findings include white matter hyperintensities (WMHs), cerebral microhemorrhages or microbleeds

Figure 1. (A, B) Axial T2 FLAIR demonstrates temporoparietal hemorrhage with surrounding patchy and confluent hyperintensities. These hyperintensities reflect vasogenic edema and extend into the gray matter, causing sulcal effacement. They exert mass effect on the occipital horn of the right lateral ventricle. There is also increased FLAIR signal in the local subarachnoid space (white arrow), consistent with sulcal subarachnoid hemorrhage. (C) Axial T2* GRE demonstrates concentric deoxyhemoglobin around the hemorrhage, with associated susceptibility effect. There is an insufficient presence of microbleeds needed for probable diagnosis of CAARI, as per the imaging criteria. At this time, the patient was not formally diagnosed and was told to obtain a follow-up MRI in one month.

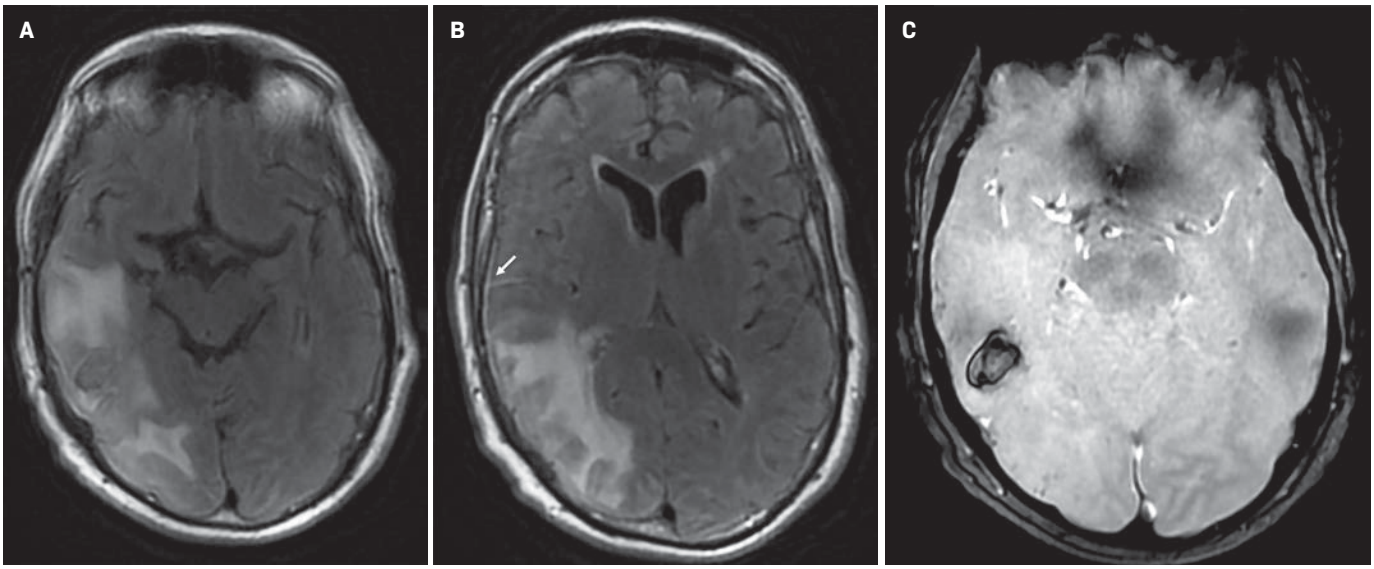

Figure 2. (A, B) Follow-up axial T2 FLAIR demonstrates showing persistence of the temporoparietal hyperintensities. (C) Axial susceptibility-weighted imaging demonstrates interval development of numerous punctate areas of signal loss, consistent with microhemorrhages.

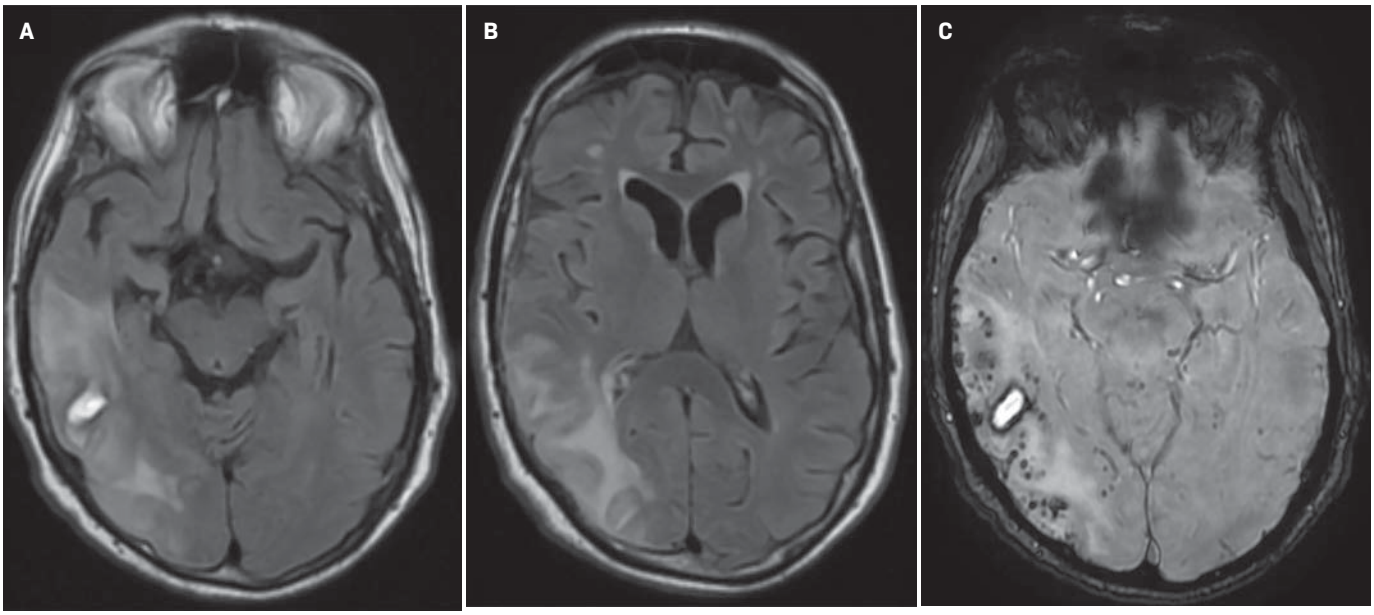

(CMBs), cortical superficial siderosis (CSS), sulcal subarachnoid hemorrhage, and cortical atrophy.[1-3] With CAARI, these findings are preserved but may differ slightly from those in traditional CAA. For example, WMHs in CAARI are unifocal or multifocal, patchy, asymmetric, and confluent.[2-4] These hyperintensities have vasogenic edema with or without mass effect and contiguous gray matter extension.[2,4]

Hyperintensities in CAARI usually reverse with resolution of edema.[4] Comparatively, hyperintensities in traditional CAA are spot-like when subcortical and have periventricular and posterior cerebral predominance without vasogenic edema.[1,5] Similarly, hyperintensities reflecting chronic small-vessel ischemia (caused by CAA or hypertensive arteriopathy) should be distinguished from the reversible, patchy hyperintensities characteristic of CAARI, as both types may be seen in some patients.

Compared to CAA, the incidence of CMBs is much higher in CAARI, and their distribution is not necessarily occipital dominant.[3,6] Cerebral microhemorrhages are best seen using T2* GRE/SWI sequences.[2,4] Hemosiderin from hemorrhage is paramagnetic and produces magnetic field inhomogeneity enhanced by T2* sequences, resulting in blooming artifact. Cerebral microhemorrhages or microbleeds are thus visualized as punctate areas of signal loss.

SWI is more sensitive to CMB depiction, owing to its high spatial resolution, three-dimensional capability, and lower section thickness compared to standard T2* GRE.[7] In CAARI, CMBs appear in a lobar distribution and can colocalize with WMHs.[3,4,6] T2* GRE/SWI also depict CSS, a chronic finding which appears as linear signal loss along pial surfaces of the brain.[7] In the acute stage, in place of siderosis, sulcal subarachnoid hemorrhage may appear as T2 FLAIR hyperintensities.[1]

White matter hyperintensities of CAARI might resemble those of posterior reversible encephalopathy syndrome and some leukoencephalopathies. T2* GRE/SWI is thus critical for differentiation, as it can depict CMBs specific for CAARI.[2] Additionally, WMHs of CAARI have a tumefactive appearance that may mimic a brain tumor.[2,6]

In the absence of brain biopsy, a diagnosis of tumor may be missed in patients with coexisting CAARI. Accordingly, CAARI is diagnosis of exclusion, and biopsy should be performed based on the clinical circumstance.[2] Moreover, diseases like primary angiitis of the central nervous system, acute disseminated encephalomyelitis, and neurosarcoidosis can imitate CAARI, but gradient-echo MRI can again help suggest a CAARI diagnosis.[2,3]

Patchy, confluent WMHs and concomitant hemorrhagic manifestations (CMBs, CSS, or prior ICH) compose the imaging criteria needed to diagnose CAARI with MRI. Besides imaging, patients must also be older than 40, have one or more typical symptoms of CAARI, and lack neoplastic or infectious causes for proper diagnosis.[8] Empiric treatment with high-dose glucocorticoids is indicated in suspected CAARI. In select cases, immunosuppressants like cyclophosphamide and azathioprine may be considered as supplemental therapy.[2,4,6]

In our case, the WMHs of CAARI were confounded by the effects of local vasogenic edema from the temporoparietal hemorrhage, making diagnosis more difficult. Additionally, initial T2* GRE did not reveal substantial evidence of CMBs, which further delayed diagnosis and treatment. Glucocorticoid treatment was begun when these white matter hyperintensities persisted on follow-up outpatient MRI and new CMBs were identified using susceptibility-weighted angiography.

This illustrates the importance of prompt follow-up imaging, especially with three-dimensional susceptibility-based sequences with high spatial resolution, in unclear cases like ours.

Conclusion

CAARI is a rare variant of CAA that causes subacute neurobehavioral symptoms, focal neurologic signs, headaches, and seizures. Patients can also have classic manifestations such as large, symptomatic ICH. Characteristic findings on MRI using T2 FLAIR and T2* gradient echo sequences permit probable diagnosis of CAARI. Brain biopsy is needed for definitive diagnosis, but empiric treatment should not be delayed when clinical and radiologic suspicion is high.

References

1) Charidimou A, Boulouis G, Gurol ME, et al. Emerging concepts in sporadic cerebral amyloid angiopathy. *Brain*. 2017;140(7):1829-1850. doi:10.1093/brain/awx047

2) Wu JJ, Yao M, Ni J. Cerebral amyloid angiopathy-related inflammation: current status and future implications. *Chin Med J (Engl)*. 2021;134(6):646-654. Published 2021 Feb 23. doi:10.1097/CM9.0000000000001427

3) Kirshner HS, Bradshaw M. The inflammatory form of cerebral amyloid angiopathy or "cerebral amyloid angiopathy-related inflammation" (CAARI). *Curr Neurol Neurosci Rep*. 2015;15(8):54. doi:10.1007/s11910-015-0572-y

4) Grasso D, Castorani G, Borreggine C, Simeone A, De Blasi R. Cerebral amyloid angiopathy related inflammation: A little known but not to be underestimated disease. *Radiol Case Rep*. 2021;16(9):2514-2521. Published 2021 Jul 3. doi:10.1016/j.radcr.2021.05.080

5) Charidimou A, Boulouis G, Haley K, et al. White matter hyperintensity patterns in cerebral amyloid angiopathy and hypertensive arteriopathy. *Neurology*. 2016;86(6):505-511. doi:10.1212/WNL.0000000000002362

6) Theodorou A, Palaiodimou L, Malhotra K, et al. Clinical, neuroimaging, and genetic markers in cerebral amyloid angiopathy-related inflammation: a systematic review and meta-analysis. *Stroke*. 2023;54(1):178-188. doi:10.1161/STROKEAHA.122.040671

7) Haller S, Haacke EM, Thurnher MM, Barkhof F. Susceptibility-weighted imaging: technical essentials and clinical neurologic applications. *Radiology*. 2021;299(1):3-26. doi:10.1148/radiol.2021203071

8) Auriel E, Charidimou A, Gurol ME, et al. Validation of clinicoradiological criteria for the diagnosis of cerebral amyloid angiopathy-related inflammation. *JAMA Neurol*. 2016;73(2):197-202. doi:10.1001/jamaneurol.2015.4078

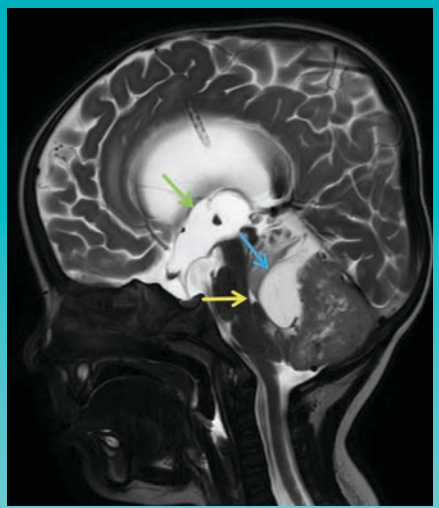

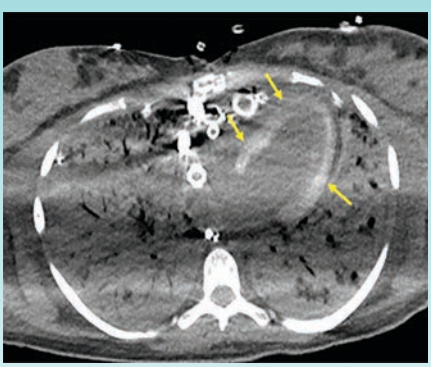

AppliedRadiology®

The Journal of Practical Medical Imaging and Management

Call for Cases

If you have an interesting case we want to know about it!

Sharing your case is a fantastic opportunity to gain recognition for your work and receive feedback from peers all over the world!

Author Guidelines* can be found at

https://appliedradiology.com/author-guidelines

- Abdominal
- Thoracic
- Genitourinary
- GI
- Emergency
- Interventional
- Vascular
- Peds
- Breast
- Neuro
- MSK
- Oncologic
- Cardiac
- Molecular Imaging
- Nuclear Medicine

* Cases undergo peer review before being accepted for publication.

PRINT / ONLINE

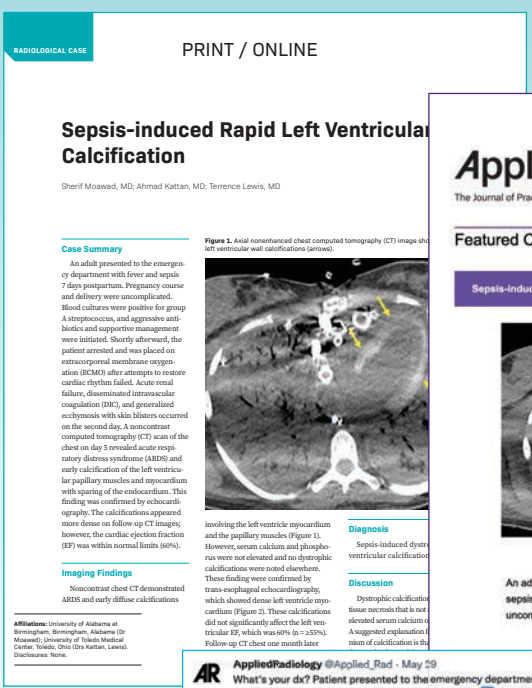
RADIOLOGICAL CASE

Sepsis-induced Rapid Left Ventricular Calcification

Sherif Moawad, MD; Ahmad Kattan, MD; Terrence Lewis, MD

Case Summary

An adult presented to the emergency department with fever and sepsis 7 days postpartum. Pregnancy course and delivery were uncomplicated. Blood cultures were positive for group A streptococcus, and aggressive antibiotics and supportive management were initiated. Shortly afterward, the patient arrested and was placed on extracorporeal membrane oxygenation (ECMO) after attempts to restore cardiac rhythm failed. Acute renal failure, disseminated intravascular coagulation (DIC), and generalized ecchymosis with skin blisters occurred on the second day. A noncontrast computed tomography (CT) scan of the chest on day 5 revealed acute respiratory distress syndrome (ARDS) and early calcification of the left ventricular papillary muscles and myocardium with sparing of the endocardium. This finding was confirmed by echocardiography. The calcifications appeared more dense on follow-up CT images; however, the cardiac ejection fraction (EF) was within normal limits (60%).

Imaging Findings

Noncontrast chest CT demonstrated ARDS and early diffuse calcifications involving the left ventricle myocardium and the papillary muscles (Figure 1). However, serum calcium and phosphorus were not elevated and no dystrophic calcifications were noted elsewhere. These finding were confirmed by trans-esophageal echocardiography, which showed dense left ventricle myocardium (Figure 2). These calcifications did not significantly affect the left ventricular EF, which was 60% (n = ≥55%). Follow-up CT chest one month later

Diagnosis

Discussion

Affiliations: University of Alabama at Birmingham, Birmingham, Alabama (Dr Moawad); University of Toledo Medical Center, Toledo, Ohio (Drs Kattan, Lewis). Disclosures: None.

EMAIL ANNOUNCEMENT

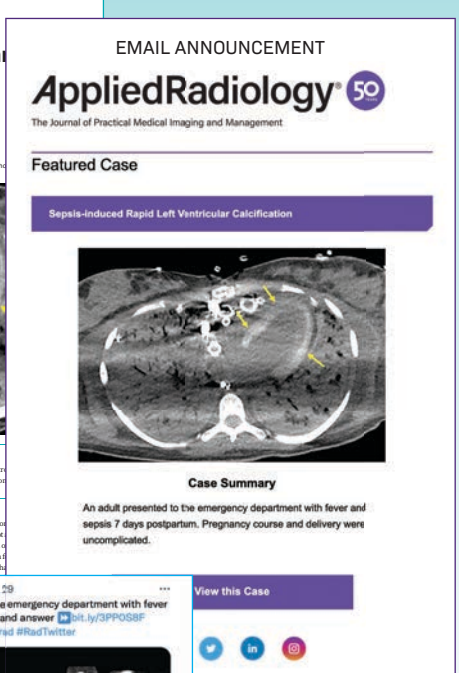
AppliedRadiology 50

The Journal of Practical Medical Imaging and Management

Featured Case

Sepsis-induced Rapid Left Ventricular Calcification

Case Summary

An adult presented to the emergency department with fever and sepsis 7 days postpartum. Pregnancy course and delivery were uncomplicated.

View this Case

SOCIAL MEDIA

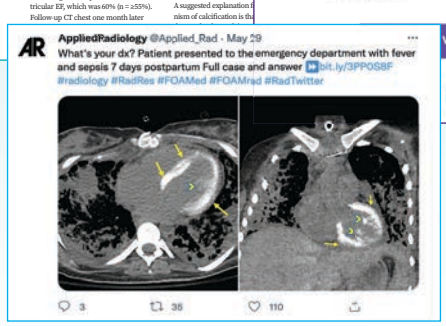
AppliedRadiology @Applied_Rad · May 29

What's your dx? Patient presented to the emergency department with fever and sepsis 7 days postpartum Full case and answer bit.ly/3PPOS8F #radiology #RadRes #FOAMed #FOAMrad #RadTwitter

3 36 110

"While we vented and ranted about the quarantine life hoping to wake up miraculously from this dystopian nightmare, we also discovered a newfound respect for the life that was, that we had left behind."

—Anindita Das

Back to Work

C. Douglas Phillips, MD

Dr Phillips is a Professor of Radiology, Director of Head and Neck Imaging, at Weill Cornell Medical College, NewYork-Presbyterian Hospital, New York, NY. He is a member of the *Applied Radiology* Editorial Advisory Board.

The Pandemic. Remember it?

Facetious question. Of course you do. That time when we all learned Zoom. I have thought a good bit about what that time past has meant to me, my friends, my family, my job, and what it has done to all of us. Nothing too deep here. You know me.

As we have gotten back to a more normal work routine, you all know the things that have changed and what it has meant to us all. Some of us are working remotely a lot now. Nothing wrong with that. Well, something is wrong with that. I used to like to dress well for work. Now, sweatpants are pretty much okay. Yes, I still do work at the hospital, but fewer days, fewer nice clothes. I don't miss the clothing expense and I have clearly saved money on suits. I am thinking that there was a hit on the economy from people not buying new clothes for the season.

The Pandemic made us all respect personal space. REALLY respect personal space. Mandatory distancing for interpersonal spacing, remember that? One thing I have noticed in our return to normalcy is that a modicum of this distance thing has remained. I really have not been crowded in a line since we started seeing each other again. Some innate memory of not wanting to get too close to everyone — they might be infectious. Score one for humanity and individuals.

Here's an odd and (at least for me) unexpected post-pandemic item: Tumor board. I am the radiology representative for a tumor board at our institution and we are in hybrid mode now. Yes, some people meet face to face again. But we have lots of folks on the Zoom call, and believe it or not, now we always have someone from any service with reason to be there, and often, several. Not just one voice from radiology, or one voice from pathology, or one from heme-onc, or radiation therapy. Several. That's another score.

Here's a thing that I miss. Working remotely doesn't let me watch clinicians wander into my reading room to steal chocolates. Or grab pens from the reception desk. I've contemplated setting up a remote camera to let me still watch these folks.

Keep doing that good work. Mahalo.

The 2024 Leaders on the Horizon Residents' Program

This exclusive program is designed to identify, cultivate, and highlight the future stars in medical imaging.

Residents are encouraged to submit a clinical research paper and/or a clinical review article for consideration. All papers should be focused on topics related to medical imaging and will be reviewed by a committee of key opinion leaders in radiology.

Residents authoring the top three (3) papers selected for each category will receive a scholarship.

Clinical Research Papers	
1st place	$7500
2nd place	$5000
3rd place	$3000

Clinical Review Papers	
1st place	$3000
2nd place	$2000
3rd place	$1000

Paper Submission Deadline: October 1, 2024

Visit appliedradiology.com/leaders to submit a paper topic today!

Supported through an unrestricted educational grant from Bracco Diagnostics, Inc.

BRACCO

LIFE FROM INSIDE

CT Suite | MR Suite | Injectors and Digital Solutions

SmartInject
SOLUTIONS FROM BRACCO

Point-of-care imaging solutions that help promote patient safety and streamline workflow

NEXO®
Contrast management system

Advance patient care with smart injectors and digital solutions from Bracco.

Learn more at **SmartInject.com**

Bracco Diagnostics Inc.
259 Prospect Plains Road, Building H
Monroe Township, NJ 08831 USA

Phone: 609-514-2200
Toll Free: 1-877-272-2269 (U.S. only)
Fax: 609-514-2446

BRACCO
LIFE FROM INSIDE

Committed to Science,
Committed **to You.**™